Technical Report Documentation Page

1. Report No.	2. Government Accession No.	3. Recipient's Catalog No.
FHWA/TX-12/0-6622-1		

4. Title and Subtitle	5. Report Date
TEXAS M-E FLEXIBLE PAVEMENT DESIGN SYSTEM: LITERATURE REVIEW AND PROPOSED FRAMEWORK	November 2011 Resubmitted: February 2012 Published: April 2012
	6. Performing Organization Code

7. Author(s)	8. Performing Organization Report No.
Sheng Hu, Fujie Zhou, and Tom Scullion	Report 0-6622-1

9. Performing Organization Name and Address	10. Work Unit No. (TRAIS)
Texas Transportation Institute The Texas A&M University System College Station, Texas 77843-3135	11. Contract or Grant No. Project 0-6622

12. Sponsoring Agency Name and Address	13. Type of Report and Period Covered
Texas Department of Transportation Research and Technology Implementation Office P. O. Box 5080 Austin, Texas 78763-5080	Technical Report: September 2010–August 2011
	14. Sponsoring Agency Code

15. Supplementary Notes

Project performed in cooperation with the Texas Department of Transportation and the Federal Highway Administration.

Project Title: Implementation of a Texas Mechanistic-Empirical Thickness Design System (TxME)

URL: http://tti.tamu.edu/documents/0-6622-1.pdf

16. Abstract

Recent developments over last several decades have offered an opportunity for more rational and rigorous pavement design procedures. Substantial work has already been completed in Texas, nationally, and internationally, in all aspects of modeling, materials characterization, and structural design. These and other assets provided the technical infrastructure that made it possible to develop the Texas Mechanistic-Empirical (TxME) pavement design system. In the first year of this project, a comprehensive literature review was made to identify and recommend available performance models in terms of rutting, fatigue cracking, low temperature cracking, endurance limit, top-down cracking, and crushing of lightly stabilized base materials. Additionally, the researchers reviewed different reliability approaches used in existing pavement design systems, and the most practical, promising reliability approach was recommended for TxME. Finally, this report discusses the framework proposed for the TxME flexible pavement design system, including pavement structure, material properties, traffic, climate, design reliability, and user interfaces.

17. Key Words	18. Distribution Statement
Flexible Pavement, Mechanistic-Empirical Design, TxME, Rutting, Cracking, Reliability	No restrictions. This document is available to the public through NTIS: National Technical Information Service Alexandria, Virginia 22312 http://www.ntis.gov

19. Security Classif. (of this report)	20. Security Classif. (of this page)	21. No. of Pages	22. Price
Unclassified	Unclassified	130	

Form DOT F 1700.7 (8-72) **Reproduction of completed page authorized**

TEXAS M-E FLEXIBLE PAVEMENT DESIGN SYSTEM: LITERATURE REVIEW AND PROPOSED FRAMEWORK

by

Sheng Hu
Assistant Research Engineer
Texas Transportation Institute

Fujie Zhou
Associate Research Engineer
Texas Transportation Institute

and

Tom Scullion, P.E.
Senior Research Engineer
Texas Transportation Institute

Report 0-6622-1
Project 0-6622
Project Title: Implementation of a Texas Mechanistic-Empirical Thickness Design System (TxME)

Performed in cooperation with the
Texas Department of Transportation
and the
Federal Highway Administration

November 2011
Resubmitted: February 2012
Published: April 2012

TEXAS TRANSPORTATION INSTITUTE
The Texas A&M University System
College Station, Texas 77843-3135

DISCLAIMER

The contents of this report reflect the views of the authors, who are responsible for the facts and the accuracy of the data presented here. The contents do not necessarily reflect the official view or policies of the Federal Highway Administration (FHWA) or the Texas Department of Transportation (TxDOT). This report does not constitute a standard, specification, or regulation, nor is it intended for construction, bidding, or permit purposes.

The United States Government and the State of Texas do not endorse products or manufacturers. Trade or manufacturers' names appear here solely because they are considered essential to the object of this report.

The researcher in charge was Fujie Zhou, P.E (Texas, #95969).

ACKNOWLEDGMENTS

This project was made possible by the Texas Department of Transportation (TxDOT) in cooperation with the Federal Highway Administration. In particular, the guidance and technical assistance provided by the project director (PD) Joe Leidy, P.E., of TxDOT proved invaluable. The following project advisors also provided valuable input throughout the course of the project, and their technical assistance is acknowledged:

- Mark McDaniel, P.E., Construction Division, TxDOT.
- Brett Haggerty, P.E., Construction Division.
- Magdy Mikhail, PhD, P.E., Construction Division.
- David Debo, Technology Service Division.
- Catherine Wolff, Transportation Planning and Programming.
- John Wright, P.E., Paris District.
- Ernie De La Gaza, P.E., Corpus Christi District.
- David Wagner, P.E., Fort Worth District.
- Suiling Cao, P.E., Houston District.

TABLE OF CONTENTS

Page

LIST OF FIGURES

Figure **Page**

LIST OF TABLES

Table **Page**

LIST OF ABBREVIATIONS

AASHTO	American Association of State Highway and Transportation Officials
AC	Asphalt Concrete
APA	Asphalt Pavement Alliance
APT	Accelerated Pavement Testing
CalME	California Mechanistic-Empirical Pavement Design Program
CAM	Crack Attenuation Mix
CMHB	Coarse Matrix High Binder
DCSE	Dissipated Creep Strain Energy
EICM	Enhanced Integrated Climatic Model
ER	Energy Ratio
ESAL	Equivalent Single Axle Load
FA	Fly-ash
FPS	Flexible Pavement System
FHWA	Federal Highway Administration
FWD	Falling Weight Deflectometer
HMA	Hot-Mix Asphalt
LVDT	Linear Variable Differential Transformer
LFA	Lime Fly-ash
M-E	Mechanistic-Empirical
MEPDG	Mechanistic-Empirical Pavement Design Guide
NCAT	National Center of Asphalt Technology
NCHRP	National Cooperative Highway Research Program
OT	Overlay Test
PCA	Portland Cement Association
PFC	Permeable Friction Course
RBL	Rich Bottom Layer

SA-CrackPro	Semi-Analytical FE Method-Based Crack Propagation Program
SIF	Stress Intensity Factor
SMA	Stone Mastic Asphalt
TxME	Texas Mechanistic-Empirical Pavement Design System
TTI	Texas Transportation Institute
TxDOT	Texas Department of Transportation
UCS	Unconfined Compressive Strength

CHAPTER 1.
INTRODUCTION

The basic geometry of a pavement system is quite simple, but flexible pavement design has never been an easy task due to varying climate, dynamic changing traffic, and complex pavement materials. Recent developments in the areas of material characterization and modeling and pavement response calculation made it possible to develop mechanistic-empirical (M-E) pavement design systems. Compared to empirical pavement design methods, the primary advantage of M-E design procedures is that they are inherently better suited to treat the variety of fundamental material properties, environmental conditions, and wheel loading conditions. The main objective of Project 0-6622 is to develop an M-E flexible pavement design system for the Texas Department of Transportation (TxDOT).

1.1 BACKGROUND AND SIGNIFICANCE OF WORK

In the mid-1990s, TxDOT implemented the Flexible Pavement System (FPS), and it has served TxDOT well in providing consistent designs statewide. However, the system has many limitations in that it does not use any results from laboratory testing, so it is impossible to determine benefits, i.e., improved design efficiencies, from improved base materials or superior asphalt mixes. Additionally, FPS performance prediction is based on pavement roughness in terms of serviceability index, rather than accounting for actual progression of distresses found in Texas highways, such as rutting, load associated cracking, and environmental cracking.

Substantial work has already been completed in Texas, nationally, and internationally in all aspects of modeling, materials characterization, and structural design. Studies recently completed have demonstrated that preliminarily calibrated models are now available to make reasonable predictions of these distresses. These new models will offer many advantages over the existing FPS system in terms of identifying trade-offs among different material types, for example, performance versus dense-grade asphalt mixes.

The development of a new enhanced flexible pavement design system will help TxDOT designers take full advantage of new materials, balance material properties, and develop more economical and reliable designs.

1.2 OBJECTIVES AND SCOPE

The main objectives of this research project are provided below:

- Improve models and testing procedures developed in Project 0-5798 and develop additional performance models and testing procedures that allow mechanistic-empirical prediction of pavement performance for Texas flexible pavement types and environmental conditions.

- Integrate performance prediction models for all flexible pavement types into program specification documents that can be used to update and enhance the FPS design system implemented in the 1990s.
- Assemble existing calibrated performance models and develop new models for surface treatment or thin pavements.
- Calibrate and validate performance prediction models using the data populated in the new Texas Flexible Pavement Database.
- Conduct case studies to demonstrate and document the advantage of the ME-based design process for Texas conditions.
- Propose framework for the TxME design system.

This report assembles background information from recently completed studies 0-5798, 0-4822, 0-5123, and other national studies. The assembled information includes performance models, traffic, climatic, and design reliability, which is the foundation of the TxME flexible pavement design system being developed under Project 0-6622. The scope and contents of this report are composed of the following items:

- Chapter 2: recommended performance models and tests. The models include asphalt layer rutting model, asphalt layer fatigue cracking model, reflection cracking model, low temperature cracking model, top down cracking model, perpetual pavement endurance limit model, granular base and subgrade rutting model, stabilized base fatigue cracking model, and stabilized base crushing failure model.
- Chapter 3: recommended reliability approach, covering literature review of possible pavement design reliability approaches and final recommendation.
- Chapter 4: proposed framework for TxME, discussing the considerations when assembling the performance models, traffic, and climate into a comprehensive design system.
- Chapter 5: conclusions and recommendations.

Additionally, the report includes several appendices, which provide more detailed information on models review and a demonstration of reliability approaches.

1.3 SUMMARY

This introductory chapter discusses the background and research objectives along with the scope and contents of the report. Specifically, this report provides the assembled information which includes performance models, traffic, climatic, design reliability, and system framework, and it will become the foundation of the TxME design system being developed.

CHAPTER 2.
PERFORMANCE MODELS AND ASSOCIATED LABORATORY TESTS FOR TxME

Performance models are critical components of any pavement design system. This chapter discusses the performance models being incorporated in the TxME design system. A total of nine models listed below and associated laboratory testing are described in this chapter.

- Asphalt layer rutting model.
- Asphalt layer fatigue cracking model.
- Reflective cracking model.
- Granular base and subgrade rutting model.
- Stabilized base fatigue cracking model.
- Stabilized base crushing failure model.
- Low temperature cracking model.
- Perpetual pavement endurance limit model.
- Top down cracking model.

The following sections describe each of the models. Specifically, detailed descriptions on the low temperature cracking model, perpetual pavement endurance limit model, and top down cracking model are provided here because these three models were not the focus of past studies in Texas and were not well addressed yet.

2.1 ASPHALT LAYER RUTTING

For the asphalt layer rutting model, the researchers selected the VESYS layer rutting model for this study. Note that the Federal Highway Administration originally developed the VESYS rutting model in the late 1970s. The MEPDG has used a similar conceptual rutting model. This model was further developed and calibrated under Project 0-5798 and is recommended for TxME (Zhou et al. 2010 and Hu et al. 2011).

2.1.1 Asphalt Layer Rutting Model for TxME

Equation 2-1 presents the asphalt rutting model developed under Project 0-5798.

$$RD_{AC} = \sum_{i=1}^{M} k_{AC} \int \left(U_i^+ - U_i^-\right) \mu_i N^{-\alpha_i} \tag{2-1}$$

where

k_{AC} = the calibration factor defined in Equation 2-2.
U_i^+ and U_i^- = deflections at the top and bottom of finite layer i due to axle group.
M = the total number of asphalt layers.

μ_i and α_i = permanent deformation parameters of asphalt layer *i*.

$$k_{AC} = f_1(T) \times f_2(E) \times f_3(h_{AC}) \tag{2-2}$$

where $f_1(T)$ is the pavement temperature correction factor, $f_2(E)$ is the modulus correction factor to alternatively consider non-linear stress dependency of rutting development, and $f_3(h_{AC})$ is the asphalt layer thickness correction factor.

The asphalt layer rutting model has been preliminarily calibrated using eight test sections of the 2006 National Center for Asphalt Technology (NCAT) test track program. The three adjustment factors, $f_1(T)$, $f_2(E)$, and $f_3(h_{OL})$ for temperature, modulus, and layer thickness, have been separately determined and are presented in Equations 2-3, 2-4, and 2-5, respectively.

$$f_1(T) = 0.191112 + \frac{3.643124}{1 + e^{18.3009 - 0.204437T}} \tag{2-3}$$

$$f_2(E) = 0.37264 + \frac{1.18771}{1 + e^{-8.90208 + 0.09879E}} \tag{2-4}$$

$$\begin{aligned} f_3(h_{OL}) = {} & \left(0.01445272 h_1^{\,3} - 0.12471319 h_1^{\,2} + 0.22193794 h_1 + 1.37640722\right) \times \\ & \left(0.00567302 h_2^{\,3} + 0.07104301 h_2^{\,2} - 0.49592553 h_2 + 2.12378879\right) \times \\ & \left(0.00199314 + \frac{0.54035153}{1 + e^{-2.61478586 + 0.58494146(h_1 + h_2)}}\right) \end{aligned} \tag{2-5}$$

where T is the asphalt layer temperature, ºF; E is the asphalt layer dynamic modulus value at 54ºC (130ºF) and 10 Hz, ksi; and h_1 and h_2 are representative layer thickness.

The major feature of the asphalt layer rutting model is to characterize layer properties rather than global parameters used in the MEPDG. For each asphalt layer, its rutting model requires permanent deformation parameters (μ_i and α_i) which can be determined from the repeated load test.

It is clear that the three key issues of the proposed asphalt layer rutting model are to

- Calculate the deflection of each asphalt layer.
- Determine permanent deformation parameters μ_i and α_i for each asphalt layer.
- Calculate accumulated rutting under different traffic loads and environmental conditions.

These issues are addressed in the following sections.

2.1.2 Calculation of Asphalt Layer Deflection

Currently, several multi-layer linear elastic programs are available for calculating pavement deflection. To be consistent with the current TxDOT pavement design program (FPS19W or FPS 21W), the research team chose the well-known multi-layer elastic program WESLEA. The WESLEA program requires the modulus and Poisson's ratio of each layer. In this study, a typical Poisson's ratio value of 0.35 was assumed for asphalt layer materials and a delegated seasonal elastic modulus was adopted. For each season, the delegated elastic modulus was determined based on the dynamic modulus master curve, average seasonal temperature of asphalt layer, and loading frequency (or vehicle operation speed). The Hot-Mix Asphalt (HMA) dynamic modulus and master curve were measured and formed following the AASHTO TP 62-03: Standard Method of Test for Determining Dynamic Modulus of Hot-Mix Asphalt Concrete Mixtures (AASHTO TP 62-03 2003).

2.1.3 Laboratory Determination of Asphalt Layer Rutting Parameters (μ and α)

The Repeated Load Permanent Deformation (RLPD) test is a stress-controlled test involving repetitive application of a haversine-shaped compressive-axial load (stress) to an unconfined specimen. The loading is 1 Hz with 0.1 sec loading time and 0.9 sec rest period, respectively, for up to 10,000 load cycles. The RLPD tests are often conducted at three test temperatures (77°, 104°, and 122°F). Figure 2-1 shows the loading configuration used at the Texas Transportation Institute (TTI). The measurable parameters include the applied load (stress), test temperature, time, loading cycles, axial permanent deformation, and strains.

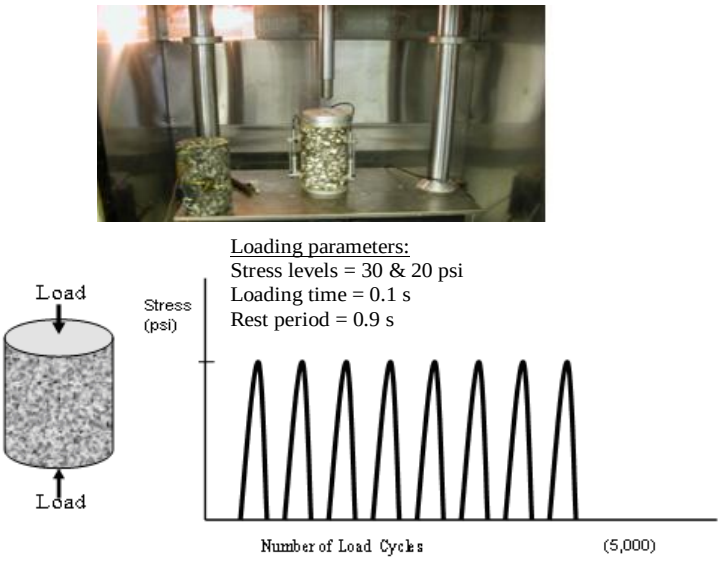

Figure 2-1. RLPD Loading Configuration.

From a plot of the accumulative axial permanent microstrain versus load repetitions on a log-log scale (Figure 2-2), permanent deformation parameters ε_r, a, b, alpha (α), and gnu (μ) were

determined consistent with the procedure that Zhou and Scullion (2002) described. These parameters constitute the VESYS5 rutting input parameters (μ and α) for asphalt mixtures and are defined as follows:

ε_r = axial resilient microstrains measured at the 100th load cycle.

a and *b* = intercept and slope of the linear portion of the permanent microstrain curve (log-log scale).

alpha (α) = rutting parameter, computed as $\alpha = 1 - b$.

gnu (μ) = rutting parameter, computed as $\mu = ab / \varepsilon_r$.

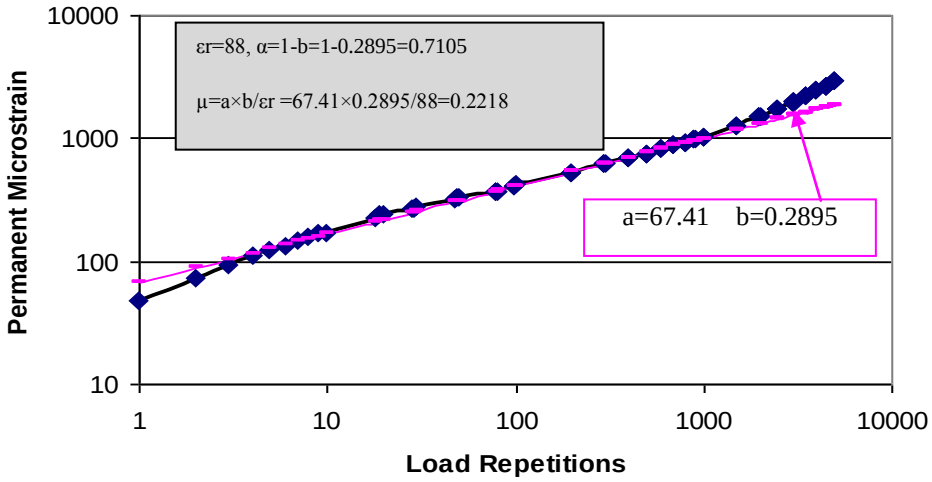

Figure 2-2. Regression Constants from Log Permanent Microstrain – Log Load Repetitions.

2.1.4 Rutting Accumulation Principle

To consider the effects of stresses of different magnitudes on the development of rutting, which results from variations in traffic loads and environmental conditions, a time-hardening procedure appears to provide a reasonable approach (Lytton et al. 1993, Epps et al. 2002).

For each season *i*, ε_i^p is computed from Equation 2-6.

$$\varepsilon_i^p = \varepsilon_i^{p(N=1)} \left[\left(N_{eqi} + n_i \right)^b - N_{eqi}^b \right] \quad (2\text{-}6)$$

where

$\varepsilon_i^{p(N=1)}$ = the permanent strain at the first load repetition.

n_i = the number of load repetitions during season *i*.

N_{eqi} = the equivalent total number of load repetitions at beginning of season *i*.

b = the slope of ($\log\varepsilon^p$ –$\log N$) curve discussed previously.

The N_{eq} is obtained for each season with the time-hardening matching scheme as follows:

$$\text{Season 1} \quad \begin{matrix} N_{eq} = 0 \\ \varepsilon_1^p = \varepsilon_1^{p(N=1)} N_1^{b_1} \end{matrix} \tag{2-7}$$

$$\text{Season 2} \quad N_{eq2} = \left[\frac{\varepsilon_1^p}{\varepsilon_2^{p(N=1)}} \right]^{\frac{1}{b_2}} \tag{2-8}$$

$$\varepsilon_2^p = \varepsilon_2^{p(N=1)} \left[\left(N_{eq2} + n_2 \right)^{b_2} - N_{eq2}^{b_2} \right] \tag{2-9}$$

$$\text{Season } i \quad N_{eq\,i} = \left[\frac{\varepsilon_{i-1}^p}{\varepsilon_i^{p(N=1)}} \right]^{\frac{1}{b_i}} \tag{2-10}$$

$$\varepsilon_i^p = \varepsilon_i^{p(N=1)} \left[\left(N_{eq\,i} + n_i \right)^{b_i} - N_{eq\,i}^{b_i} \right] \tag{2-11}$$

2.1.5 Summary of Asphalt Layer Rutting Model

The VESYS layer rutting model is considered a reasonable approach for predicting rut depth; it provides the added flexibility of allowing use of either linear or nonlinear elastic theory. The major feature of the recommended rutting model is to characterize layer properties rather than global parameters that MEPDG used. For each layer, the VESYS rutting model requires permanent deformation parameters: α_i and μ_i, which assures a more accurate rutting prediction.

Additionally, to consider the effects of stresses of different magnitudes on the development of rutting which result from variations in traffic loads and environmental conditions, a time-hardening procedure was incorporated.

2.2 ASPHALT LAYER FATIGUE CRACKING

Fatigue cracking is one of the major distress modes considered in flexible pavement design and has been studied for several decades. Different types of fatigue cracking models have been reviewed under Project 0-5798, such as the Shell Oil model (Bonnaure et al. 1980), Asphalt Institute (MS-1) model (Asphalt Institute 1981), MEPDG model (NCHRP 2004), CalME model (Ullidtz et al. 2006), Viscoelastic Continuum Damage Mechanistics (VCDE)-based model (Christensen Bonaquist 2005), and Overlay Tester (OT)-based fatigue cracking model (Zhou et al. 2007), etc. Each fatigue cracking model has its advantages; however, except for the OT-based model, these models mainly focus on the crack initiation stage and the crack propagation stage is often not directly considered. It is well-known that to accurately predict fatigue cracking, it is necessary to include both crack initiation (N_i) and crack propagation (N_p) in

the model. Thus, the OT-based fatigue cracking model is identified to be incorporated into the future TxME system.

2.2.1 Recommended Asphalt Layer Fatigue Cracking Model

The proposed OT-based fatigue cracking model is composed of three components:

- Fatigue life model.
- Fatigue damage model.
- Fatigue amount model.

Note that the fatigue life model described below originated from study 0-5798 (Zhou et al. 2008), and the fatigue damage model and fatigue amount model are similar to those used in the MEDPG.

Fatigue Life Model

The fatigue life (N_f) is the sum of the number of load repetitions needed for micro-cracks to coalesce to initiate a macro-crack (crack initiation life, N_i) and the number of load repetitions required for the macro-crack to propagate to the surface (crack propagation life, N_p):

$$N_f = N_i + N_p \tag{2-12}$$

The following equations estimate crack initiation life N_i:

$$N_i = k_1\left(\frac{1}{\varepsilon}\right)^{k_2} \tag{2-13}$$

$$k_1 = 10^{6.97001 - 3.20145 k_2 - 0.83661 \log E} \tag{2-14}$$

$$k_2 = n \tag{2-15}$$

where ε is maximum tensile strain at the bottom of asphalt layer, E is dynamic modulus, and n is a fracture property.

Crack propagation life N_p is calculated based on the well-known Paris' law (Paris 1963):

$$N_p = \int_{c_0}^{h} \frac{1}{A(K)^n} dc \tag{2-16}$$

$$N_p = \sum \Delta N_{pi} \tag{2-17}$$

$$\sum \Delta N_{pi} = \frac{\sum \Delta c_{pi}}{k_{p1} A K_I{}^n + k_{p2} A K_{II}{}^n} \tag{2-18}$$

where

c_0 = the initial crack length (based on Lytton's recommendation [Lytton et al. 1993], c_0=7.5 mm is used).

h = the asphalt layer thickness, K_I and K_{II} are stress intensity factors (SIF) caused by bending and shearing stresses, respectively.

A and n = fracture properties determined from the OT testing.

Δc_{pi} = the crack propagation length caused by ΔN_{pi} (number of load repetitions).

k_{p1} and k_{p2} = field calibration factors.

Fatigue Damage Accumulation Model

The accumulated fatigue damage (D) caused by a specified number of load repetitions (n) is estimated using Miner's law:

$$D = \sum \frac{n}{N_f} \tag{2-19}$$

Fatigued Area Model

A sigmoidal model is proposed for predicting the fatigued area:

$$fatigued\_area(\%) = \frac{100}{1 + e^{-7.89 \log D}} \tag{2-20}$$

where D is the accumulated fatigue damage estimated from Equation 2-19.

Note that the *fatigued_area(%)* is the percentage of fatigue cracking area over the wheel path area. Also note that Equation 2-20 has a sigmoidal function form, which is bound with 0 percent cracking as a minimum and 100 percent cracking as a maximum. Specifically, it was assumed that *fatigued_area(%)* equals 50 when D equals 1.

In this model, the stress intensity factor K can be computed using the specifically developed pavement SIF FE program, SA-CrackPro, which is comparably accurate but much faster and simpler to use than some commercial 3D FE packages such as ANSYS or ABAQUS (Hu et al. 2008). To determine K, full pavement structures including all the asphalt layers, base layers, and subgrade have to be considered. Besides, for a pavement that has multiple asphalt layers, the fracture properties A and n of each asphalt layer are involved. This assures that the contributions of all asphalt layers to pavement fatigue life are considered during the crack propagation stage.

The researchers used measured fatigue cracking data from seven test sections of the 2006 test cycle at the NCAT Test Track to preliminarily calibrate this asphalt fatigue cracking model. Then the calibrated model was further validated using the fatigue cracking data of two test sections of the 2003 test cycle at the NCAT Test Track. The final values of the calibration factors k_{p1} and k_{p2} are k_{p1} =2 and k_{p2}=4. It is obvious that further calibration and validation are needed, especially for Texas materials and environmental conditions.

As can be seen in the OT-based fatigue cracking model, fracture properties *A* and *n* are the key parameters when determining the crack propagation life N_p. Additionally, the crack initiation parameters k_1 and k_2 also depend on the *n* value. Therefore, a brief description about how to use the OT test to determine fracture properties A and n is given below.

2.2.2 Two-Step OT Test for Determining Fracture Properties *A* and *n*

Over the past several years, the standard OT test with 0.64 mm (0.025 in.) maximum opening displacement (TxDOT's test procedure: Tex-248-F) has been used as a quick screening test for crack-prone mixes. When the standard OT test was used for determining HMA fracture properties, two problems were identified.

- The unknown specimen modulus (in tension mode) that is critical in determining the fracture parameter *A* value (Zhou et al. 2007).
- The maximum opening displacement of 0.64 mm (0.025 in.) under the standard OT test is too big for many Texas limestone mixes, resulting in a very low number of cycles to failure, which is not enough for fracture properties determination.

Thus, a two-step OT test was proposed (Zhou et al. 2007) for HMA fracture properties determination.

Step 1. OT Modulus Test (OT-E) to Determine Modulus

To use the OT to measure the specimen modulus *E* (in tension mode) the researchers first modified the test procedure by gluing only the ends of the specimens to new end plates. External linear variable differential transformers (LVDTs) were also added to enhance measurement accuracy. Figure 2-3a shows a glued specimen within the glue jig. Figure 2-3b illustrates the standard OT base plates, assembled connecting plates, external LVDTs, and the specimen with mounted LVDTs. Note that the gauge length of the LVDT is 88 mm (3.5 in.).

Secondly, the main purpose of the OT-E test is to determine the *E* value for later calculation of the fracture property *A*. Thus, the proposed OT-E test will be conducted at the same test temperature and frequency in a displacement controlled tension mode as those used for the standard OT test. For example, if the OT is run at 25°C and 0.1 Hz (10 sec per cycle), the corresponding OT modulus test should be performed at 25ºC and 0.1 Hz as well. Its opening

displacement should be much smaller than the standard test so that no damage will occur to the specimen. The recommended opening displacement is 0.023 mm (0.0009 in.), and the corresponding strain level within the specimen is about 75 microstrains ($\mu\varepsilon$), which is consistent with the MEPDG dynamic modulus test (AASHTO TP62-03 2003). Figure 2-4 shows an example of an OT-E test loading curve and corresponding strain curve (haversine-shaped) measured by LVDTs. The sample modulus (in tension mode) can then be determined based on these curves.

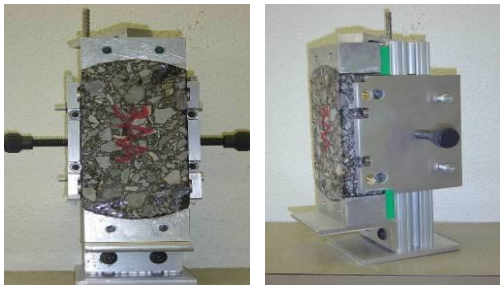

(a) Specimen and Glue Jig.

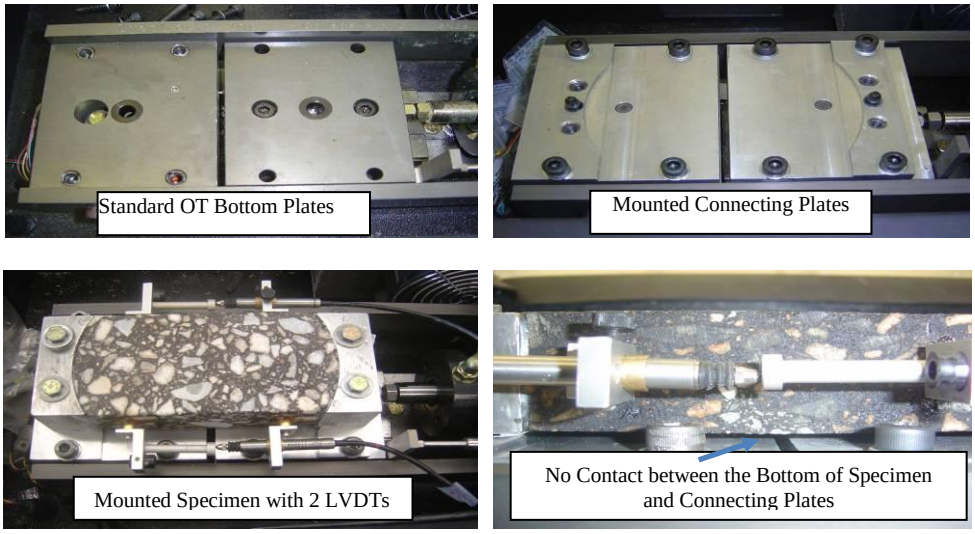

(b) Plates and LVDTs.

Figure 2-3. OT-E Test Specimen, Glue Jig, Plates, and LVDTs.

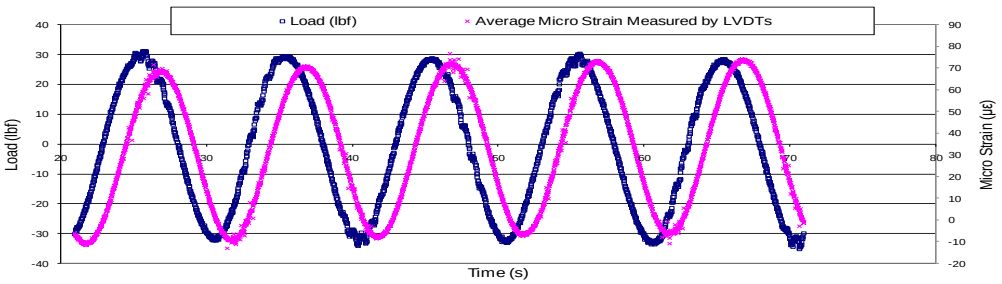

Figure 2-4. Load and Corresponding Strain Curve.

Step 2. OT Test to Determine A and n

This test procedure is similar to TxDOT test method Tex-248-F but with the following minor changes:

- Reduce the opening displacement to 0.43 mm (0.017 in.) from the standard 0.63 mm (0.025 in.).
- Run the OT until it reaches 100 cycles. If the OT sample fails in less than 50 cycles, reduce the opening displacement to 0.015 in. or less; run the other replicate again until it reaches a minimum of 50 cycles.

After performing the two-step OT test, fracture properties (*A* and *n*) can be determined following the five steps listed in Zhou et al. (2007). It is worth noting that the OT-based test procedure briefly discussed above and all other crack evaluation procedures currently address only Mode I fracture (opening and/or bending mode loading). The Mode II fracture (shearing mode loading) is under development. Currently, it is assumed that Modes I and II share the same fracture properties (*A* and *n*).

2.2.3 Summary of Asphalt Layer Fatigue Cracking Model

The OT-based fatigue cracking model is identified to be a rational choice to model asphalt layer fatigue cracking. The main features of the proposed OT-based fatigue cracking model include

- Consideration of both crack initiation and crack propagation.
- Full consideration of the contribution of all asphalt layers.
- The use of a simple OT test for determining the fracture properties required for predicting both crack propagation and cracking initiation.

This asphalt fatigue cracking model has been calibrated using NCAT test track data under Project 0-5798. However, it should be further calibrated to Texas local conditions under this study.

2.3 REFLECTIVE CRACKING MODEL

The proposed reflective cracking model includes three components: reflective crack propagation model, reflective damage model, and reflective cracking amount model. These three models are exactly the same as those developed under TxDOT Research Project 0-5123.

Reflective Crack Propagation Model

A reflective cracking model has been developed and calibrated under Project 0-5123. Equation 2-21 presents the basic model.

$$\Delta C = k_1 A\left(K_{bending}\right)^n \Delta N_i + k_2 A\left(K_{shearing}\right)^n \Delta N_i + k_3 \left(K_{thermal}\right)^n \tag{2-21}$$

where

ΔC = daily crack length increment.
ΔN = daily load repetitions.
A and n = HMA fracture properties which can be determined by the aforementioned OT test.
$K_{bending}$ = SIF caused by traffic load in bending.
$K_{shearing}$ = SIF caused by traffic load in shearing.
$K_{thermal}$ = SIF caused by thermal load.
k_1, k_2, and k_3 = calibration factors.

Note that regression equations for $K_{bending}$, $K_{shearing}$, and $K_{thermal}$ have been developed based on extensive finite element computations under the Project 0-5123.

Reflective Cracking Damage Model

The reflective cracking damage model is presented in Equation 2-22.

$$D = \sum \Delta C / h \tag{2-22}$$

where h is the overlay thickness, and $\sum \Delta C$ is the total crack length.

Reflection Cracking Amount Model

A sigmoidal function (Equation 2-23) is used to describe the development of the reflection cracking amount:

$$RCR = \frac{100}{1 + e^{C_1 \log D}} \tag{2-23}$$

where *RCR* is reflective cracking rate (%), C_1 is the calibration factor, and *D* is the reflective cracking damage from Equation 2-22.

Reflective cracking model has been calibrated and validated under the TxDOT Research Project 0-5123 and was incorporated in the overlay design system TxACOL, which was getting implemented through Project 5-5123-03. Any updating of the reflective cracking model (calibration factors, and new SIF regression equations, etc.) during implementation will be incorporated in the future TxME system.

2.4 GRANULAR BASE/SUBGRADE RUTTING

After reviewing all existing rutting models for unbound materials, Project 0-5798 identified that the VESYS layer rutting model presented in Equation 2-24 (Kenis 1978) is a good candidate for unbound materials.

$$RD_{granular} = \sum_{i=1}^{M} k_{granular} \int \left(U_i^+ - U_i^-\right) \mu_i N^{-\alpha_i} \tag{2-24}$$

where

$k_{Granular}$ = calibration factor.
U_i^+ and U_i^- = deflection at top and bottom of finite layer *i* due to axle group.
M = total number of granular base layers.
μ_i and α_i = permanent deformation parameters of layer *i*.

Limited studies on granular base materials have been conducted under Project 0-5798, and the influence of moisture on permanent deformation of granular base materials was not investigated. The research team strongly believes that further study on the influence of moisture should be pursued and included in the rutting model development under this new research project. Finally, the developed granular base rutting models will be calibrated using the field performance data populated in the Texas Flexible Pavement Database (Project 0-6658).

2.5 STABILIZED BASE FATIGUE CRACKING

Two fatigue cracking models were identified under Project 0-5798 and are presented below:

MEPDG fatigue cracking model

$$\log N_f = \frac{(0.972\beta_{c1} - (\frac{\sigma_t}{M_r})}{0.0825 * \beta_{c2}} \tag{2-25}$$

PCA fatigue cracking model

$$N_f = \left(\frac{\beta_{c4}}{\sigma_t / M_r} \right)^{\beta_{c3} \cdot 20} \quad (2\text{-}26)$$

where

N_f = number of repetitions to fatigue cracking of the stabilized layer.
σ_t = maximum traffic induced tensile stress at the bottom of the stabilized layer (psi).
M_r = 28-day modulus of rupture (flexural strength) (psi).
β_{c1}, β_{c2}, β_{c3}, and β_{c4} = field calibration factors.

Calibration factors for two types of cement treated materials were developed for:

- Cement treated base: β_{c1}=1.0645, β_{c2}=0.9003, β_{c3}=1.0259, and β_{c4}=1.1368.
- Fine-grained soil cement: β_{c1}=1.8985, β_{c2}=2.5580, β_{c3}=0.6052, and β_{c4}=2.1154.

The two major material inputs that the proposed models required are resilient modulus (used to calculate tensile stress σ_t) and modulus of rupture M_r of the stabilized materials.

2.5.1 Resilient Modulus Test

The standard resilient modulus test for stabilized materials that the MEPDG proposed is not recommended for routine use. The test is very difficult to run on cement-treated materials. The strain levels are very low, requiring accurate instrumentation. During this test, seating loads do not ensure uniform contact with cement-treated materials, where even small unevenness of the surface causes major differences in strains measured on either side of the test sample.

The limited test program that Scullion et al. (2006) conducted indicated that the seismic modulus device is a better, more repeatable test for estimating the resilient modulus of stabilized materials. The seismic modulus equipment is available within TxDOT, and the resilient modulus can be estimated to be 75 percent of the measured seismic modulus (Scullion et al. 2006).

One more attractive method for most users is to relate the design values to the standard seven-day Unconfined Compressive Strength (UCS) value. The recommended relationships (Scullion et al. 2006) are given below.

- For cement treated bases:

$$\text{28-day Modulus of Rupture (ksi)} = 7.30 * \sqrt{UCS} \quad (2\text{-}27)$$

$$\text{Resilient Modulus (ksi)} = 36.5 * \sqrt{UCS} \quad (2\text{-}28)$$

- For fine-grained soil cement:

$$\text{28 day Modulus of Rupture (ksi)} = 6.32^* \sqrt{UCS} \quad (2\text{-}29)$$

$$\text{Resilient Modulus (ksi)} = 31.6^* \sqrt{UCS} \quad (2\text{-}30)$$

- For cement treated bases:

  Resilient Modulus 600 ksi, Modulus of Rupture 125 psi, Poisson's Ratio 0.20

- For fine-grained soil cement:

  Resilient Modulus 300 ksi, Modulus of Rupture 60 psi, Poisson's Ratio 0.20

2.5.2 Modulus of Rupture Test

Figure 2-5 shows a modulus of rupture test set-up. Samples for the test can be fabricated in triplicate using a 6-in. × 6-in. × 20-in. beam mold and be compacted in two lifts at 72 blows per lift with a 10-lb tamper. These samples can then be moist cured for 28 days before determining the modulus of rupture in accordance with TEX-448-A: Flexural Strength of Concrete Using Simple Beam Third-Point Loading.

Figure 2-5. Modulus of Rupture Test Setup.

2.6 STABILIZED BASE CRUSHING FAILURE

Different from fatigue cracking that usually starts at the bottom of the layer and progresses upwards through the layer, crushing occurs at the top (upper 2–3 in.) of a lightly stabilized base layer. De Beer (1989) initially founded the crushing or compression failure mechanism of

cementitiously stabilized materials. Based on the HVS testing results, de Beer (1989) proposed a crushing model (Equation 2-31) that is a function of the ratio of vertical stress (σ_t) to UCS:

$$N_c = 10^{8.21\left(1-\frac{\sigma_t}{1.2\times UCS}\right)} \quad (2\text{-}31)$$

Except for the work that de Beer had done in South Africa, the study on crushing failure and modeling is very limited, and no standard test procedure has been proposed. Therefore, both a laboratory test procedure and associated crushing models should be developed for Texas conditions under this study.

2.7 LOW TEMPERATURE CRACKING

Although low temperature cracking is not often observed in south Texas, it does exist in north Texas, in areas such as the Amarillo and the Lubbock Districts. Generally, contraction strains induced by cooling lead to thermal tensile stress development in the restrained surface layer. Depending on the magnitude of these stresses and the asphalt mixture's resistance to fracture, transverse cracks may develop at different points along the length of the pavement. A brief discussion on low temperature cracking is presented below, since it was not fully investigated under Project 0-5798.

2.7.1 Background

Before the SHRP A-005 project (Lytton et al. 1993), there were no existing models to predict thermal cracking performance (amount of cracking versus time) using fundamental, low-temperature mixture properties. Empirical models have been developed to predict the number of cracks or crack spacing, but these models do not include time as a variable and are primarily based on asphalt binder properties rather than mixture properties. Other existing models predicted a mixture's cracking potential (Finn et al. 1986, Roque and Ruth 1990), but did not predict thermal cracking performance in terms of amount of cracking versus time.

Lytton et al. (1983) developed a model called THERM, which provides thermal cracking predictions as a function of time, but relies on estimated mixture properties rather than mixture properties directly measured at low temperatures. Therefore, the SHRP A-005 program undertook the development of a new thermal cracking model that predicted thermal cracking performance (the amount of cracking versus time) using mixture properties measured from the indirect tension (IDT) test, along with site-specific environmental and structural information. The resulting thermal cracking model was called TCMODEL, which was updated and incorporated into MEPDG software (Witczak et al. 2000).

The low temperature cracking model proposed in this study is similar to the one used in the MEPDG. However, the aforementioned enhanced OT test (Zhou et al. 2007) will determine the

fracture properties A and n in this model rather than the IDT test. In addition, an alternative cracking amount model will be recommended.

2.7.2 Low Temperature Cracking Model in MEPDG

The model in MEPDG is composed of two major components: crack propagation model and cracking amount model.

Crack Propagation Model

$$\Delta C = A(\Delta K)^n \tag{2-32}$$

where, ΔC is change in the crack depth due to a cooling cycle, *A and n* are fracture properties, and:

$$n = 0.8 * (1 + \frac{1}{m}) \text{ (Lytton et al. 1983)} \tag{2-33}$$

where *m* is the slope of the linear portion of the log compliance – log time master curve determined from creep tests (see Figure 2-6).

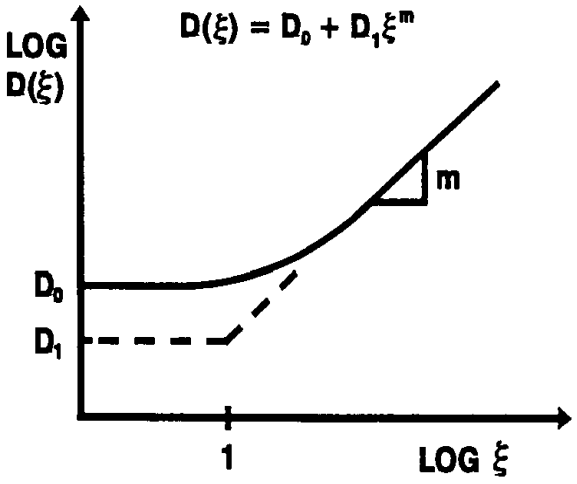

Figure 2-6. Power Model for Creep Compliance Master Curve.

$$\log A = 4.389 - 2.52 * \log(k * \sigma_m * n) \tag{2-34}$$

where *k* is a coefficient determined through field calibration, *k* = 10,000, and σ_m is the mixture strength based on IDT test (Witczak et al. 2000).

In Equation 2-32, ΔK is the change in the thermal stress intensity factor K due to a cooling cycle, and K is determined by the following equation (Witczak et al. 2000):

$$K = \sigma(\xi)(0.45 + 1.99C^{0.56}) \tag{2-35}$$

where C is current crack length, $\sigma(\zeta)$ is thermal stress at reduced time ζ, determined by:

$$\sigma(\zeta) = \int_0^{\zeta} E(\zeta - \zeta') \frac{d\varepsilon}{d\zeta'} d\zeta' \tag{2-36}$$

where, $E(\zeta - \zeta')$ is the relaxation modulus at reduced time $\zeta - \zeta'$, ε is the strain at reduced time ζ (= $\alpha(T(\zeta') - T_0)$), α is the linear coefficient of thermal expansion/contraction, $T(\zeta')$ is the pavement temperature at reduced time ζ', T_0 is the pavement temperature when $\sigma = 0$, and ζ' is the variable of integration.

Cracking Amount Model

The model shown in Equation 2-37 was used to predict the amount of cracking per unit length of pavement section. Essentially, the amount of cracking is a function of the probability that the crack depth is equal to or greater than the thickness of the surface layer. As shown in Figure 2-7, this probability is determined by assuming that the logarithm of the depth of cracks in the pavement is normally distributed with mean equal to log C_0 (the crack depth predicted by the model), and a variance of σ^2. The amount of cracking is computed as follows:

$$AC = \beta_1 * N\left(\frac{\log C / D}{\sigma}\right) \tag{2-37}$$

where

AC = amount of thermal cracking, ft/500ft.
β_1 = regression coefficient determined through field calibration =353.5.
P( ) = probability that ( ) is true.
N ( ) = standard normal distribution evaluated at ( ).
σ = standard deviation of the log of the depth of cracks in the pavement =0.769.
C = crack depth.
D = thickness of surface layer.

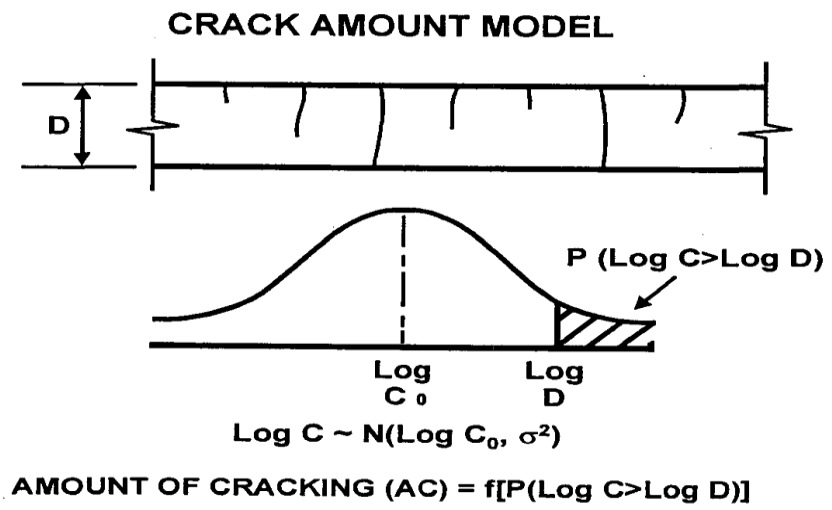

Figure 2-7. Crack Amount Model: Crack Depth Distribution (after Witczak et al. 2000).

Under the SHRP program in 1993, Roque et al. originally developed the calibration factors β_1 and σ. Later, the MEPDG research team refined these factors using 22 GPS sections (SHRP general pavement sections), 14 Canadian SHRP sections, and five MnRoad sections.

Note that this model does not predict any more than 50 percent of the total possible amount of cracking that can develop in the pavement. This corresponds to the instant when the average crack depth is equal to the thickness of the surface layer, which implies that 50 percent of cracks in the pavement are deeper than the thickness of the surface layer and 50 percent of the cracks have not penetrated through the surface layer. Based on the field observations, a maximum amount of 400 ft of cracking per 500 ft of pavement that corresponds to a crack frequency of one crack per 15 ft of pavement, was selected as the maximum amount of thermal cracking that would typically develop in a pavement. Thus, the model predicts a maximum amount of cracking of about 200 ft per 500 ft of pavement (i.e., one crack per 30 ft). Therefore, when the model predicts 200 ft of cracking after five years of service, the proper interpretation is that the pavement can be expected to have at least 200 ft of cracking after five years (Witczak et al. 2000).

2.7.3 Recommended Alternative Cracking Amount Model

In essence, the amount of cracking amount model in MEPDG (Equation 2-37) is used to correlate the ratio of crack length *C* over layer thickness *D* to the observed amount of thermal cracking, in length or in number of cracks. To be consistent with the crack amount model for either reflective cracking or fatigue cracking, the following model would be recommended as an alternate.

First, determine the damage ratio, as follows:

$$D = \sum \Delta C / h \tag{2-38}$$

where D is the damage ratio, h is the asphalt concrete layer thickness, and ∑ΔC is the total crack length determined using the crack propagation model.

Then, a sigmoidal model is used to describe the development of the thermal cracking amount:

$$AC = \frac{100}{1 + e^{C \log D}} \times B \tag{2-39}$$

where *AC* is amount of thermal cracking (ft/mile), *B* and *C* are calibration factors, and *D* is the damage ratio from Equation 2-38.

2.7.4 Summary of Low Temperature Cracking Model

The low temperature cracking model which is similar to the one used in the MEPDG is recommended for use in the TxME. Two significant differences from the MEPDG model are noted here:

- The fracture properties *A* and *n* in the proposed model will be determined by the aforementioned enhanced OT test directly. As can be seen from Equation 2-33, the *A* and *n* determination method MEPDG uses is based on an empirical relationship with IDT results. With the measured *A* and *n* values, the MEPDG low temperature cracking needs to be calibrated against actual pavement performance.
- An alternative cracking amount model was recommended to be consistent with the crack amount model of reflective cracking or fatigue cracking.

2.8 ENDURANCE LIMIT MODEL FOR PERPETUAL PAVEMENT

In recent years, there has been a push toward designing a long-lasting thick HMA pavement, commonly referred to as a perpetual pavement. The asphalt pavement alliance (APA) has defined a perpetual pavement as "an asphalt pavement designed and built to last longer than 50 years without requiring major structural rehabilitation or reconstruction, and needing only periodic surface renewal in response to distresses confined to the top of the pavement" (Newcomb 2002). There is a belief that for these perpetual pavements bottom-up fatigue cracking does not occur. The concept of the HMA fatigue endurance limit—a level of strain below which there is no cumulative damage over an indefinite number of load cycles—has been proposed to explain this occurrence. Therefore, additional pavement thickness, greater than that required to keep strains below the endurance limit, would not provide additional life. This concept has significant design and economic implications.

Since 2001, Texas has been designing and constructing perpetual pavements on some of its heavily trafficked highways where the expected 20-year truck-traffic estimate of 18 kip Equivalent Single-Axle Loads (ESALs) is in excess of 30 million. To date, more than 10 in-service perpetual pavement sections are being monitored and evaluated, and a performance database of these perpetual pavement sections was developed (Walubita et al. 2009). It is necessary to validate and calibrate this endurance limit concept and so-called model before incorporating it in the future TxME.

2.8.1 Background

The concept of an endurance limit is widely recognized in many areas of materials science, especially that of ferrous metals. Barret et al. (1973) describe the endurance limit for metals as being a stress below which, the plot of stress versus cycles to failure becomes essentially horizontal for uncracked materials, and fatigue does not occur. Although this limit has been extensively studied and defined in metal and other material areas, relatively less work was done for HMA, a typical viscoelastic material.

Monismith and McLean (1972) first demonstrated the existence of a fatigue endurance limit below which asphalt mixtures tend to have an extraordinarily long fatigue life and proposed an endurance limit of 70 $\mu\varepsilon$ for asphalt pavements. The log-log relationship between strain and bending cycles converged below 70 $\mu\varepsilon$ at approximately 5 million cycles (Figure 2-8). Maupin and Freeman (1976) noted a similar convergence. Nunn (1997) in the United Kingdom (UK) and Nishizawa et al. (1997) in Japan proposed concepts for long-life pavements where classical bottom-up fatigue cracking would not occur. Nishizawa et al. (1997) reported an endurance limit of 200 $\mu\varepsilon$ based on the analysis of in-service pavements in Japan. Similarly, strain levels at the bottom of the asphalt layer of between 96 and 158 $\mu\varepsilon$ were calculated based on backcalculated stiffness data from the falling weight deflectometer for a long-life pavement in Kansas (Wu et al. 2004). Other engineers propose that one should limit the strain anywhere from 60 to 100 $\mu\varepsilon$ based on laboratory testing (Romanoschi et al. 2008). Another experimental pavement project in China allowed perpetual pavement design to reach the less conservative value of 125 $\mu\varepsilon$ (Yang et al. 2005).

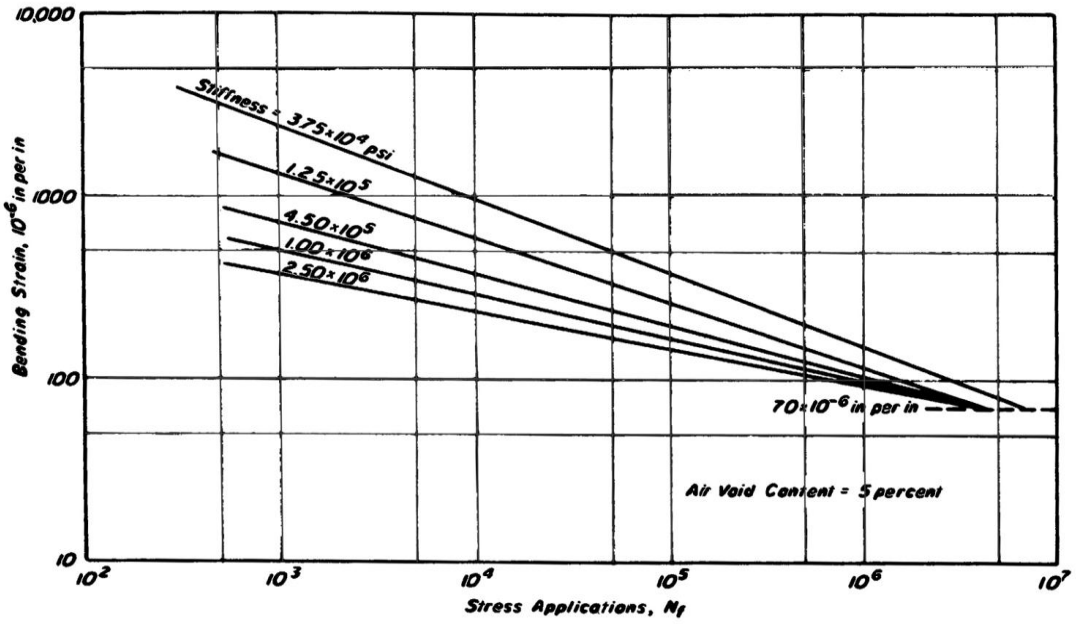

Figure 2-8. Strain vs. Stress Applications to Failure Relationships (after Monismith and McLean 1972).

Most recently, NCAT has led a research effort for NCHRP Project 9-38 to investigate the endurance limit for HMA (Prowell et al. 2010). This study involves conducting fatigue tests for a number of mixtures over a wide range of strain levels. Tests requiring up to 50 million cycles to failure were conducted. The Asphalt Institute has also been involved in the portion of the work to test samples having fatigue lives up to 50 million cycles. The primary objectives of that study were to determine if HMA mixtures do have an endurance limit and to provide guidance on determining this limit for various mixture types. The results indicated that HMA mixtures appeared to have an endurance limit that varies with mix type, so there is not just one limit that can be used for all mixes.

Based on measured strains from the NCAT Test Track from sections that have not experienced fatigue cracking, Willis (2008) proposed a cumulative frequency distribution of allowable strains for perpetual pavements design. Priest (2005) initially proposed a similar concept.

An active NCHRP Project 09-44A "Validating an Endurance Limit for HMA Pavements: Laboratory Experiment and Algorithm Development" is under way with the following objectives:

- Further identify the endurance limit as a potential function of mixture composition, binder rheology, pavement temperature, etc.
- Develop an algorithm to incorporate this endurance limit into the MEPDG and other selected pavement design methods.

The following sections further discuss NCHRP 9-38 investigations and findings, field measured strain distributions from the NCAT Test Track, and considerations for incorporating endurance limits into M-E design procedures. The last section provides the summary and recommendations.

2.8.2 NCHRP 9-38 Project Investigations and Findings

In theory, samples tested at a strain level below the endurance limit should last for an indefinite or infinite number of loading cycles. However, it is impossible to test samples to an infinite number of cycles. Therefore, a practical definition of the endurance limit or a laboratory life representative of the endurance limit is needed.

Practical Definition of Endurance Limit

The literature has defined 40 to 50 years as a reasonable lifetime to be considered as a long-lasting or perpetual pavement. Therefore, it would be safe to assume that the maximum possible number of load repetitions expected in a 40-year period is approximately 500 million. This period of time could be considered a practical target for evaluating parameters (strain or energy), indicating an endurance limit (Prowell et al. 2010). Research conducted during the SHRP recommended a shift factor of 10 between laboratory, strain-based beam fatigue results and field performance equating to 10 percent cracking in the wheel-path (Leahy et al. 1995). Considering this shift factor, laboratory testing to 50 million cycles would equate to approximately 500 million loading cycles in the field or approximately the maximum possible loading in a 40-year period. Based on these analyses, a mix that can last 50 million cycles or more of fatigue life in the laboratory indicates a long-life pavement that is subjected to similar strain levels within the structure.

Laboratory Study

NCHRP 9-38 (Prowell et al. 2010) developed a controlled laboratory experimental plan with the primary objective of testing the hypothesis that there is an endurance limit for HMA mixtures. As a secondary objective, the NCHRP 9-38 researchers investigated some of the HMA material properties that affect the endurance limit.

Four-point beam fatigue testing was conducted according to AASHTO T 321, "Determining the Fatigue Life of Compacted Hot-Mix Asphalt (HMA) Subjected to Repeated Flexural Bending." In this procedure, beam specimens (380-mm length, 63-mm width, 50-mm height) are loaded under strain-controlled conditions using sinusoidal loading at 10 Hz at a temperature of 20°C (see Figure 2-9). The literature indicated that beam fatigue tests were the most commonly used form of fatigue test in the United States. Testing was conducted in a constant strain mode.

Figure 2-9. Beam Fatigue Apparatus and Specimen (after Prowell et al. 2010).

AASHTO T 321 indicates typical strain levels between 250 and 750 $\mu\varepsilon$. The literature suggests that the endurance limit in the laboratory is on the order of 70 $\mu\varepsilon$ and possibly up to 200 $\mu\varepsilon$ in the field. Each of the cells in the experimental plan was to be tested at six strain levels beginning on the high side: 800, 400, 200, 100, 70, and 50 $\mu\varepsilon$ (Prowell et al. 2010). At least two replicates were tested for each cell. Once the fatigue lives of both replicates at a given strain level exceeded 50 million cycles, the next lower strain level was not tested. Testing at 10Hz, approximately one million load repetitions can be applied to a beam fatigue sample in a given day. Thus 50 days of testing were required to test a single sample to 50 million cycles. The air void contents of the optimum asphalt content samples were targeted at 7 ± 0.5 percent.

A working definition of the endurance limit was developed as a framework for testing within the experimental plan. The literature indicated that the primary material properties affecting fatigue life are binder content, binder stiffness, and air void content. The literature indicated that aggregate gradation, type, shape, and angularity have more limited effects (Prowell et al. 2010).

Extrapolation Method

As noted previously, testing was conducted to 50 million cycles. These tests can be very time-consuming, taking as much as two months to conduct one test. Besides, samples tested below the fatigue endurance limit are expected to have an essentially infinite fatigue life. Therefore, the failure point of these samples needed to be extrapolated. The NCHRP 9-38 researchers explored four techniques to extrapolate the stiffness versus loading cycle data, such as AASHTO T321 exponential function, the single- and three-stage Weibull functions, and the ratio of dissipated energy change (RDEC) method (Prowell et al. 2010).

According to the conclusions of NCHRP 9-38, the single-stage Weibull model produced fairly accurate extrapolations that appear to be conservative. Therefore, the single-stage Weibull model was recommended for extrapolating low strain fatigue test results to confirm the existence of the endurance limit.

Findings

The NCHRP 9-38 project had the following findings:

- The test data support the existence of an endurance limit.
- The strain level corresponding to the endurance limit appears to be mix dependent.
- Optimum plus asphalt content/reduced in-place air voids may increase the endurance limit slightly.
- Visually, the endurance limit appears to be more sensitive to binder properties than to asphalt content/air void content.
- An endurance limit of approximately 170 $\mu\varepsilon$ was determined for the PG 67-22 mix at optimum asphalt content. The endurance limit for the PG 76-22 mixture appears to be on the order of 220 $\mu\varepsilon$, and approximately 300 $\mu\varepsilon$ for the PG 76-22 at optimum plus.
- The design thickness for a perpetual pavement is very sensitive to the measured endurance limit. Considering a typical traffic stream, a 50 $\mu\varepsilon$ change in the endurance limit resulted in a 7- to 8- in. change in HMA thickness with the MEPDG. This sensitivity highlights the need for accurate determination of the endurance limit.

2.8.3 Field Measured Strain Distribution from NCAT Test Track

The NCAT Pavement Test Track is comprised of 46 experimental test sections in Opelika, Alabama. In 2000, all 46 sections were built with a minimum thickness of 23 in. of bituminous material to help control the potential for bottom-up fatigue cracking. At the conclusion of the first experiment (10 million equivalent single-axle loads [ESALs]), no fatigue cracking had been observed at any of the 46 sections (Willis 2008).

After the 2000 test cycle, many sections were rebuilt to cater to other investigative needs. When the 2003 NCAT Test Track experiment began, many of the original test sections were left in place to receive another 10 million ESALs of traffic. The additional traffic did not prove detrimental to the pavement structure in terms of fatigue cracking, which was still not observed after 20 million ESALs of traffic.

The third experiment at the NCAT Test Track began to traffic the pavement on November 10, 2006. At this point, only eight of the original 2000 Test Track sections remained in place. Of those sections, as of December 4, 2008, 30 million ESALs had trafficked over these eight test sections and signs of fatigue cracking have yet to be witnessed.

2003 Test Track Field Strain

Compare to the 2000 Test Track, the eight sections from the 2003 Test Track were considerably thinner ranging from 5 to 9 in. of total HMA (see Figure 2-10).

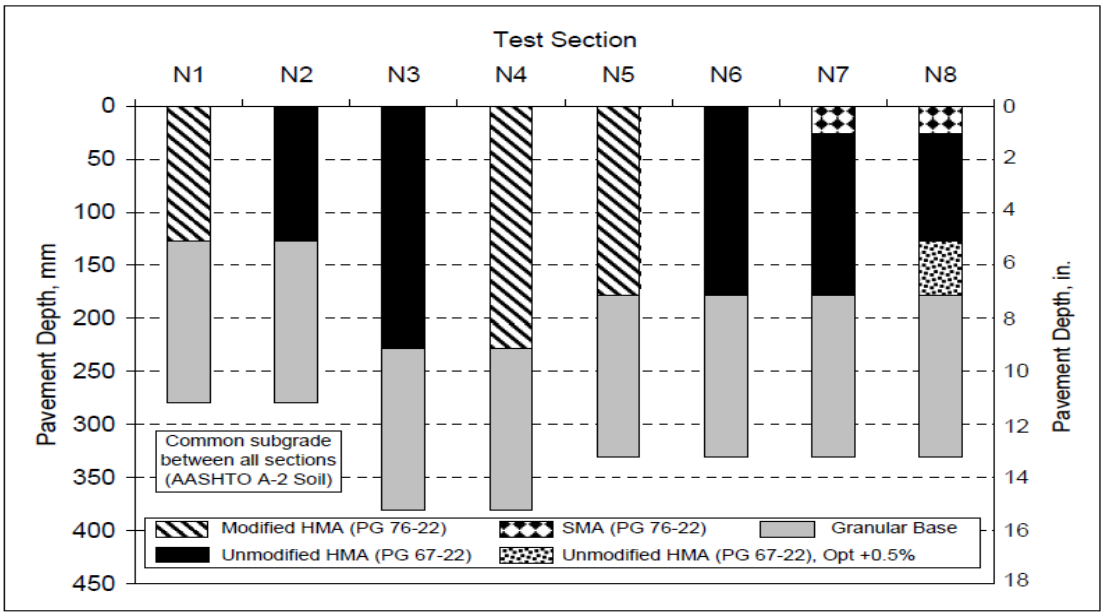

Figure 2-10. Structural Sections at the 2003 NCAT Test Track (after Willis 2008).

Each of these structural test sections was instrumented with strain gauges and temperature probes at depths of 0, 2, 4, and 10 in. Dynamic strain data were collected monthly from the beginning of trafficking until fatigue cracking was first noticed in April 2004.

Among these sections, five of the sections experienced fatigue cracking: N1, N2, N5, N6, and N7. Sections N3 and N4 did not show signs of fatigue cracking. Section N8 failed early due to the bonding problem between layers so that it was not included in the analysis (Willis 2008).

To develop strain distribution plots for each section, hourly strains are necessary; however, measuring and processing continual strain at the Test Track was impractical. Therefore, strain and temperature relationships are needed to calculate an hourly strain value for each vehicle.

After estimating the strains, it was vital to know how many strain repetitions of that specific strain magnitude were experienced in the pavement. This was completed by knowing the strain previously calculated, the truck configuration from the traffic database, and the number of laps

completed each hour. Once the number of strain events having occurred for each truck was determined, the number of strain events was multiplied by the number of laps completed in one hour to calculate the total number of strain repetitions inflicted by each particular truck in an hour.

After the total number of strain repetitions imposed by each truck every hour was calculated, the percentage of total strain repetitions at each microstrain magnitude needed to be determined. This was completed by dividing the number of total strain repetitions each hour by the total number of strain repetitions over the entire performance period of the pavement (Willis 2008).

To create a cumulative distribution for the estimated strain values, the strains were sorted by strain magnitude in ascending order. At this point, a running sum of the percentage column was calculated to determine the percentiles associated with each strain magnitude. Once the cumulative distributions were determined for each structural section, the 1st, 99th, and every 5th percentile were manually picked from the completed spreadsheets to develop cumulative distribution plots as illustrated in Figure 2-11 (Willis 2008).

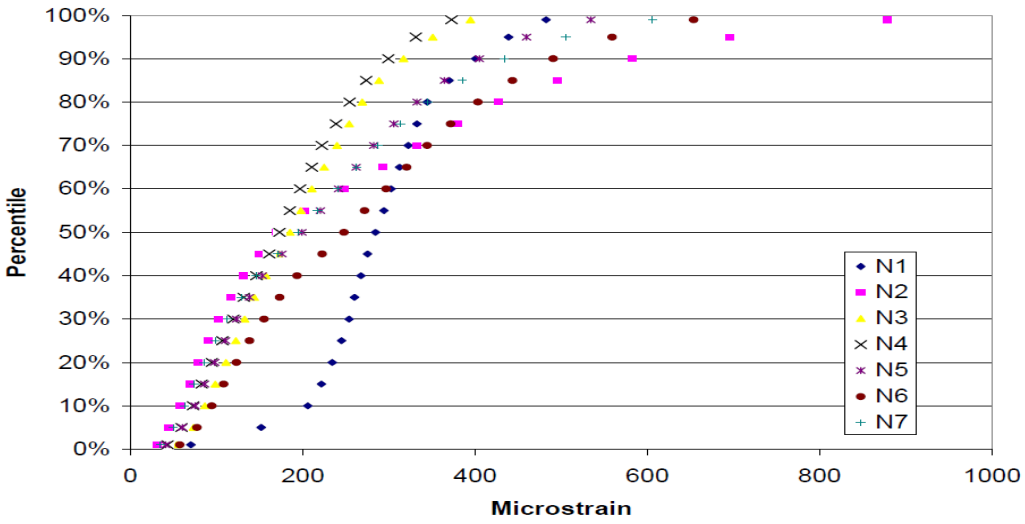

Figure 2-11. Cumulative Distribution Plots for 2003 Test Sections (after Willis 2008).

2003 Test Track Field Strain Analysis

Among these sections, N3 and N4 did not show signs of fatigue cracking during the 2003 trafficking cycle. The strains started out with low strains comparable to those in failed sections; however, from the 25th until the 50th percentile, the strains track very well with sections that failed in fatigue. The 55th percentile seemed to be the breaking point for sections N3 and N4 where failed sections began to escalate into higher strains.

Upon comparing the cumulative distribution functions for sections N3 and N4 with the often-used laboratory fatigue thresholds of 70 or 100 με, one would find that for both sections less than 10 percent of the strain measurements fall below 70 με. In section N3, less than 15 percent of the strain measurements were below 100 με, and this value was under 25 percent for section N4.

Therefore, it can be inferred that measured strains in the field can exceed the laboratory fatigue threshold without fatigue damage occurring.

In conclusion, the difference between the cumulative distributions of the cracked and non-cracked sections is the most useful result of this analysis. The strain profiles between the test sections that performed well and those that did not are distinctly different after the 60th percentile strains.

2006 Test Track Field Strain

Similarly, the field strain cumulative distribution plots for 2006 test track was obtained and presented in Figure 2-12.

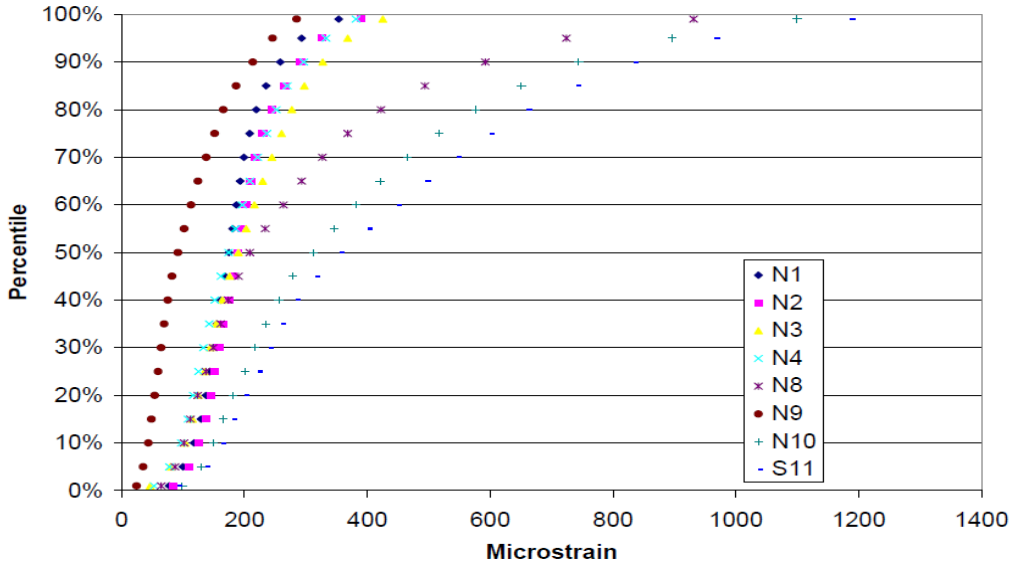

Figure 2-12. Cumulative Distribution of Strains for 2006 Structural Sections (after Willis 2008).

Among the analyzed 2006 sections, three of the eight experienced fatigue cracking (N8, N10, and S11). Sections N1's and N2's experiments were cut off early because of observed cracking; however, forensic investigations have shown that the cracking experienced in these two sections `were top-down cracking and not bottom-up fatigue. The three other sections (N3, N4, and N9) have not experienced bottom-up cracking at this point.

The two sections that failed early in fatigue (N10 and S11) had strain profiles that behaved very similarly. Even at the 5th percentile strain, both sections have strain measurements above 125 $\mu\varepsilon$, and the values continue to escalate from that point.

Section N8 is another section that eventually experienced fatigue cracking. Unlike Sections N10 and S11, N8's early strain profile reflects those of the non-cracked sections very well. Section N8 was specifically designed to perform in a perpetual manner; however, while thick, it was also built on a very poor subgrade material, which may have influenced the structure's ability to disperse strain. At the 50th percentile strain, there is a 20 $\mu\varepsilon$ difference between this section and the maximum strain value of a section that did not experience fatigue cracking. As the percentiles get closer to the 99th, these discrepancies continue to increase.

If one were to compare the cracked profiles versus the non-fatigue cracked profiles, a clear breakpoint occurs around the 45th percentile. At this point, the cracked sections begin to diverge greatly from the non-cracked sections. N3's and N4's strain profiles represent the least conservative strain profiles that were able to withstand trafficking without fatigue cracking. These two sections have also received double the traffic of any other section in the 2006 study. Therefore, these two sections should be considered when determining the uppermost bound for a field-based measured fatigue threshold.

Criteria Based on Strain Distribution

Among the analyzed 2003 and 2006 sections, N3 and N4 were able to withstand 19 million ESALs without fatigue cracking. The strains seen in these two sections were much higher than those seen from the previous Test Track cycle. Therefore, the combination of higher strains and extended trafficking without cracking made them ideal for consideration in the development of strain criteria for perpetual pavements.

Using four strain profiles developed for Sections N3 and N4, the researchers calculated an average strain distribution. Previous research had found gauge precision at the NCAT Test Track to be approximately 30 με between duplicate strain gauges (Willis 2008). From Figure 2-13, when gauge variability (±15 με) was considered, all four profiles fell within the gauge tolerance of the average strain distribution. Therefore, the average strain profile was determined to be an upper bound for strain criteria in flexible perpetual pavement design. Table 2-1 lists the exact values for each percentile.

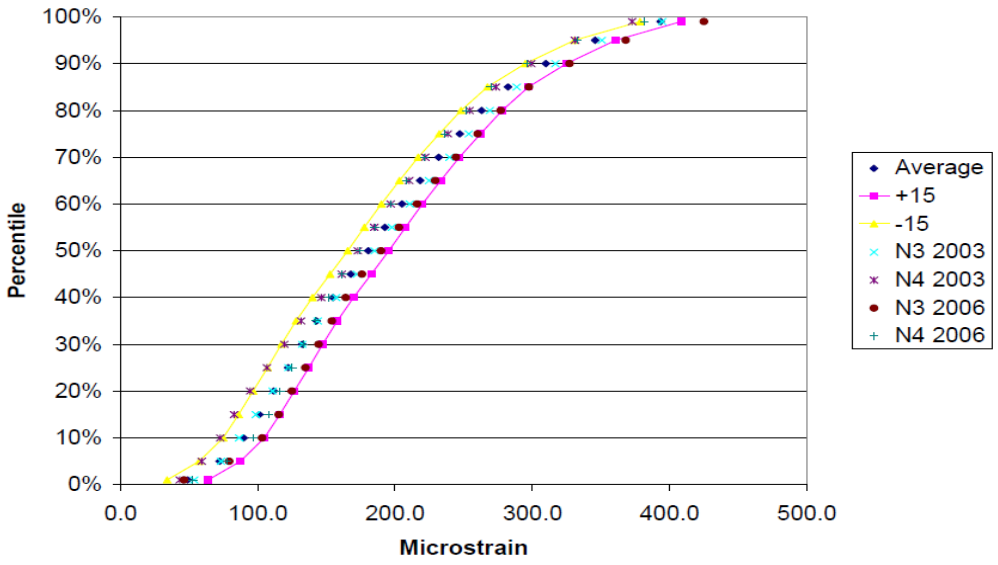

Figure 2-13. Average Strain Distribution with Confidence Bands (after Willis 2008).

Table 2-1. Strain Criteria for Perpetual Pavements (after Willis 2008).

Percentile	Fatigue Limit
99	394
95	346
90	310
85	282
80	263
75	247
70	232
65	218
60	205
55	193
50	181
45	168
40	155
35	143
30	132
25	122
20	112
15	101
10	90
5	72
1	49

2.8.4 Considerations for Incorporating the Endurance Limit into M-E Design Procedures

According to the preceding discussions, several considerations should be given when incorporating endurance limit into M-E Design procedures:

- Firstly the temperature effect should be considered. Tsai et al. (2008) tested mixes at three temperatures (10ºC, 20ºC, and 30ºC) as part of a reflective-cracking study. They tested six samples at each temperature with two strain levels. The result showed that the influence of temperature existed but no stable trend could be concluded.

- The second consideration is the effect of loading frequency and rest period. One hypothesis is that the fatigue endurance limit is driven partly by the ability of asphalt mixtures to heal. Healing occurs more readily during a longer rest period. Therefore, a mixture's fatigue capacity or endurance limit may be higher during longer rest periods. This implies that if two roads have similar distribution of axle loads but different volumes, the lower volume road should have the larger endurance limit. Otherwise, the design thickness would be the same.

- The third consideration should be given to whether a single value best represents the endurance limit. As discussed previously, based on measured strains from the NCAT Test Track from sections that have not experienced fatigue cracking, Willis (2008) proposed designing perpetual pavements based on a cumulative frequency distribution of allowable strains.

- Finally, NCHRP 9-38 pointed out that "For pavements designed using equivalent annual or equivalent seasonal temperatures, the use of a single value for the endurance limit appears to be reasonable. However, field data from the NCAT Test Track which indicate pavements can withstand a cumulative distribution of strains which includes strain levels that exceed the mixtures endurance limit, determined at a single temperature, as described in this study and still exhibit perpetual behavior. Further, there is evidence that the endurance limit, determined from beam fatigue tests, varies as a function of temperature. Thus, future efforts to incorporate the endurance limit into the ME-PDG should consider a distribution of acceptable strains or endurance limits which vary as a function of temperature" (Prowell et al. 2010).

According to these considerations, the research team envisioned two levels of potential methods when incorporating the endurance limit into TxME design system:

- Level 2: When traffic input is ESALs, 18 kip axle load will be applied at the equivalent annual temperature. The tensile strain at the bottom of asphalt layer will be determined and compared to the single endurance limit value (mix and binder type related).

- Level 1: When traffic input is load spectra, then maximum tensile strains at the bottom of the asphalt layer under different load levels and different temperature conditions will be determined and the corresponding strain distribution will be evaluated and then compared with the user defined strain distribution criteria.

The research team will also keep a close eye on the ongoing NCHRP 9-44A "Validating an Endurance Limit for HMA Pavements: Laboratory Experiment and Algorithm Development" to incorporate/validate the latest findings.

2.8.5 Summary of Endurance Limit Model

Thick HMA pavements (perpetual pavements) have been in service for 40 or more years without any evidence of bottom-up fatigue cracking. This field experience suggests that an endurance limit, a level of strain below which fatigue damage does not occur for any number of load repetitions, is a valid concept for HMA mixtures.

NCHRP 9-38 provided a practical definition of the endurance limit. This project also developed several techniques used to extrapolate beam fatigue data, such as exponential extrapolation, single or three-stage Weibull model, and ratio of RDEC. The single-stage Weibull model produced fairly accurate extrapolations that appear to be conservative. The data supported the existence of an endurance limit for each of the mixes tested. This limit has been shown to vary with mix type so there is not just one limit that can be used for all mixes. Besides, there is evidence that the endurance limit varies with test temperature.

Field data from the NCAT Test Track indicate pavements can withstand a cumulative distribution of strains, which includes strain levels that exceed the mixtures endurance limit and still exhibit perpetual behavior. Thus, Willis (2008) proposed designing perpetual pavements based on a cumulative frequency distribution of allowable strains.

Currently, MEPDG does not fully incorporate the endurance limit concept. Active NCHRP 9-44A "Validating an Endurance Limit for HMA Pavements: Laboratory Experiment and Algorithm Development" is in progress with the following objectives:

- To further identify the endurance limit as a potential function of mixture composition, binder rheology, pavement temperature, etc.
- To develop an algorithm to incorporate this endurance limit into the MEPDG and other selected pavement design methods.

For this study, the research team envisioned two levels of methods to incorporate the endurance limit into TxME design system and will keep a close eye on the ongoing NCHRP 9-44A to potentially incorporate/validate the newest findings.

2.9 TOP-DOWN CRACKING

Top-down cracking has not been widely reported in Texas, but it is a potential distress for thick perpetual pavements and is discussed in the following text.

2.9.1 Background

In the past, most research and even pavement design procedures focused on fatigue cracking, which normally originates at the bottom of asphalt layers and propagates upwards toward the pavement surface. However, observations from cracked roads in different countries including South Africa (Hugo 1985), France (Dauzats et al. 1987), the Netherlands (Gerritsen et al. 1987), Japan (Matsuno and Nishizawa 1992), the UK (Nunn 1997), Canada, and the United States have shown that cracking can originate in the surface of pavements; this type of cracking is sometimes called surface cracking and other people call it top-down cracking. The basic consensus on top-down cracking is that

- It is longitudinal.
- It occurs in thicker asphalt pavements.
- It happens at an early stage of pavement life.

To further differentiate top-down cracking from surface cracking, which can occur either in the transverse or longitudinal direction, this report defines top-down cracking as cracking that initiates at the surface and propagates downward in the longitudinal direction.

In the late 1990s, Myers et al. (1998) reported that the top-down longitudinal cracking represented 90 percent of the observed cracking in pavements scheduled for rehabilitation in Florida. They also noted that this type of cracking is generally observed on pavements within five to ten years following construction. The cracks were most often longitudinal with surface crack widths of about 3 to 4 mm (0.12 to 0.16 in.) decreasing with depth. The total crack depth ranged from about 25 mm (1 in.) to the full depth of the HMA layer. Uhlmeyer et al. (2000) reported that top-down cracking is common in thicker Washington State DOT HMA-surfaced pavements (top-down cracking was typically observed when the average HMA thickness was about 160 mm [6.3 in.] or greater). Such cracks were generally contained in the wearing course and averaged 46 mm (1.8 in.) in depth. The top-down cracks generally initiated within three to eight years of paving. Later, Colorado and other states also observed this type of cracking. Although the top-down longitudinal cracking is not a dominant distress in Texas right now, it still is necessary to review this type of cracking and identify any available lab test methods and models. This is because Texas has built several full-depth perpetual pavements, and there are many other Texas highways where the total HMA thickness exceeds 6 in.

Top-down longitudinal cracking has become a hot topic in recent years, and it has been the focus of two NCHRP projects (NCHRP 1-42 and 1-42A). However, the top-down longitudinal cracking issue has not been fully understood or well modeled yet. This report documents current

knowledge on top-down longitudinal cracking in terms of mechanisms, existing laboratory testing, and modeling. A discussion and summary is presented at the end of this section. Appendix A presents the latest top-down longitudinal cracking model developed under NCHRP 1-42A.

2.9.2 Top-Down Longitudinal Cracking Mechanisms

Because top-down longitudinal cracking usually occurs in or near the wheel paths in a pavement, traffic must play an important role in the process. There are at least four mechanisms of top-down longitudinal cracking proposed in the literature:

- Construction related mechanism (segregation and hairline cracks induced by compaction roller).
- Away-from-tire bending mechanism.
- Near-tire non-uniform shearing stress mechanism.
- Thermal effect mechanism.

Other factors such as aging are also important to top-down cracking. Detailed mechanisms are discussed below.

Construction Related Top-Down Cracking

The construction-related top-down cracking has been extensively observed and reported on I-25 in Colorado (Anderson et al. 2001, Harmelink et al. 2003, Harmelink et al. 2008). Initial forensic analysis concluded that a number of contributing factors caused the surface-initiated cracking. One of the factors was attributed to pockets of segregation at the bottom of the lift (see Figure 2-14). Apparently, there is a vertical segregation: some finer aggregates near surface and the coarse aggregates below the finer aggregates. However, this vertical segregation is invisible from the surface during construction. After this so-called top-down cracking was discovered on this first project, other pavements started manifesting similar traits. Harmelink et al. (2003) then conducted a statewide evaluation, which found that 18 out of 28 sites examined contained top-down cracking. Additionally, there was a connection between type of paving equipment used on each project and the presence of longitudinal cracking (see Figure 2-15). To address this top-down cracking issue, the Colorado Department of Transportation took three actions:

- Changed the mix design to allow for increased asphalt content.
- Established a task force to develop a specification for (subsurface) segregation.
- Worked with paving equipment manufactures to develop an anti-segregation retrofit for laydown machines.

As a result of these efforts, top-down cracking in Colorado has been generally eliminated or at least greatly reduced (Harmelink et al. 2008).

Figure 2-14. Top-Down Cracking on I-25, Colorado (after Harmelink et al. 2008).

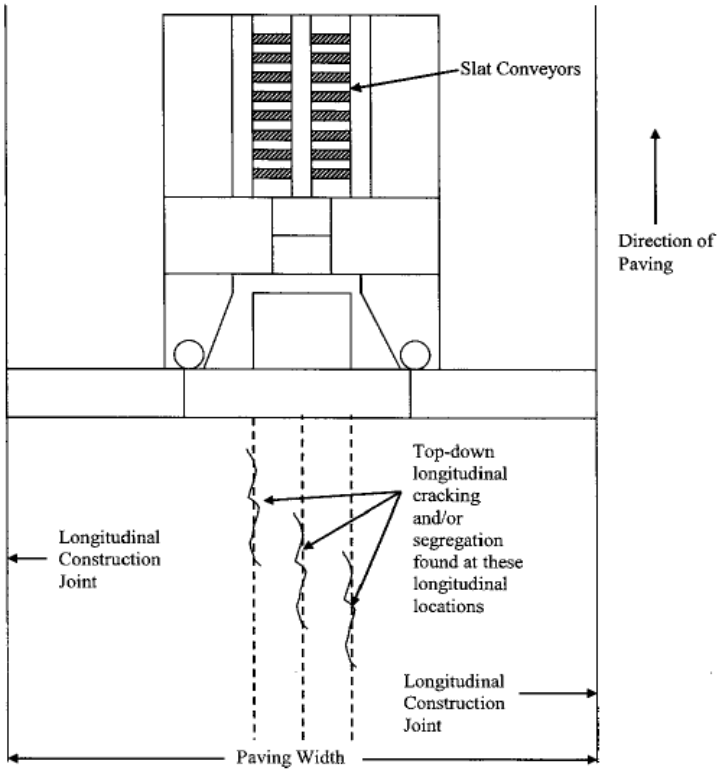

Figure 2-15. Paver Top View and Associated Cracks (after Harmelink et al. 2008).

Another construction-related top-down cracking cause was reported in Canada. El Halim et al. (2004) showed that asphalt rollers induce hairline construction cracks at the surface of the compacted layer that can subsequently propagate under traffic and thermal loading.

Generally speaking, the construction-related top-down cracking has not been the major focus of current research in terms of lab testing and modeling. Instead, the other two mechanisms—the away-from-tire bending mechanism and the near-tire shearing mechanism—have been well-investigated (although modeling of these behaviors is still not robust) and will be discussed below.

Away–from-Tire Bending-Related Top-Down Cracking

One of the top-down mechanisms is related to the bending-induced surface tension away from the tire (i.e., bending mechanism, see Figure 2-16). Soon et al. (2004) reported that horizontal tensile stresses and strains are found at the surface away from the load due to the negative curvature of the surface. Although these stresses and strains are typically lower in magnitude than those at the base of the layer, aging of the asphalt surface mix may weaken its resistance to cracking. Under the bending mechanism, it is often assumed that the excessive tensile strain at or near the pavement surface governs crack initiation and propagation, and aging of the asphalt surface mix accelerates the crack initiation-propagation process. This type of top-down cracking often occurs in pavements with thin to medium thick asphalt layers (Zou 2009).

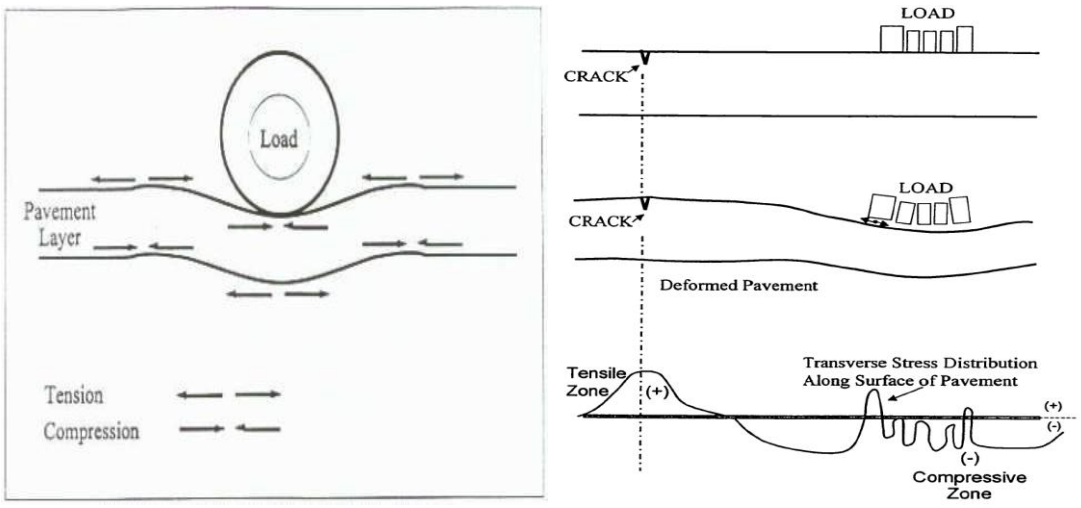

Figure 2-16. Top-Down Longitudinal Cracking: Bending Mechanism.

This bending mechanism of top-down longitudinal cracking has been proposed and incorporated into the MEPDG program. Actually the latest top-down longitudinal cracking model under NCHRP 1-42A was also developed based on such a mechanism, although the NCHRP 1-42A model is much better than that currently installed in the MEPDG (see later sections). The good

part of the bending mechanism theory is that it is not necessary to consider the non-uniform distribution of tire-pavement contact stress so that a multi-layer elastic system with uniform stress distribution can be used to analyze and predict top-down longitudinal cracking. The bad part is the notion that this is a uniform stress distribution because the actual tire-pavement contact stress is non-uniform, which many believe is the major contributor to top-down longitudinal cracking.

Near-Tire Non-Uniform Stress (Shearing)-Related Top-Down Cracking

Many pavement engineers and researchers believe that non-uniform stress distribution caused the top-down longitudinal cracking. For simplicity, most pavement analyses assume the tire-pavement contact stress as a circular loading with uniform stress. However, the reality is that the tire-pavement contact stress is far from uniform. A number of researchers investigated the detailed contact pressure distributions beneath rolling tires (De Beer et al. 1997, Myers et al. 1999, Weissman 1999, Fernando et al. 2006). De Beer et al. (1997) developed a Vehicle-Road Pressure Transducer Array (VRSPTA) and measured the three-dimensional contact stress beneath slow-moving pneumatic truck tires. Several different truck tires were investigated, ranging from bias/cross ply to radials. The De Beer et al. study yielded the following significant findings:

- The contact pressure distribution is three dimensional and highly non-uniform.
- Maximum vertical contact pressure could be up to twice the tire inflation pressure.
- The transverse (lateral) contact stress (at right angles to the direction of travel) under a smooth tire indicates inward shear (toward the center of the tire) with zero stresses at the tire center (zero resultant force).
- The longitudinal contact stresses (in the direction of travel) for free rolling tires indicate that these stresses are lowest in magnitude with the peak stress typically occurring near to the front and rear positions of the tire.
- The contact stresses under grooved tires are more variable compared to a smooth tire, but the patterns are overall similar to those measured from the smooth tire.

Later, Fernando et al. (2006) used the VRSPTA device and measured the non-uniform tire pressure distribution of select tires used on Texas trucks. A typical set of measured stresses is shown in Figure 2-17.

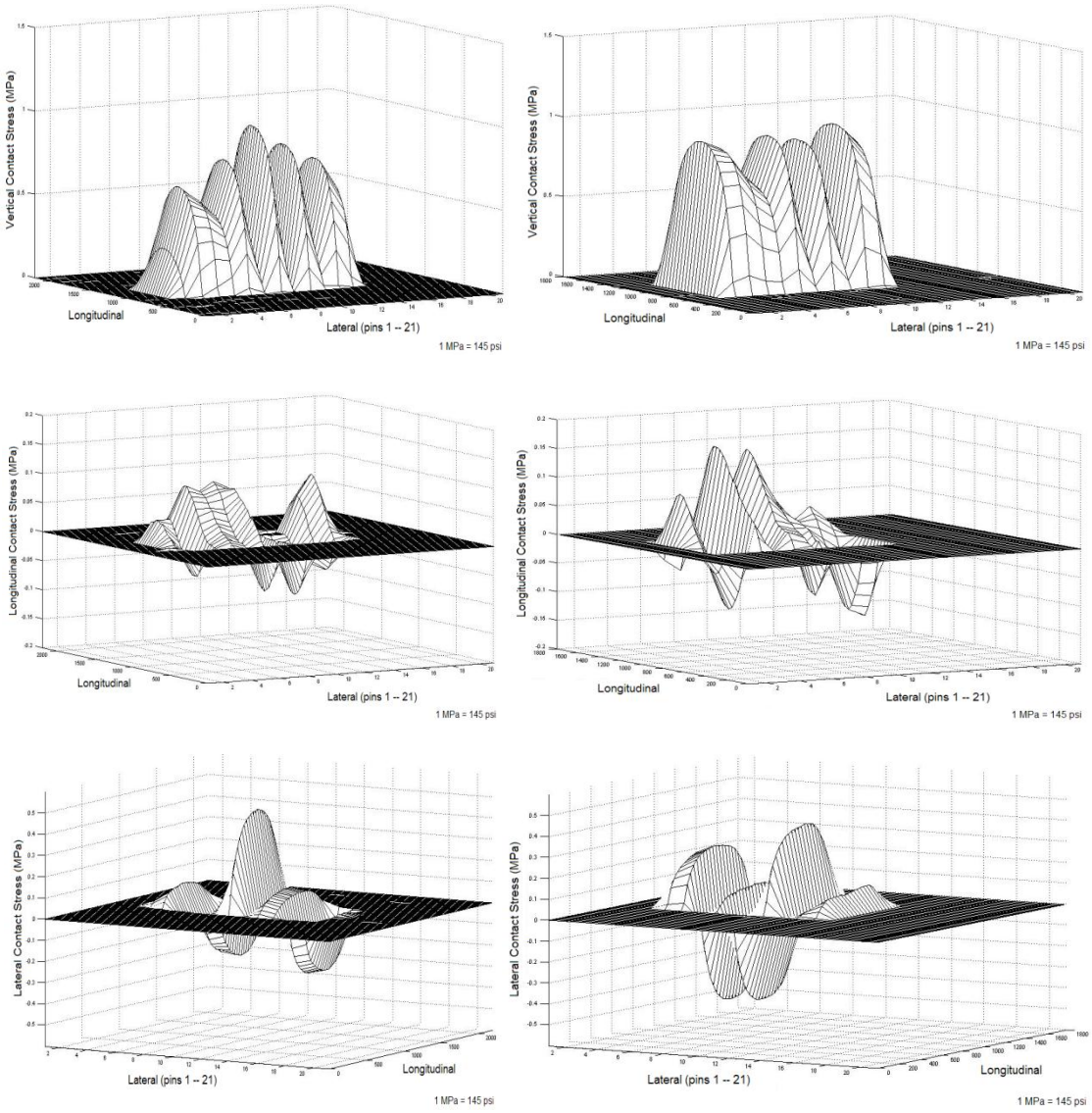

Figure 2-17. Typical Set of Measured Tire/Pavement Contact Stresses (after Fernando et al. 2006).

Different types of truck tires have different tire-pavement contact stress. Figure 2-18 shows the difference between a radial tire and a bias ply tire. Both Groenendijk (1998) and Myers et al. (1999) found that the contact stress of a radial tire is different from that of bias ply tires.

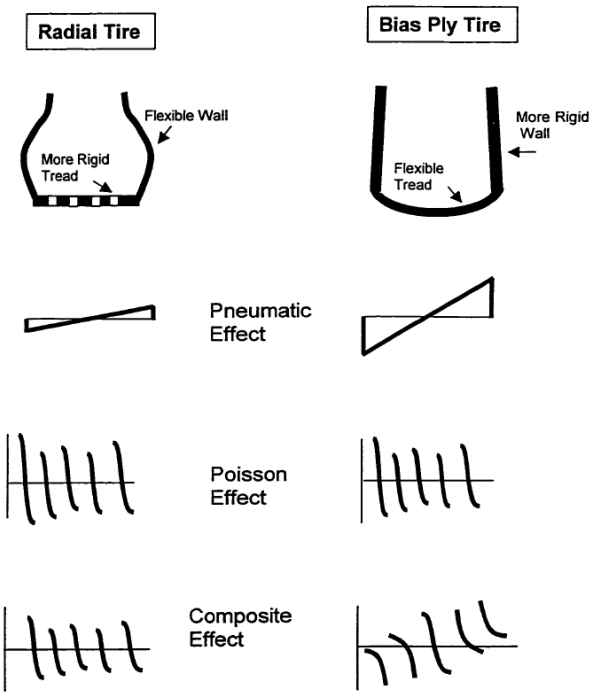

Figure 2-18. Transverse Contact Stress Induced by Radial and Bias Ply Truck Tires (after Myers 2000).

Based on computer modeling, Myers et al. (1998) concluded that tensile stresses under the treads of the tire—not the tire edges—were the primary cause of the cracks; wide-based tires caused the highest tensile stresses. They noted that the tensile stresses dissipate quickly with depth, suggesting that this might be the reason the cracks essentially stop growing.

Different from the findings that Myers et al. (1998) reported, Christensen et al. (2004) found that the octahedral shear stress may cause the top-down cracking initiation and propagation. Figure 2-19 shows the octahedral shear stress distribution at different pavement depths. The octahedral shear stress directly under the edge of the tire increases rapidly to a value of about 280 kPa and remains nearly constant down to the maximum depth of 37.5 mm. Furthermore, the magnitude of this stress is substantial; Anderson et al. reported an average IDT strength of 1100 kPa (160 psi) for mixtures made with 12 widely differing binders at temperatures of 4.4° and 15.5°C. This corresponds to an allowable octahedral shear stress of 520 kPa (75 psi), so the maximum octahedral shear stress, which extends undiminished through much of the pavement, is over 50 percent of the allowable stress. Shear failure under the edge of the tire is entirely consistent with the observation that top-down cracking tends to occur near the edges of wheel paths. The importance of shear stresses in the formation and growth of top-down cracks should not be neglected.

Although there is no consensus on top-down cracking initiation and propagation mechanisms, it is very possible that the top-down cracking is initiated through the combined action of tire-

pavement tensile stresses and shear stresses. Then the top-down cracking is propagated deeper into the pavement largely by the action of high shear stresses under the edge of a tire.

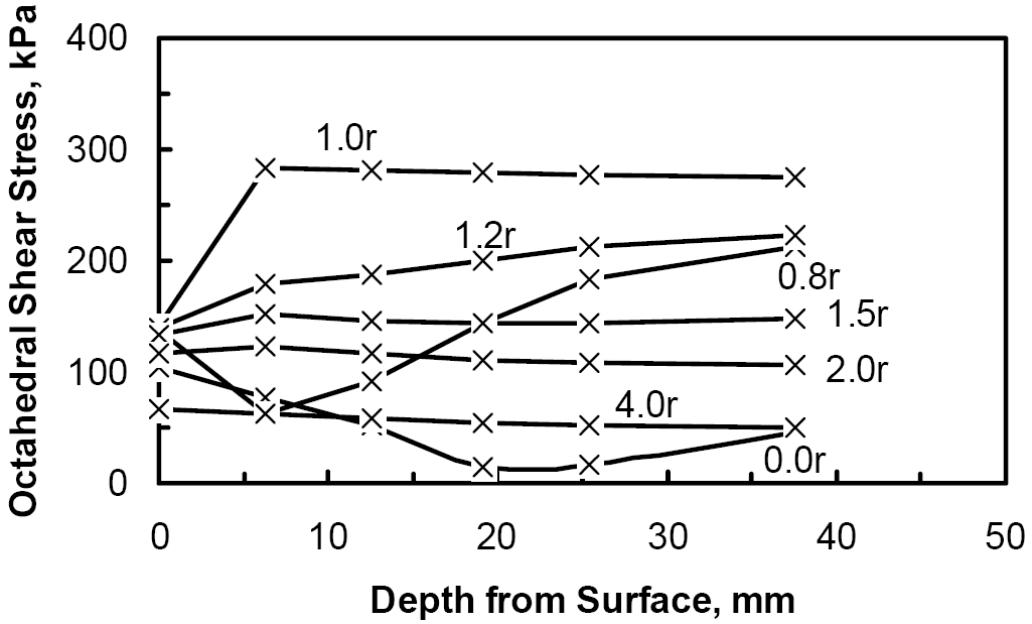

Figure 2-19. Octahedral Shear Stress in an Asphalt Concrete Pavement as a Function of Depth, at Different Radial Distances from the Applied Load (thickness = 200 mm, E_1 = 5500 MPa, E_2 = 140 MPa, P = 24 kN, p = 690 kPa).

Thermal Effect

Daily temperature variation also has impact on top-down cracking. For example, rapid cooling from higher temperatures (i.e., after rainfall) can cause negative temperature gradients, which can lead to tensile stresses in the upper part of asphalt layer. Indeed, this mechanism was proposed as the explanation for longitudinal top-down cracking observed in Japan (Matsuno and Nishizawa 1992).

Myers (2000) also found that temperature and modulus gradients appear to be critical to the initiation and propagation of surface cracks. Furthermore, the driving force in surface cracks will vary, depending on the position of the applied load relative to the crack and the crack length (see Figure 2-20). Those factors should be considered in pavement design and management. For example, a surface crack might initiate and grow relatively quickly to a certain depth, and then stabilize for a time.

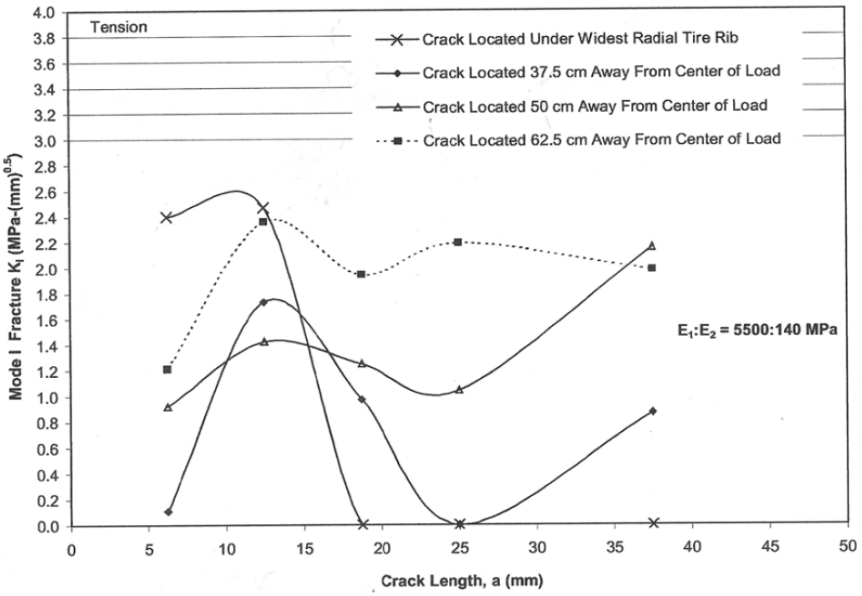

Figure 2-20. Stress Intensity Factors as a Function of Crack Length at Various Distances from Applied Load (after Myers 2000).

However, the traditional thermal stress causes top-down transverse cracking rather than top-down longitudinal cracking so that it is unreasonable to directly use the traditional thermal stress to explain the top-down longitudinal cracking. Apparently, detailed 3-D thermal stress analysis is necessary to fully understand the contribution of thermal stress to top-down longitudinal cracking.

Aging Effect

As Hugo et al. (1985) noted, aging and/or moisture damage near the surface of the pavement can significantly affect the stiffness, tensile strength, and tensile stress/strain of the top surface mix near the pavement surface. Leech and Nunn (1997) conducted rheological tests on a number of UK Hot Rolled Asphalt (HRA)-wearing course binders (recovered from materials up to 25 years old) to investigate the variation in aging with depth. They found that the most severe aging occurs in the top few millimeters of the wearing course increasing the stiffness of the binder. Aging can cause the surface mix near the pavement surface to become brittle and consequently reduces crack resistance of the mix, making it easier for top-down cracking to propagate downwardly.

In summary, the mechanisms of top-down longitudinal cracking have not been fully understood. However, here are some consensuses on top-down longitudinal cracking found from the literature reviewed:

- Accumulated damage associated with repeated traffic loading is the primary mechanism of top-down cracking in asphalt concrete pavements.

- Both tire-contact surface tension stresses and shear stresses contribute to top-down cracking. Contact stresses are probably more important in the initiation of top-down cracks, while shear stresses primarily cause propagation of these cracks to significant depths in the pavement.
- Aging and thermal stresses or temperature gradients can contribute significantly to the occurrence of top-down cracking.
- Segregation during construction, particularly slat-conveyor segregation near the wheel paths, can cause or exacerbate top-down cracking in asphalt concrete pavements.
- Pavement thickness probably affects the occurrence of top-down cracking, but there is no clear agreement among researchers concerning how pavement thickness affects this form of distress. Stiffness gradients in pavements arising from binder grade selection, mix design, age hardening, and/or temperature gradients also probably contribute to top-down cracking, but the nature and magnitude of this contribution is not yet clear.
- Computational fracture mechanics is a useful research tool for predicting top-down cracking propagation.

2.9.3 Top-Down Longitudinal Cracking Model

Top-down cracking in asphalt concrete pavements is a complex phenomenon involving two primary damage mechanisms and numerous contributing factors. It is therefore difficult to model, though proper application of available technology should provide a good basis for evaluating this mode of distress. As discussed previously, traffic-associated fatigue and thermal stresses primarily cause the damage leading to top-down cracking. Poor construction (including segregation), age hardening, and moisture damage all exacerbate the damage that these mechanisms have caused. The fatigue damage at the pavement surface is more complicated than that occurring at the bottom of the bound material in a flexible pavement because the state of stress is more complicated—both shear stresses and tensile stresses are present with both contributing to damage in the pavement. Thermal stresses can contribute to top-down cracking in two ways: through thermal fatigue, where relatively low thermal stresses slowly damage the pavement; and through acute thermal cracking, where very low temperatures cause sudden fracture of the pavement surface.

Top-down cracking is a very complicated distress. So far, a widely accepted top-down cracking model does not exist. That is why NCHRP is going to initiate the third project on top-down cracking beginning in FY2012. The following section summarizes the work that Roque and his associates have done in Florida and under the NCHRP 1-42A. Note that the models that Roque and his associates have developed deal only with the bending mechanism.

Energy Ratio Based Top-Down Cracking Model

Based on the work at the University of Florida (UF), Zhang et al. (2001) identified that dissipated creep strain energy (DCSE) is a good indicator to rank the cracking resistance of asphalt mixes. In addition, Zhang et al. (2001) verified that the DCSE limit is a fundamental property that can be obtained from relatively simple tests (i.e., resilient modulus and strength tests) using the Superpave Indirect Tension Test (IDT) equipment. Figure 2-21 shows a typical stress-strain response of mixture from the IDT tensile strength test. The fracture energy (FE) is determined as the area under the stress-strain curve (area OAB). The elastic energy (EE) at fracture is calculated as the triangular area (CAB), in which the resilient modulus of the mixture (M_R) is determined using the IDT resilient modulus test. The DCSE is then obtained by subtracting the EE from FE.

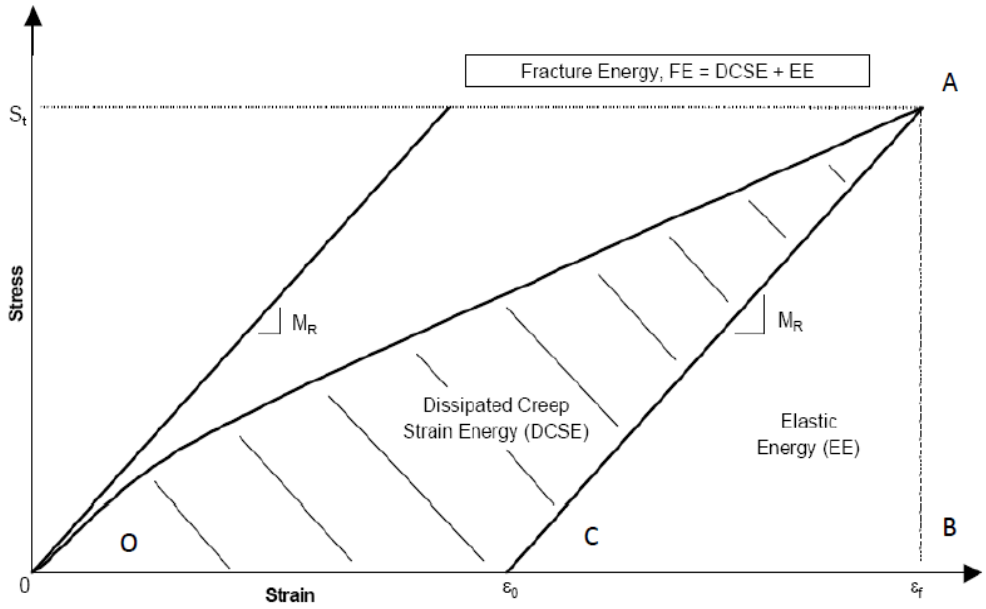

Figure 2-21. Dissipated Creep Strain Energy (after Zhang et al. 2001).

With this energy concept, the researchers at UF (Zhang et al. 2001, Roque et al. 2002) proposed a new HMA fracture mechanics (HMA-FM) model that predicts crack initiation and propagation through basic principles of viscoelastic fracture mechanics. This model is based on a critical condition concept that specifies crack initiation and growth develop only under specific loading, environmental, and healing conditions that are critical enough to exceed the mix's energy threshold/limit.

However, as shown in the work of Myers and Roque (2002), fairly complex mechanisms appear to be involved in the development of tensile stress conditions that can induce and propagate top-down longitudinal cracks at the surface of the asphalt pavements. Computer models required to predict these stresses, let alone the resulting crack initiation and propagation resulting from

these stresses, are clearly at a high level of sophistication. So Roque et al. (2004) derived a parameter termed the energy ratio (*ER*) based on a detailed analysis and evaluation of 22 field test sections in Florida. The ER was defined as:

$$ER = DCSE_f / DCSE_{\min} \tag{2-40}$$

where $DCSE_f$ is the dissipated creep strain energy limit of the mix, and $DCSE_{min}$ is the minimum dissipated creep strain energy required for the number of cycles to failure to exceed 6000 (Roque et al. 2004), which can be determined in Equation 2-41:

$$DCSE_{\min} = m^{2.98} \cdot D_1 / A \tag{2-41}$$

where, *m* and *D1* are the creep compliance power law parameters (determined using SuperPave IDT creep compliance test at 0°C, 10°C, and 20°C and construct master curve at the reference temperature of 20°C). See Figure 2-22. Parameter *A* is a function of tensile strength S_t (in MPa) and tensile stress σ in the asphalt concrete pavement, which is expressed as:

$$A = 0.0299 \cdot \sigma^{-3.10} \cdot (6.36 - S_t) + 2.46 \times 10^{-8} \tag{2-42}$$

Note that both the SuperPave IDT tensile strength *St* (in MPa) and resilient modulus tests at 10°C are required to determine S_t and resilient modulus M_R. The tensile stress σ (in psi) is predicted using the measured M_R and other layer moduli as determined from Falling Weight Deflectometer (FWD) tests for a typical pavement structure.

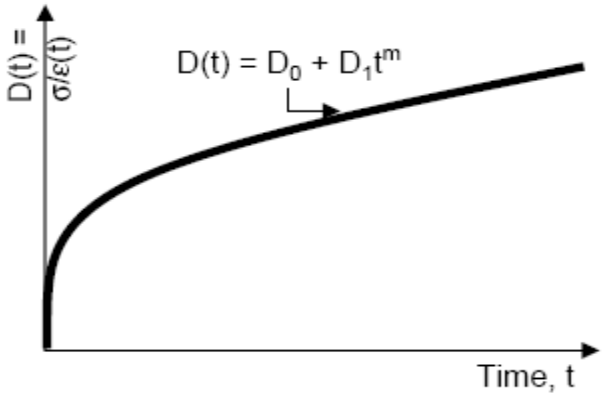

Figure 2-22. Creep Compliance Power Law Parameters.

The 6000 cycles should not necessarily be taken to have a real meaning as far as, for example, the number of ESALs required to cause a certain amount of cracking in the field. This number of cycles is simply a design condition that was identified to relate well to the top-down cracking performance of mixes in the field (Roque et al. 2004). It should also be emphasized here that this tensile stress σ is at the bottom (not surface) of the pavement. Roque et al. (2004) explained

that "…the magnitude of the load induced portion of these surface tensile stresses is related to the bending characteristics of the pavement structure. In other words, pavement structures that result in higher load-induced tensile stresses at the bottom of the pavement also result in higher load-induced tensile stresses at the surface of the pavement when appropriate conditions are present for these stresses to develop. Therefore, the load-induced tensile stress at the bottom of the pavement was used as a surrogate to represent the relative difference in surface tensile stresses between different pavement structures. This should not be taken to mean that the magnitude of the surface tensile stresses is expected to be the same as at the bottom of the pavement, but simply that both stresses will increase when bending increases."

As can be seen from these definitions, the ER accounts for effects of both damage and fracture properties of asphalt mix on top-down cracking performance. A higher ER implies better cracking performance. Besides, when considering the development of mix specification criteria based on the ER, it quickly became evident that traffic level would need to be considered. Figure 2-23 presents the relationship between minimum required ER and traffic level.

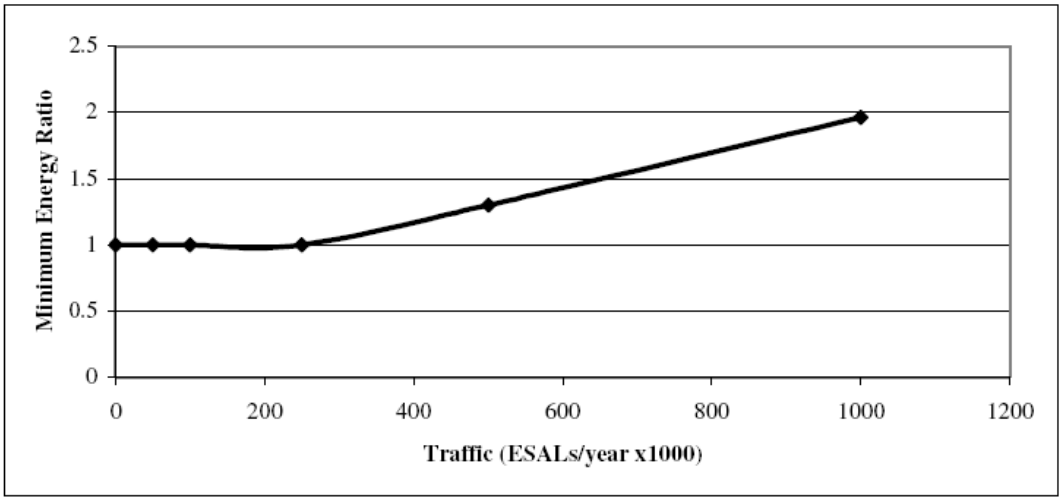

Figure 2-23. Minimum Energy Ratio Adjusted for Traffic Level (after Roque et al. 2004).

Because ER was developed based on the evaluation of load-induced cracking performance, it may not provide a reliable basis to assess pavements located in areas where the thermal effect cannot be neglected. In order to combine the effects of load and thermal, Kim et al. (2008) developed a method to calculate thermally induced damage and the failure time (FT) to 100 mm crack length for a thin plate subject to specified thermal loading conditions. This method was then used in conjunction with the HMA-FM model to perform a detailed analysis and evaluation of 11 field test sections in Florida, which resulted in a new parameter termed the modified energy ratio (MER) defined as follows:

$$MER = IFT / MTR \quad (2\text{-}43)$$

where MTR is the minimum time requirement used to discriminate the performance of cracked and uncracked pavement sections. IFT is the integrated failure time expressed as follows:

$$IFT = FT \times AMT / MTV \times ER \quad (2\text{-}44)$$

where AMT is the annual mean air temperature and MTV is the mean temperature variation (*AMT* and *MTV* are correction factors to account for temperature inputs other than the single harmonic function used to calculate FT); and ER is the energy ratio. Clearly, the MER approach essentially introduced a correction factor into the ER equation so that both loading and thermal effects can be accounted for during evaluation of top-down cracking performance.

The ER concept was later incorporated into a top-down cracking design tool for Florida (Wang et al. 2007). So far, the Florida Department of Transportation (FDOT) has not yet implemented the use of this tool.

In summary, the ER or MER approach is an indirect approach which can be thought of as a simplified version of HMA-FM model. However, the effect of aging and healing on the top-down cracking performance during the entire service life of asphalt concrete pavements was not considered. In addition, the thermally-induced damage needs to be directly involved in the computation of damage accumulation so that damage recovery due to healing can be applied in a more consistent way.

NCHRP 1-42A Top-Down Cracking Models

Building on the DCSE concept, Roque and his associate proposed an enhanced top-down cracking model under NCHRP 1-42A. Figure 2-24 shows the framework of the top-down cracking model in NCHRP 1-42A. The enhanced system has five main parts:

- The inputs module.
- The material property model.
- Indirect tensile test.
- Pavement response model.
- Pavement fracture model.

Appendix A has details about these models. The following section briefly summarizes the models.

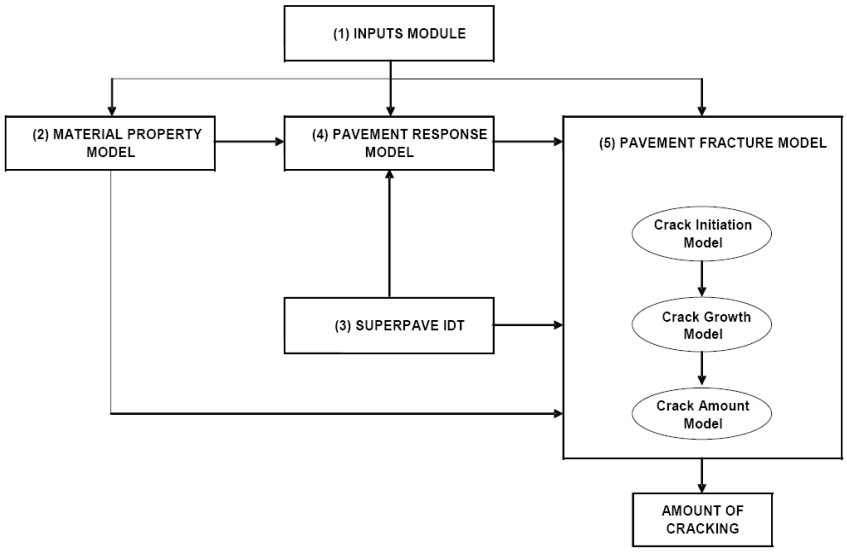

Figure 2-24. Framework of the Top-Down Cracking Performance Model (after Roque et al. 2010).

The inputs module provides pavement material and structural properties, temperatures within HMA layer (as predicted using an enhanced integrated climatic model), and traffic volume (in ESALs). Because the use of load spectra to represent the traffic would have significantly increased the complexity of model development and its use on model accuracy was unknown, the research team decided to express the traffic in terms of ESALs (assuming an even spacing of ESALs over time). Table 2-2 summarizes the sub-models of the HMA-FM-based system along with the input requirements. The Superpave IDT was used to determine damage and fracture properties on field cores as part of the calibration efforts. Three types of tests were performed with the Superpave IDT:

- Resilient modulus.
- Creep compliance (for damage rate).
- Tensile strength (for fracture energy limit).

See Appendix A for more detailed information about these models.

Table 2-2. Input Required for the NCHRP 1-42A Model (Roque et al. 2010).

Sub-model	Sub-model component	Input requirement
Material property model	AC stiffness aging model	Basic mixture characteristics (gradation, binder type, mix volumetrics)
		Temperature, loading time, and aging time
	AC tensile strength aging model	Stiffness (from AC stiffness aging model)
		Material coefficients
	Fracture energy limit aging model	Stiffness (from AC stiffness aging model)
		Initial fracture energy
		Aging parameter k1 (to be determined in calibration)
	Healing model	Stiffness (from AC stiffness aging model)
		Initial fracture energy
		Critical stiffness
Pavement response model	Load response model	Structural properties of each layer (thickness, modulus, and Poisson's ratio)
		Stiffness (from AC stiffness aging model)
		Equivalent single axle load
	Thermal response model	Structural property of AC layer (thickness)
		Relaxation modulus master curve parameters: E_i, λ_i, η_v
		Temperature and thermal contraction coefficient
Pavement fracture model	Crack initiation model	Load and thermal-induced stresses (from response models)
		Creep compliance master curve parameters: m, D1, ηv
		Mixture fracture and healing properties (from material property model)
		Traffic (in ESALs)
	Crack growth model	Time and location of initial crack (from crack initiation model)
		Structural properties of each layer (thickness, modulus, and Poisson's ratio)
		Stiffness (from AC stiffness aging model)
		Thermal-induced stresses (from thermal response model)
		Stress intensity factor for an edge crack
		Creep compliance master curve parameters: m, D1, η_v
		Mixture fracture and healing properties (from material property model)
		Traffic (in ESALs)
	Crack amount model	Change of crack depth over time (from crack growth model)

At the end of the NCHRP 1-42A report, Roque et al. (2010) emphasized that "the simplified integrated system is not ready nor intended for immediate implementation, because (1) it is necessary to evaluate damage zone effects on performance predictions; (2) it is necessary to further verify the material property sub-models developed in this study (i.e., models for aging, healing, damage, and fracture criteria); and (3) validation and calibration of the integrated performance model needs to be performed on a broader range of pavements and environmental conditions. The intent of the simplified integrated system was to demonstrate the potential of a fully integrated system. …" Apparently significant work is still needed to have an implementable top-down cracking model.

2.9.4 Summary and Discussion

Generally speaking, the top-down longitudinal cracking is very complex, and it is not fully understood. So far, there is no implementable top-down longitudinal cracking model. In terms of laboratory characterization and mechanistic modeling of the top-down longitudinal cracking, more research is still needed. Roque et al. (2010) identified the following areas to be further investigated:

- Aging and healing models: There is a need to further investigate the material property aging and healing models including submodels for viscoelastic properties and damage and fracture properties.
- The near-tire mechanism: The effects of tire type and cross slope on shear-induced tension near the tire edge should be considered for incorporation into the unified near-tire mechanism.
- Model calibration and validation using field data: A calibration and validation effort with a broader range of field sections is needed to ensure the accuracy of the integrated top-down cracking performance model.
- Traffic: Constant ESAL loading distribution was used. It would be more realistic to use an equivalent daily loading history that has a more representative load spectra and distribution (i.e., more trucks during certain times of the day). Also, load wander likely plays a role in performance associated with the near-tire mechanism. Therefore, it should be considered in future model development.

Right now the research team does not recommend any top-down longitudinal cracking model for inclusion into the TxME design system. Instead, the team recommends a specific study on the top-down cracking, especially the potential for top-down cracking in perpetual pavements in Texas.

CHAPTER 3.
RECOMMENDED RELIABILITY APPROACH

3.1 INTRODUCTION

It is well known that the pavement design and construction involve a lot of uncertainties and variation from the specified design parameters. To address the uncertainties and variability, a reliability concept is often incorporated into the pavement design and analysis process. In general, reliability is often defined as "the ability of a system or component to perform its required functions under stated conditions for a specified period of time" (Bagowsky 1961). Specifically for pavement design and analysis, the reliability is referred to as the probability that a pavement section designed using the process will perform satisfactorily in terms of pavement distresses over the traffic and environmental conditions for the design period. Even though mechanistic concepts provide a more accurate and realistic methodology for pavement design, a practical method to consider the uncertainties and variations in design and construction is still needed so that pavements can be designed for a desired level of reliability (i.e., pavements will perform as designed).

This chapter focuses on components of pavement design/performance variability and reliability approaches used in existing pavement design and analysis systems. The following section presents the main findings and discussion of potential reliability approaches for the TxME pavement design. Detailed background information on different reliability approaches and examples are presented in the appendices:

- Appendix B: Existing reliability approaches used in existing pavement design and analysis systems.
- Appendix C: Examples and demonstration of reliability approaches including closed-form, Rosenblueth 2^n, Rosenblueth 2n+1, and Monte Carlo simulation methods.

3.2 SOURCES OF VARIATION AND UNCERTAINTY FOR PAVEMENT DESIGN AND ANALYSIS

There are always errors between actual pavement distresses and the ones predicted using models. The actual distress could be higher or lower than the mean expected value. The distribution of the error term for a given distress about the mean expected prediction is a function of the many sources of variation and uncertainty, including:

- Errors in estimating traffic loadings.
- Fluctuations in climate over many years.
- Variations in layer thicknesses, materials properties, and subgrade characteristics along the project.

- Differences between mean as-designed and as-built materials and other layer properties.
- Prediction model limitations and errors.

Figure 3-1 presents a correlation between fatigue damage (from Miner's model) and alligator/fatigue cracking of a flexible pavement. The figure presents the calibrated fatigue cracking model (represented as a solid line) along with the original data points used in calibrating the model (represented as dots). In the figure, the actual data are scattered about the line representing the final calibrated-validated model.

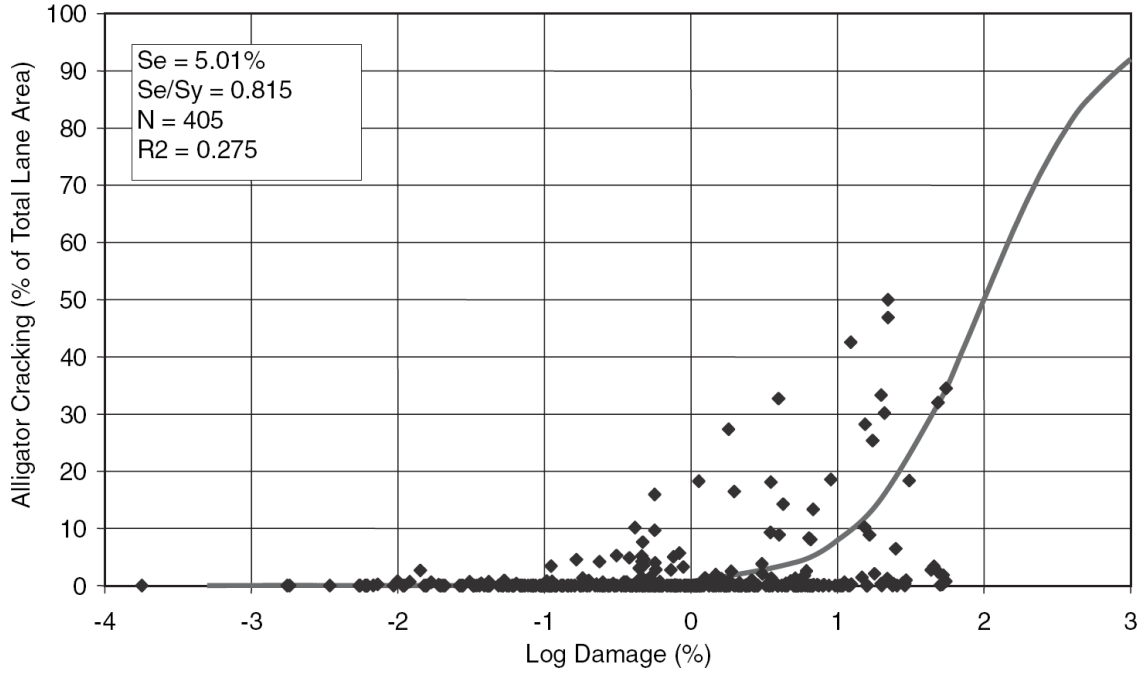

Figure 3-1. Bottom-Up Fatigue (Alligator) Cracking Calibration and Model (NCHRP 2004).

Many factors, of which the pure model error is only a part, caused the scatter. Knowledge of the error components and their respective magnitudes is essential to the estimation of the model error. In turn, the estimation of the model error is important to reliability design because it directly affects the performance prediction. The major components of the scatter are:

- Input error – this is the error associated with estimating each design input for each pavement test section such as HMA mix properties, HMA layer thickness, base and subgrade moduli, traffic loads, climate over life, etc.
- Measurement error of distress – this is the error associated with measuring the distress quantity being predicted from each pavement section used in calibration.
- Pure error – this error represents the random variation between the distresses exhibited by supposedly replicate sections. Although the causes of this error were not

determined, construction processes and material properties caused unknown variations that partly explain its occurrence.

- Model or lack-of-fit error – this error reflects the inability of the model to predict actual pavement performance due to its own inherent deficiencies, such as missing inputs or inadequate functional form or damage accumulation algorithm (e.g., Miner's model). This is the real model error associated with prediction. Once the models have undergone final calibration and validation, this error remains a constant until the model is improved in the future.

3.3 EXISTING APPROACHES FOR INCORPORATING RELIABILITY INTO PAVEMENT DESIGN AND ANALYSIS

Different approaches have been employed to consider reliability in a variety of pavement design and analysis systems. Researchers reviewed five pavement design and analysis systems:

- Reliability approach used in TxDOT's current FPS system.
- Reliability approach used in the AASHTO 1993 design guide.
- Reliability approach used in the MEPDG.
- Reliability approach used in the VESYS design system
- Reliability approach used in the CalME.

3.3.1 FPS19W (FPS21W) and AASHTO 1993

Both TxDOT's FPS19W (FPS21W) and the AASHTO 1993 Guide incorporate reliability through simply adjusting estimated traffic (or ESALs) in the design period. The standard deviation of traffic was preset or assumed. With that, higher reliability means a larger adjusting factor for estimated traffic, and consequently results in thicker pavement. Appendix B has a more thorough discussion on the FPS system and the AASHTO 1993 Guide.

3.3.2 MEPDG

Different from adjusting the estimated traffic in the FPS19W/FPS21W and the AASHTO 1993 Guide, the MEPDG design reliability is achieved through adjusting pavement distress using the following equation:

$$\text{Distress\_P} = \text{Distress\_mean} + \text{STD}_{\text{distress\_mea}} \times Z_P \qquad (3\text{-}1)$$

where *Distress_P* is distress level corresponding to the reliability level *P*, *Distress_mean* is distress predicted using the MEPDG deterministic model with mean inputs, $STD_{distress\_mean}$ is standard deviation of distress corresponding to distress predicted using the deterministic model

with mean inputs, and Z_P is standardized normal deviate corresponding to reliability level P (e.*g.*, *Z_P=0 corresponding to 50% reliability and Z_P=1.645 corresponding to 95% reliability based on one-sided confidence interval*).

Figure 3-2 further demonstrates the MEPDG reliability concept. The key points (or assumptions) behind this concept are

- All predicted distresses are normally distributed.
- The standard deviation of each predicted distress (e.g., fatigue cracking) can be substituted by that of measured data, since the MEPDG itself is deterministic and cannot predict the standard deviation of each distress.

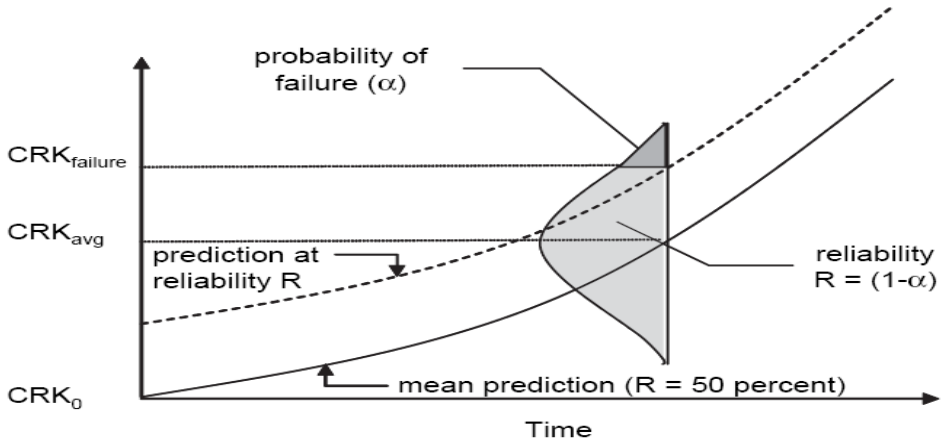

Figure 3-2. MEPDG Reliability Concept for a Given Distress (after Darter et al. 2005).

3.3.3 VESYS Program

The Federal Highway Administration (FHWA) originally developed the VESYS program the several decades ago (Kenis 1978). One of the main features of the program is that it considers the variability of pavement materials and traffic, and then evaluates the reliability of the pavement design. The VESYS program considers not only the reliability of pavement distresses (such as fatigue cracking, rutting, roughness, and low-temperature cracking) but also the pavement present serviceability index (PSI). Moavenzadeh and Elliott (1968) developed closed-form probabilistic solutions for this three-layer linear viscoelastic boundary value problem, and later Brademeyer (1975) refined and expanded the work. Therefore, the VESYS program, different from other design programs, evaluates reliability (or probability) of pavement distress using a closed-form function. It is ideal to have a closed-form function for predicting pavement distresses, but the reality is that there is no such simple function for pavement responses induced by various traffic loading scenarios and changing climate.

3.3.4 CalME

CalME is a computer program that the pavement research center at the University of California created for the California Department of Transportation (Caltrans). The program was developed to fill the need for a mechanistic–empirical analysis tool for designing new pavements and asphalt overlays (Ullidtz et al. 2010). CalME considers input variability and evaluates reliability of pavement distress through Monte Carlo simulation. Currently, for nine uncertain variables, 1000 simulations may be needed (Wu 2011). The beauty of the Monte Carlo simulation is that there is no need to assume the distribution of pavement distress. The major drawback of the Monte Carlo simulation is the running time: it often takes too long to tolerate for pavement design and analysis.

Table 3-1 presents a summary of all five existing pavement design programs in terms of reliability. There is no clear ideal approach.

Table 3-1. Summary and Comparison among Different Reliability Approaches.

Reliability approach	Advantages	Disadvantages	Iteration numbers	Examples of design system
Adjusting traffic	Simple	Cannot account for impact of the variability of other inputs on pavement design	1	▪ FPS19W/ (FPS21)W ▪ AASHTO 1993
Adjusting prediction	Simple	Cannot account for variability of inputs directly	1	MEPDG
Monte Carlo simulation	▪ Accurate ▪ Accounts for all input variability ▪ Obtains the distribution of response	Has long computation time	>1000	CalME
Closed-form function	▪ Efficient ▪ Accounts for design input variability	▪ Very complicated to get a closed-form pavement response function (if not impossible) ▪ Requires partial derivatives	1	VESYS

To further address this issue, TTI researchers reviewed the latest development in this area. They found that the Rosenblueth 2n+1 method has high potential for evaluating pavement design reliability. Detailed information on the Rosenblueth 2*n*+1 method is presented in the next section.

3.4 ROSENBLUETH SIMULATION METHOD

Normally, the Taylor series expansion is used to determine the mean and variance of a function if there is a closed-form function for predicting pavement distress. This method requires each term to be known in the function and the existence and continuity of the first and second derivatives. Rosenblueth (1975) developed a simple method known as the Point-Estimate method, which is similar to the finite difference procedure that can be used directly to determine the mean and variance of any function without knowing its formulation. The basic idea of the Point-Estimate method is to replace a continuous random variable with a discrete random variable. Specifically for reliability/probability, the continuous random variable (represented by a mean and standard deviation) is replaced by two masses representing the distribution of the function with the characteristic that the discrete distribution has the same mean and variance as the continuous one. Rosenblueth proposed two types of Point-Estimate methods: the 2^n simulation method and 2*n*+1 simulation method (*n* is the number of random variables).

3.4.1 Rosenblueth's 2^n Simulation Method

To illustrate the 2^n simulation method, an example with a function $y = f(X1, X2, X3)$ is presented. Figure 3-3 shows the schematic of probability density curves of three random variables *X1*, *X2*, and *X3*. In this figure μ_{xi} and σ_{xi} are the mean value and standard deviation of each random variable *Xi*, *i*=1, 2, and 3, respectively. Thus, in the Rosenblueth Point-Estimation method, for each variable *Xi*, only two points such as $\mu_{xi} - \sigma_{xi}$ and $\mu_{xi} + \sigma_{xi}$ are needed to represent the distribution.

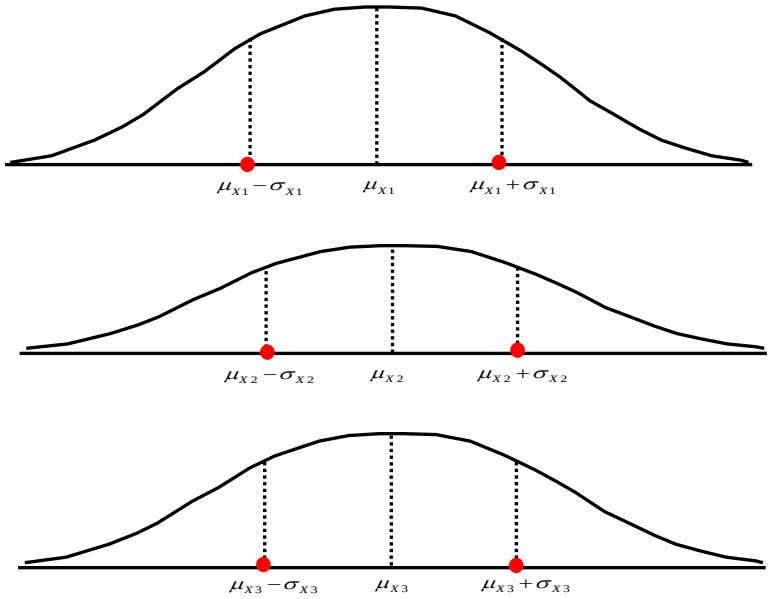

Figure 3-3. Schematic of Probability Density Curves and Representative Points for Variables X1, X2, and X3.

Therefore, for the function $y = f(X1, X2, X3)$, 8 ($=2^3$) simulations need to be made to determine the mean value (μ_y) and standard deviation (σ_y), such as:

$$y_1=f(\mu_{x1} - \sigma_{x1}, \mu_{x2} - \sigma_{x2}, \mu_{x3} - \sigma_{x3}) \quad (---) \quad (3\text{-}2)$$

$$y_2=f(\mu_{x1} - \sigma_{x1}, \mu_{x2} - \sigma_{x2}, \mu_{x3} + \sigma_{x3}) \quad (--+) \quad (3\text{-}3)$$

$$y_3=f(\mu_{x1} - \sigma_{x1}, \mu_{x2} + \sigma_{x2}, \mu_{x3} - \sigma_{x3}) \quad (-+-) \quad (3\text{-}4)$$

$$y_4=f(\mu_{x1} - \sigma_{x1}, \mu_{x2} + \sigma_{x2}, \mu_{x3} + \sigma_{x3}) \quad (-++) \quad (3\text{-}5)$$

$$y_5=f(\mu_{x1} + \sigma_{x1}, \mu_{x2} - \sigma_{x2}, \mu_{x3} - \sigma_{x3}) \quad (+--) \quad (3\text{-}6)$$

$$y_6=f(\mu_{x1} + \sigma_{x1}, \mu_{x2} - \sigma_{x2}, \mu_{x3} + \sigma_{x3}) \quad (+-+) \quad (3\text{-}7)$$

$$y_7=f(\mu_{x1} + \sigma_{x1}, \mu_{x2} + \sigma_{x2}, \mu_{x3} - \sigma_{x3}) \quad (++-) \quad (3\text{-}8)$$

$$y_8=f(\mu_{x1} + \sigma_{x1}, \mu_{x2} + \sigma_{x2}, \mu_{x3} + \sigma_{x3}) \quad (+++) \quad (3\text{-}9)$$

Then, the mean value and standard deviation of the function y can be determined as:

$$\mu_y = \frac{\sum_{i=1}^{8} y_i}{8} \quad (3\text{-}10)$$

$$\sigma_y = \sqrt{\frac{\sum_{i=1}^{8}(y_i - \mu_y)^2}{8}} \qquad (3\text{-}11)$$

This method has the following advantages:

- It is unnecessary to know the distribution type of the input random variables if the distribution is (or is close to) symmetric.
- Only the mean value and standard deviation are needed.
- The total simulations will be much less than the Monte Carlo simulation if the number of random variables is small.

Meanwhile, there are two disadvantages with this method:

- There is not much of an advantage if the number of random variables is large because the total simulation number of the Point-Estimate method is 2^n (*n* is the number of random variables).
- The Cumulative Distribution Function of the dependent variable is unknown.

To address the disadvantages and specifically to reduce the number of simulations (2^n), Rosenblueth later proposed a rapid and equally valid method: the 2*n*+1 simulation method, which is presented next.

3.4.2 Rosenblueth's 2*n*+1 Simulation Method

Instead of 2^n simulations, the 2*n*+1 simulation method needs 2*n*+1 (*n* is number of random variables) simulations only. The basic idea is to evaluate a function of random variables at 2*n*+1 key combinations and then use this information to estimate the mean and coefficient of variation of the function. Again, the same function of $y = f(X1, X2, X3)$ is used here to describe Rosenblueth's 2*n*+1 method.

Step 1: Define y_0 as the value of the function *y* when all input variables are equal to their mean values; that is, $y_0 = f(\mu_{X1}, \mu_{X2}, \mu_{X3})$.

Step 2: The value of the function *y* is evaluated at an additional 2*n* points as follows. For each random variable *Xi*, evaluate the function at two values of *Xi*, which are shifted from the mean μ_{Xi} by $\pm\sigma_{Xi}$ while all other variables are assumed to be equal to their mean values. These values of the function will be referred to as y_i^+ and y_i^-. The subscript denotes the variable that is shifted, and the superscript indicates the direction of the shift. In mathematical notation,

$$y_i^+ = f(\mu_{X1}, \mu_{X2}, \ldots, \mu_{Xi} + \sigma_{Xi}, .., \mu_{Xk}) \qquad (3\text{-}12)$$

$$y_i^- = f(\mu_{X1}, \mu_{X2}, \ldots, \mu_{Xi} - \sigma_{Xi}, \ldots, \mu_{Xk}) \quad (3\text{-}13)$$

For n=3,

$$y_1^+ = f(\mu_{X1} + \sigma_{X1}, \mu_{X2}, \mu_{X3}) \quad (3\text{-}14)$$

$$y_1^- = f(\mu_{X1} - \sigma_{X1}, \mu_{X2}, \mu_{X3}) \quad (3\text{-}15)$$

$$y_2^+ = f(\mu_{X1}, \mu_{X2} + \sigma_{X2}, \mu_{X3}) \quad (3\text{-}16)$$

$$y_2^- = f(\mu_{X1}, \mu_{X2} - \sigma_{X2}, \mu_{X3}) \quad (3\text{-}17)$$

$$y_3^+ = f(\mu_{X1}, \mu_{X2}, \mu_{X3} + \sigma_{X3}) \quad (3\text{-}18)$$

$$y_3^- = f(\mu_{X1}, \mu_{X2}, \mu_{X3} - \sigma_{X3}) \quad (3\text{-}19)$$

Step 3: For each random variable, calculate the following two quantities based on y_i^+ and y_i^-:

$$\bar{y}_i = \frac{y_i^+ + y_i^-}{2} \quad (3\text{-}20)$$

$$V_{y_i} = \frac{y_i^+ + y_i^-}{y_i^+ - y_i^-} \quad (3\text{-}21)$$

Step 4: Calculate the estimated mean and standard deviation of the function y as follows:

$$\mu_y = y_0 \prod_{i=1}^{k} \frac{\bar{y}_i}{y_0} \quad (3\text{-}22)$$

$$\sigma_y = \mu_y \sqrt{\{\prod_{i=1}^{k} (1 + V_{yi}^2)\} - 1} \quad (3\text{-}23)$$

Using the $2n$+1 simulation method, the number of simulations is substantially reduced when the number of random variables is large, which is significant to pavement design with many inputs to consider. The $2n$+1 simulation method is recommended as one of the reliability approaches for consideration in the TxME design program.

The examples and verifications for the Rosenblueth methods (both 2^n and $2n$+1 simulation methods) will be demonstrated in Appendix C: Examples and Comparisons among Closed-form method, Rosenblueth methods, and Monte Carlo method. The accuracy and validity of the 2^n and $2n$+1 simulation methods are verified by comparison with the closed-form method and the Monte Carlo method.

3.5 SUMMARY AND RECOMMENDATION

As discussed above, the most simple and effective approach is the adjusting-traffic-only approach used in both FPS19W/FPS21W and the AASHTO 1993 design guide. However, its major problem is that the impact of the variability of other input variables cannot be considered. For the MEPDG approach, the input uncertainty is not considered directly; the standard deviation of prediction is determined through measured data. The Monte Carlo simulation approach is a good one, but the simulation time is often too long to tolerate. Therefore, for pavement designs the most promising reliability approach is Rosenblueth's $2n+1$ method. But the drawback of Rosenblueth's $2n+1$ method is that the cumulative distribution curve of the dependent variable is unknown. Therefore, the research team will investigate and explore both the Rosenblueth's $2n+1$ method and the Monte Carlo simulation method. The final decision will be made after trying out these two methods with actual pavement designs for typical Texas conditions.

CHAPTER 4.
PROPOSED FRAMEWORK FOR TxME

TxME design system aims to enable TxDOT designers to take full advantage of new materials and to make more economical and reliable designs. The main goals of a proposed framework are

- To assemble all the implementable performance models.
- To provide a user-friendly interface to make the verification/calibrations of these models feasible.

For any pavement design and analysis, there are always at least three categories of input that need to be considered:

- Pavement structure and associated material properties.
- Traffic.
- Climate.

For this study, since the input uncertainty is included, a fourth category—reliability-related input—is also needed. This chapter discusses these four input categories and other aspects related to TxME.

4.1 PAVEMENT STRUCTURE DIFFERENTIATION AND ASSOCIATED DISTRESS MODES

For new roads, flexible pavements in Texas highways can roughly be divided into three types:

- Surface treatment or thin pavements.
- Conventional pavements.
- Very thick pavements (perpetual pavements), all loosely dependent on the thickness of asphalt layers.

The reason for making a differentiation between flexible pavements is that each different type of flexible pavement has a specific distress mode. For example, there is a potential for subgrade shear failure in a surface treatment or thin pavement, but such failure will not happen in a perpetual pavement. Similarly, for base layers, two categories can be identified based on the material type: stabilized base and granular (flexible) base.

For asphalt concrete (AC) overlays, there are basically two main types: AC overlay over existing AC pavements, and AC overlay over existing PCC pavements. Due to the significant difference in behavior between PCC with and without reinforced steel reinforcement (modulus, joint load

transfer efficiency, etc.), the latter can be divided further into two categories: AC overlay over existing JPCP pavement, and AC over existing CRCP pavement.

Each type of pavement structure and associated distresses are discussed below.

4.1.1 Thin-Surfaced Pavement

Texas has many miles of excellent-performing surface treatment or thin (≤ 1.5") asphalt pavements. Thin-surfaced pavement design is typically not addressed in either the NCHRP or other studies, but they must be an integral part of the proposed TxME design system.

Depending on the type of base material, granular or stabilized, thin-surfaced pavements will have different failure modes, and consequently different models are needed to predict field performance of those pavements.

Failure Modes for Thin-surfaced Pavements with Granular Base

For this pavement type, subgrade shearing failure and/or base and subgrade permanent deformation are the two principle types of failures—subgrade shear failure under one-pass loading and rutting (or permanent deformation) under multi-pass loading. It has been decided that the shear failure under one-pass loading will be handled using LoadGage developed under Project 0-4519; and this study will focus on the permanent deformation development under multi-pass loading.

As presented in Chapter 2, the VESYS layer rutting model is recommended for that purpose, and the triaxial repeated load test will be used for determining the VESYS layer rutting model parameters.

Failure Modes in Thin-Surfaced Pavements with Stabilized Base

Fatigue cracking and crushing failure are two concerns for this pavement type. Fatigue cracking models for stabilized materials were discussed in Chapter 2. Regarding the crushing failure, this study will develop a crushing model based on the work that de Beer had done in South Africa in 1989.

In summary, since the surface layer is very thin, it is assumed that any failure or deformation in the base will immediately reflect to the surface. Additionally, the surface layer is too thin to be treated as a common AC layer to predict thermal cracking. Thus for surface treatment or thin pavements, if the base is granular base, the development of rutting (including base rutting, and subgrade rutting) will be predicted; if the base is stabilized base, the development of fatigue cracking and crushing failure will be analyzed under TxME.

4.1.2 Conventional Pavement

As the word *conventional* implies, this type of pavement is the most common type and widely used in Texas. Depending on the type of base material, granular or stabilized, conventional pavements also have different potential failure modes and, consequently, different field performances must be predicted.

Failure Modes for Conventional Pavements with Granular Base

For conventional pavements with granular base, the total surface rutting, AC fatigue cracking, and AC low temperature cracking are potential major failures. Note here that the total surface rutting includes that from AC layers, granular base layers, and the subgrade.

To predict rutting, the aforementioned asphalt layer rutting model, granular base, and subgrade rutting model will be employed. Similarly, the AC fatigue cracking model and the low temperature cracking model discussed in Chapter 2 will be used for predicting fatigue cracking and low temperature cracking development, respectively.

Failure Modes for Conventional Pavements with Stabilized Base

For a stabilized base layer, rutting will be ignored while fatigue cracking will be fully considered. So, for conventional pavements with stabilized base, asphalt layer rutting, subgrade rutting, asphalt layer fatigue cracking, and stabilized base fatigue cracking will be analyzed. Also, low temperature cracking of the asphalt layer will be included in the TxME design system.

4.1.3 Perpetual Pavements

Several considerations are presented below in terms of perpetual pavements:

- The perpetual pavements are designed to be long-lasting pavements with enough structural integrity and thickness to preclude distresses such as conventional bottom-up fatigue cracking and subgrade shear failure.
- Literature review showed that an endurance limit, influenced by mix type, is an important controlling factor for perpetual pavement design. It will be validated through analyses of the Texas perpetual pavement sections, and incorporated into the TxME design system.

- Previous research also indicated that top-down cracking (longitudinal cracking) may happen in perpetual pavements. However, no technically sound M-E model is available for the top-down cracking, so that no top-down cracking model is recommended for the TxME design system right now. Instead, the researchers recommend a specific study on the top-down cracking in perpetual pavements in Texas.
- Low temperature cracking (transverse cracking) is another potential distress for perpetual pavements and will be incorporated into the TxME design system.

In summary, rutting, fatigue cracking, endurance limits, and low temperature cracking will be predicted for perpetual pavements.

4.1.4 AC Overlays

Regardless of the existing pavement type (rigid or flexible), reflective cracking and AC overlay rutting are two major distresses which will be considered in the TxME design system. Additionally, for an AC overlay on existing AC pavements, AC fatigue cracking is another potential failure mode being considered in the TxME design system.

In summary, AC overlay rutting, reflective cracking, and AC fatigue cracking (for AC over existing AC pavements only) will be included in the TxME design system.

4.1.5 Summary of Pavement Structure and Associated Distress Modes

Figure 4-1 summarizes the pavement structures and associated distress modes considered in the TxME design system.

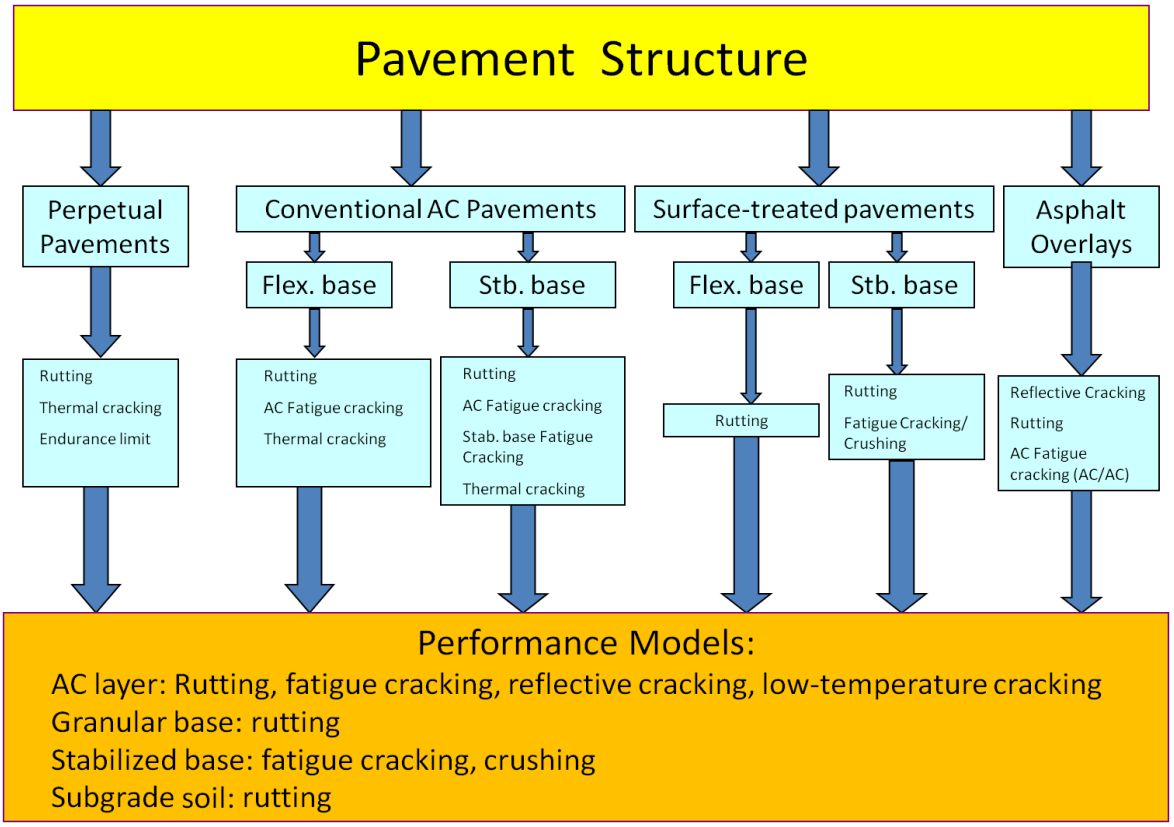

Figure 4-1. Pavement Structure Types and Predicted Performances.

4.2 MATERIAL TYPES AND ASSOCIATED PROPERTIES

In general, a flexible pavement structure is composed of four types of layers:

- Asphalt layers.
- Base layers.
- A subbase layer.
- The subgrade.

Material properties of each layer are highly related to material types. The material types and associated material properties being included in the TxME design system are described below.

4.2.1 Material Types

For asphalt layers, there are overall eight types of materials included in the FPS21W:

- Surface treatment material.
- Dense-graded AC.
- Superpave AC.
- Coarse Matrix High Binder (CMHB) AC.
- Stone Matrix Asphalt (SMA).
- Rich Bottom Layer (RBL) AC.
- Crack Attenuating Mix (CAM).
- Permeable Friction Course (PFC).

For now all eight of these mix types are incorporated into the TxME design system, and necessary change will be made according to the TxDOT's new HMA specification.

For base layers, the following six types of materials will also be included:

- Fly-ash (FA) or Lime Fly-ash (LFA) treated base.
- Lime stabilized base.
- Cement Stabilized base.
- Asphalt treated base.
- Emulsion asphalt treated base.
- Flexible base (granular base)

For the subbase layer, two major categories of materials—Lime (Cement) Stabilized soil/subgrade and Emulsion asphalt treated soil/subgrade—are considered.

For subgrade, a selection of default subgrade properties will be available based on the selected soil type for the county the project is located in.

4.2.2 Material Properties

For each material, modulus and Poisson's ratio are always needed for pavement analysis. Other engineering properties may also be required, depending on distress modes. For example, for AC material, dynamic modulus, fracture, and rutting properties are the most basic properties required for predicting rutting and cracking development versus time. For stabilized base, the modulus of rupture, unconfined compressive strength, fatigue cracking parameters, and crushing parameters are necessary to predict fatigue cracking or crushing failure.

In the TxME design system, the material property inputs correlate to the pavement structure type and associated distress modes. For example, if the pavement structure is surface treatment or thin pavement with stabilized base, then the crushing parameters are necessary for prediction of crushing failure. However, these inputs are not necessary for conventional pavement or

perpetual pavement with stabilized base, since the crushing prediction is not required. The detailed input interface for material properties will be described in a later section.

4.3 TRAFFIC

Two approaches have been used to consider the influence of traffic loading on pavement performance: traditional ESALs and the more recent load spectra approach used in the MEPDG. A two-level approach (Level 1-load spectra and Level 2-ESALs) will be considered in the TxME design system.

4.4 CLIMATE

Environment is another important factor for pavement design. The enhanced integrated climatic model (EICM) is believed to accurately predict pavement temperatures and moisture within the pavement structure. The research team has extensive knowledge and experience with the EICM, and will incorporate the EICM into the TxME design system.

4.5 RELIABILITY INPUT

As discussed in Chapter 3, the Rosenblueth 2*n*+1 method merits high consideration for addressing the design reliability within the TxME design system. The Monte Carlo simulation method is also worth further investigation. The proposed reliability input for each item is described below.

- For pavement structure and material properties: the general inputs for the variables (such as pavement layer thickness) are one mean value and one standard deviation (or coefficient of variation which equals standard deviation divided by mean value).
- For climate, no reliability input is needed; the research team ignored the uncertainty for three reasons:
  - The climate data are represented by hourly climatic data through many years, which results in tens of thousands variables.
  - There is no practical way available to determine the variations between these variables.
  - The variation of climate is ostensibly considered through using many years rather than one-year climate data.
- For traffic, if the input is ESALs, then one mean value and one coefficient of variation of *20 Year 18 kip ESALs* can be representative. However, if the input is load spectra, then the mean value and coefficient of variation of the Annual Average Daily Truck Traffic (AADTT) can be used as reliability input. The uncertainty of other variables, such as axle load distribution, etc., will be ignored for the same reasons as the proceeding climate data consideration.

The proposed reliability input for the TxME design system is a table that lists the potential uncertain variables and their coefficients of variation. Through this table, users can decide which variables need to be incorporated and can modify the coefficients based on measured data. Section 4.6.7 shows this table in the reliability input user interface.

4.6 PROPOSED TxME USER INTERFACE

The proposed user interfaces for the TxME design system are briefly illustrated below.

4.6.1 Connection with FPS

Figure 4-2 envisions the potential connection between TxME and the current FPS. With this connection, the user can conduct preliminary designs using the current FPS and then import the relevant data into TxME to predict the performance (with the material properties input, etc.). The idea is to provide a better transition for current TxDOT pavement designers.

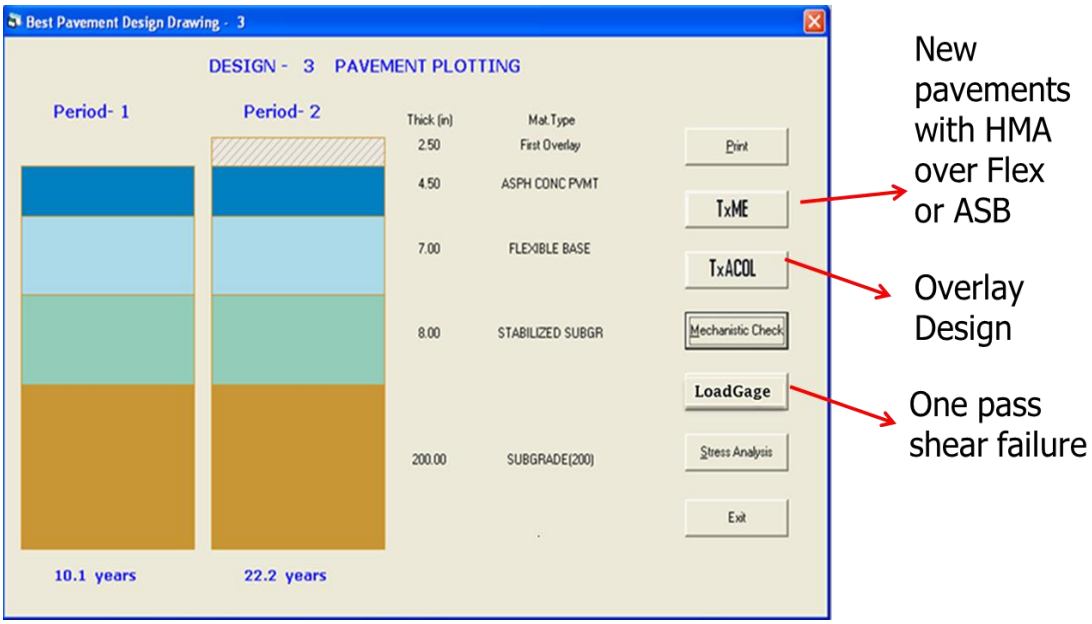

Figure 4-2. Envisioned Connection between FPS and TxME.

4.6.2 Main Screen

Figure 4-3 presents the main screen of the application. In this screen, four major input categories are listed in the left side on the node tree, such as Structure, Climate, Traffic, and Reliability. Double-clicking each node activates the corresponding input window on the right side.

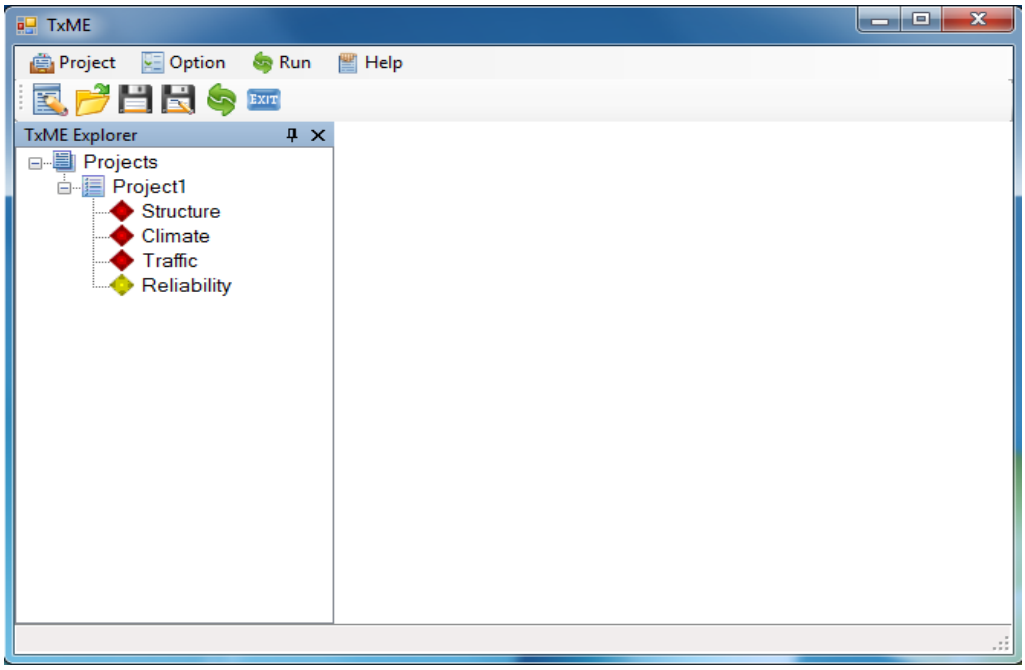

Figure 4-3. Main Screen of User Interface.

4.6.3 Pavement Structure

Figure 4-4 presents the pavement structure input screen. On this screen, different AC layer materials, base layer materials, and sub-base layer material icons are listed in the upper right part of the window. The lower left part of the window shows the pavement structure. With these materials, users can build their own pavement structures. Note that for the design just run in FPS, the program will automatically load the FPS inputs as the default pavement structure through the TxME button shown in Figure 4-2.

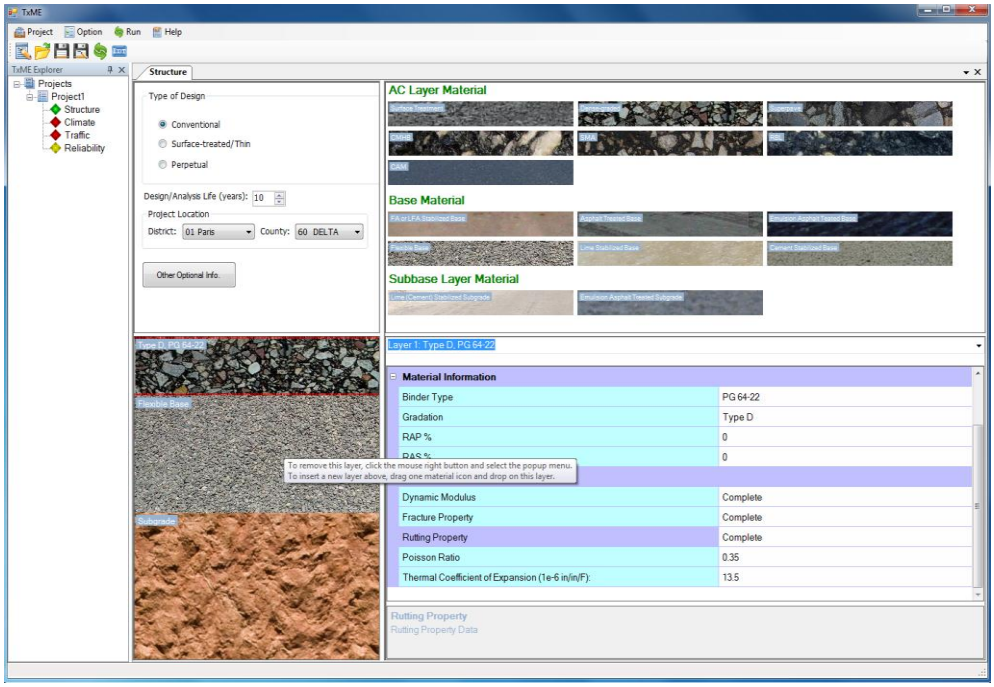

Figure 4-4. Pavement Structure Information Input Screen.

4.6.4 Material Property

For each layer, the user can input the corresponding material properties in the lower right part of the screen (see Figure 4-4). For some property inputs such as Thickness, Poisson Ratio, etc., the user only needs to input some numbers. For more complicated inputs such as dynamic modulus, the user needs to click the item and the corresponding input screen will pop up. Several material property input screens are illustrated below, including:

- Figure 4-5, presenting the dynamic modulus inputs for AC layers.
- Figures 4-6 and 4-7, presenting the fracture property and rutting property inputs, respectively.
- Figure 4-8, presenting the stabilized base material property inputs.
- Figure 4-9, presenting the flexible base or subgrade material rutting property inputs, with monthly values.

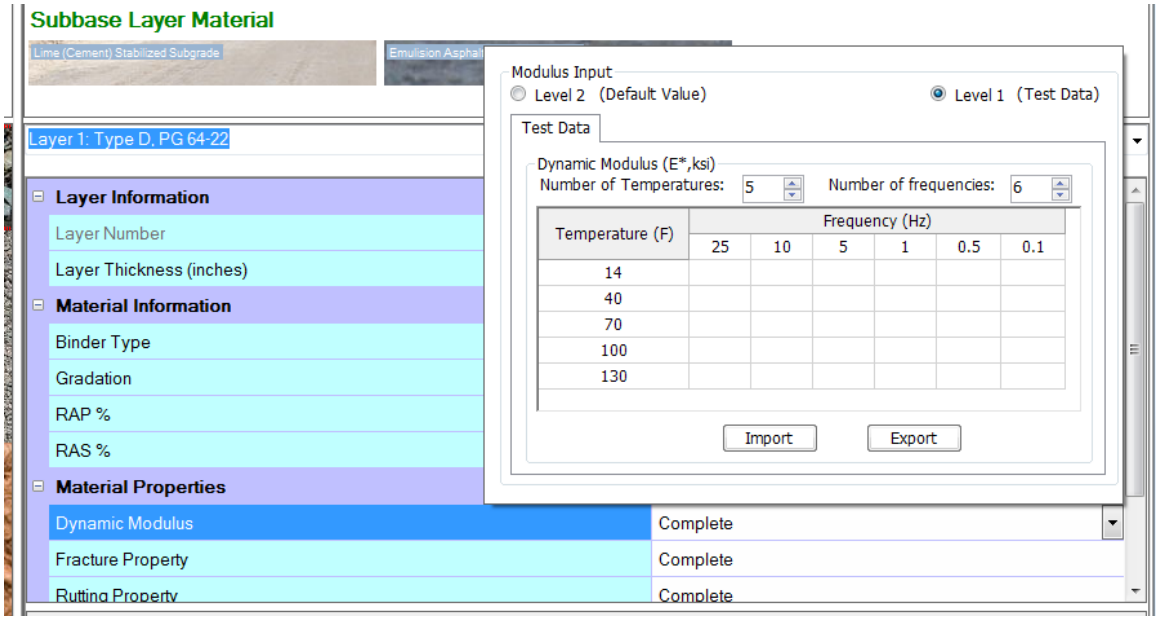

Figure 4-5. AC Layer Dynamic Modulus Input Screen.

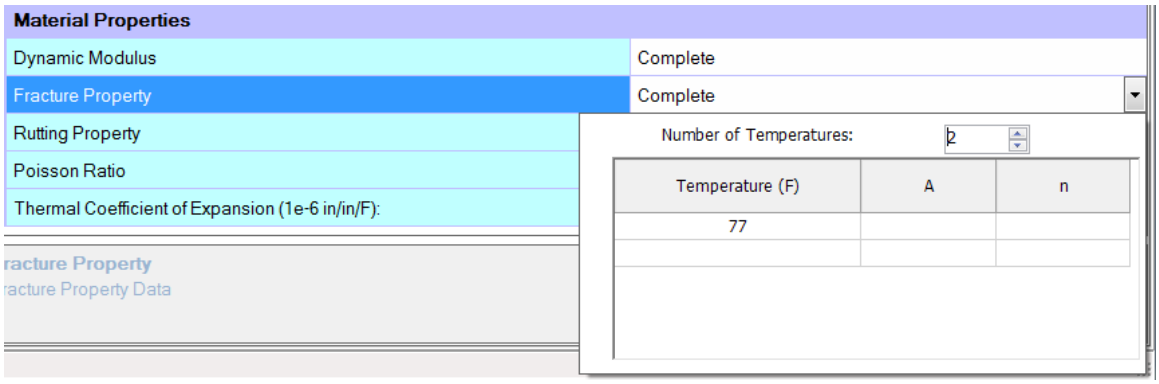

Figure 4-6. AC Layer Fracture Properties Input Screen.

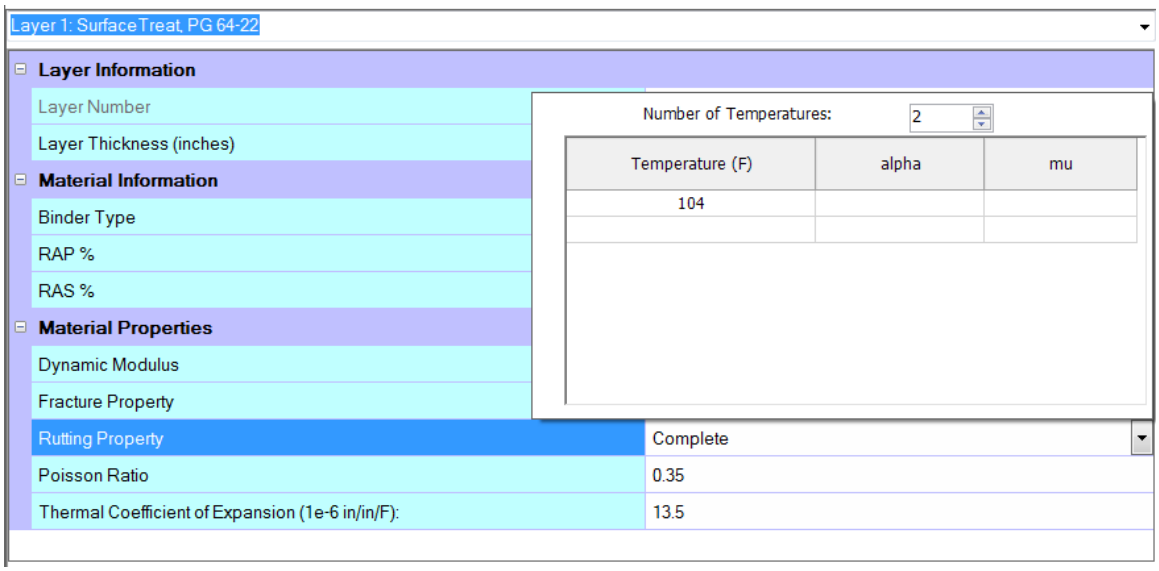

Figure 4-7. AC Layer Rutting Properties Input Screen.

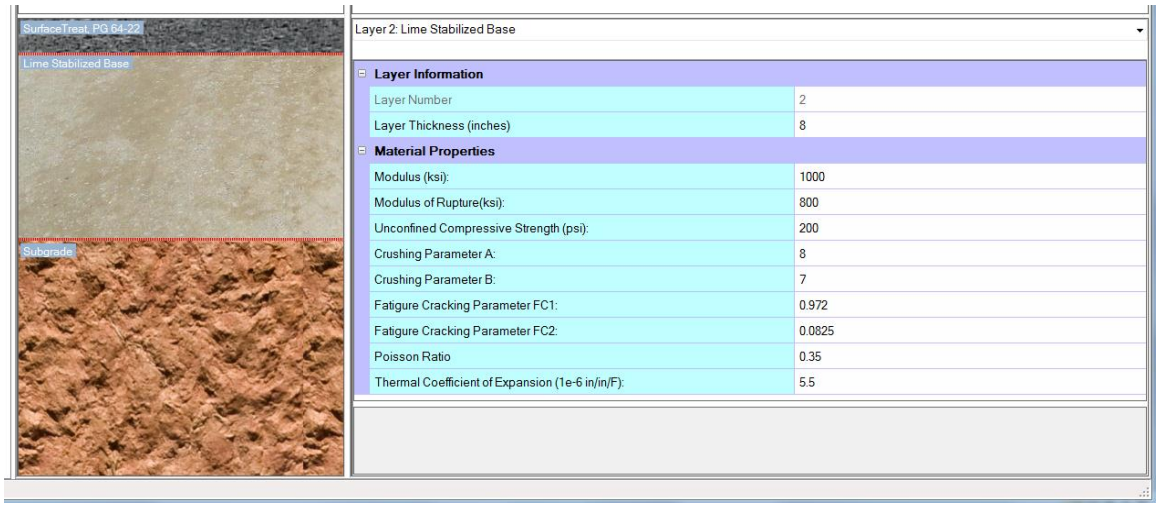

Figure 4-8. Stabilized Base Material Properties Input Screen.

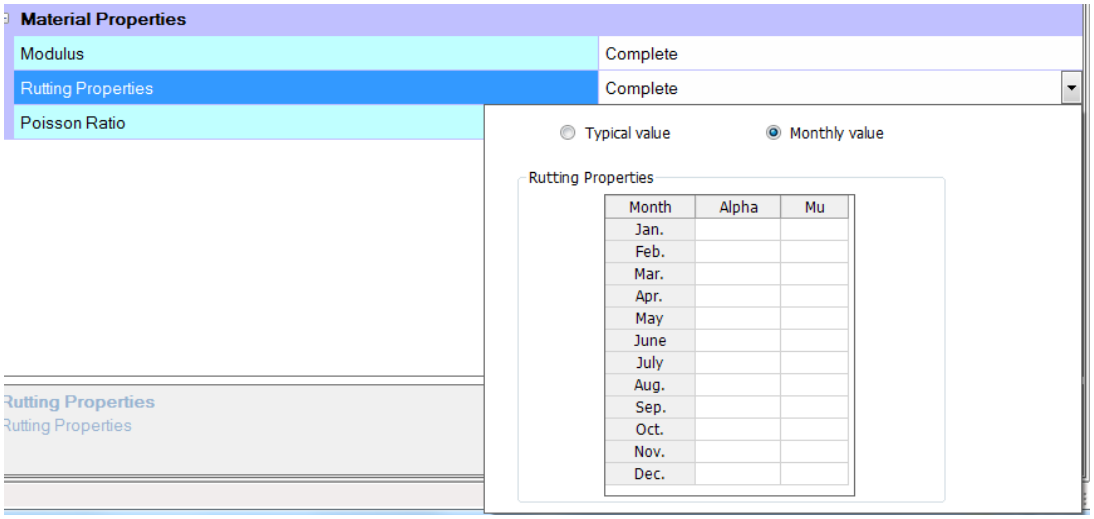

Figure 4-9. Flexible Base/Subgrade Rutting Properties Input Screen.

4.6.5 Traffic

Figures 4-10 to 4-13 present the traffic input screens. Figure 4-10 shows Level 2: ESALs input, and Figure 4-11 shows Level 1: load spectra input. When the user clicks the "Monthly Adjustment" or "Axle Load Distribution" button in Figure 4-11, screens such as Figure 4-12 or Figure 4-13 pop up. These screens let the user define the axle load distributions for each vehicle class and their monthly variations.

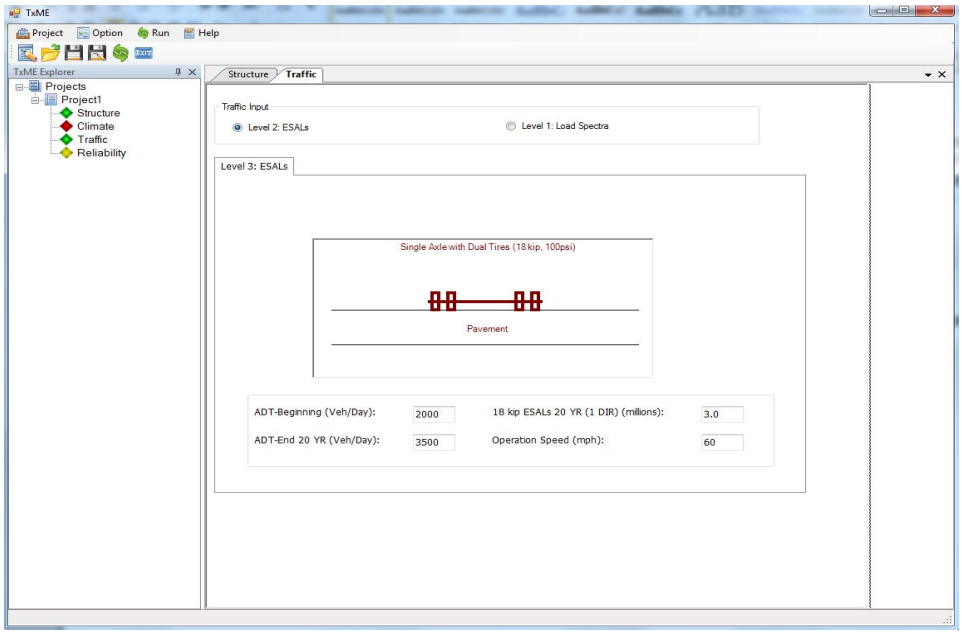

Figure 4-10. Traffic Level 2 (ESALs) Input Screen.

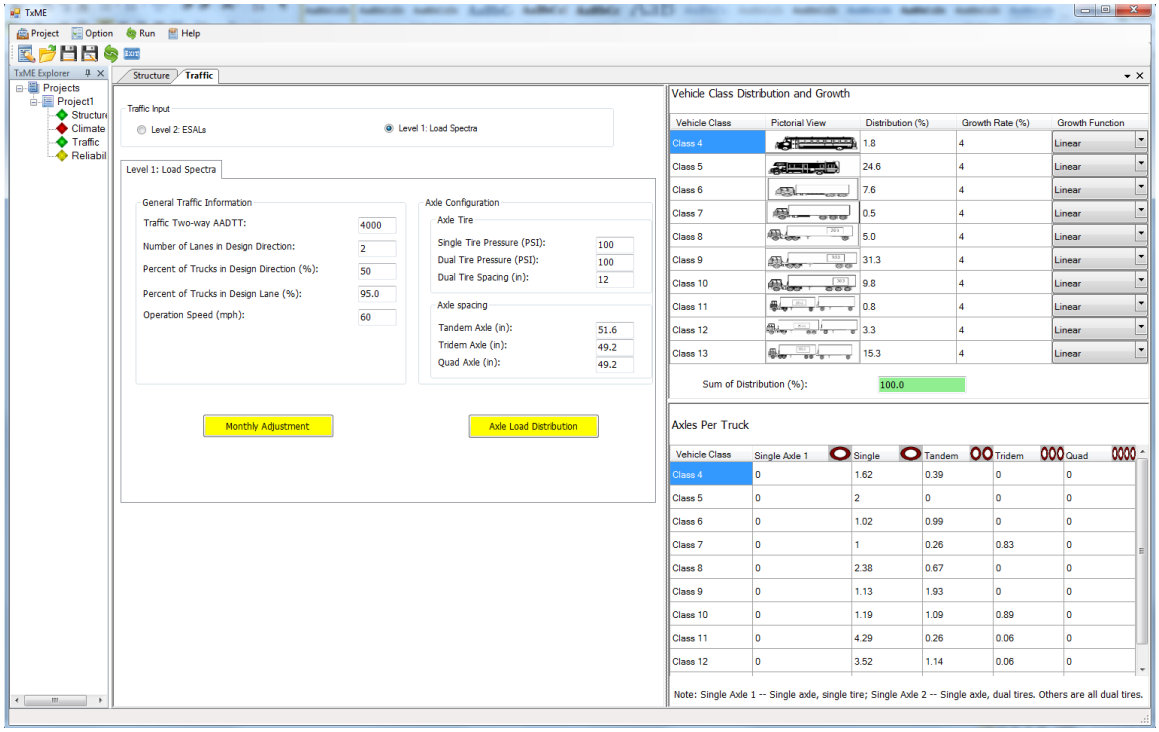

Figure 4-11. Traffic Level 1 (Load Spectra) Input Screen.

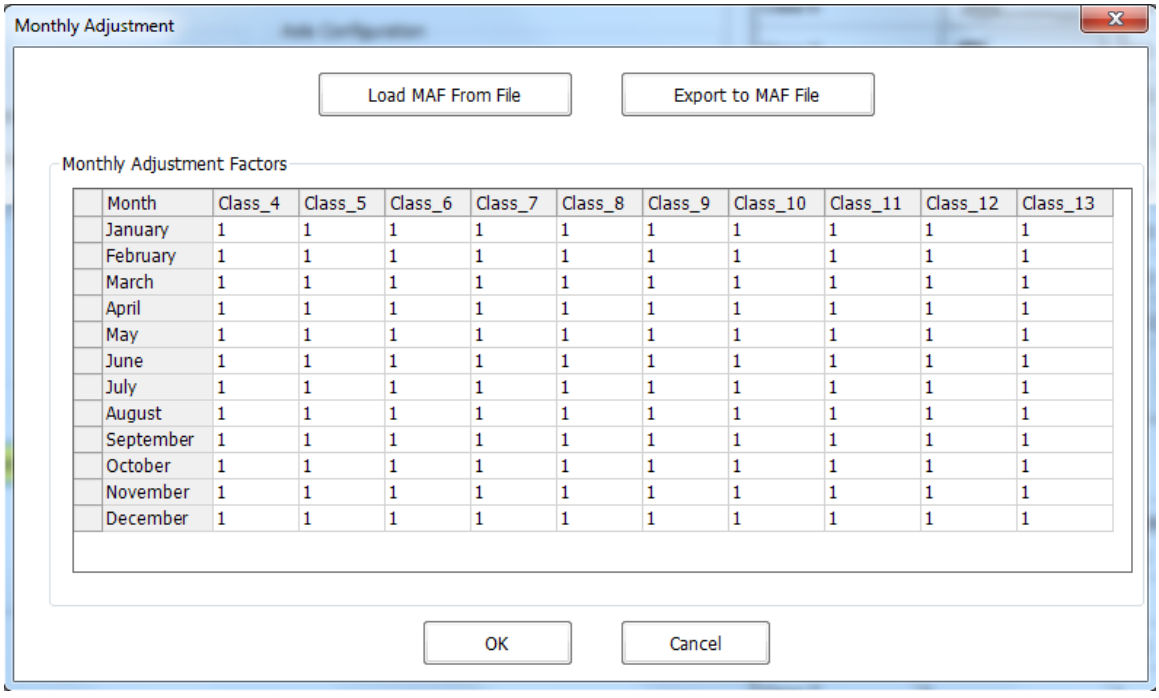

Figure 4-12. Traffic Monthly Adjustment Input Screen.

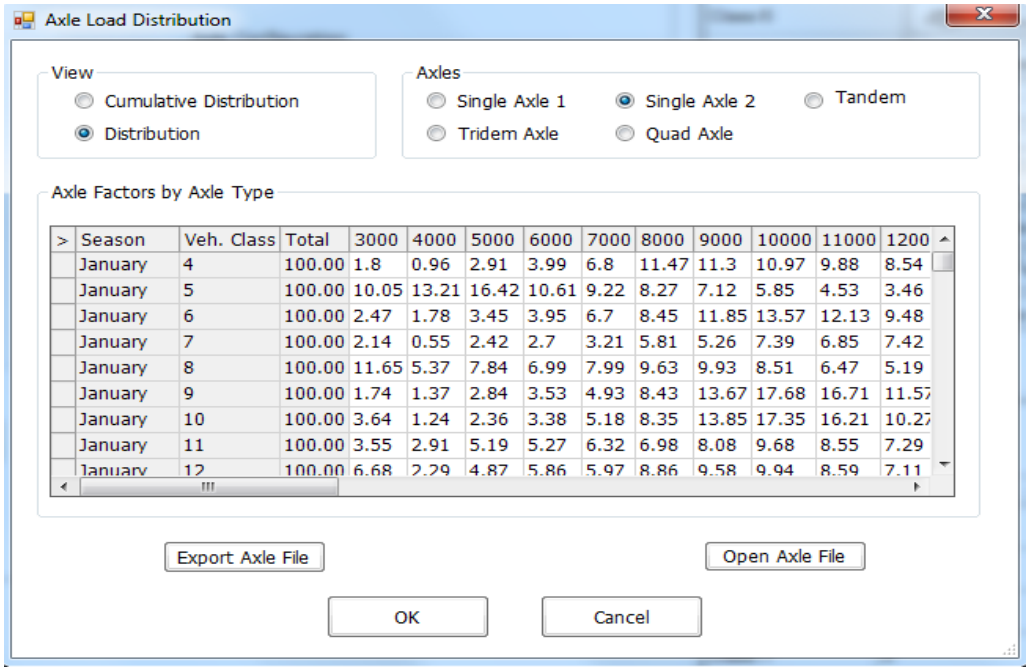

>	Season	Veh. Class	Total	3000	4000	5000	6000	7000	8000	9000	10000	11000	1200
	January	4	100.00	1.8	0.96	2.91	3.99	6.8	11.47	11.3	10.97	9.88	8.54
	January	5	100.00	10.05	13.21	16.42	10.61	9.22	8.27	7.12	5.85	4.53	3.46
	January	6	100.00	2.47	1.78	3.45	3.95	6.7	8.45	11.85	13.57	12.13	9.48
	January	7	100.00	2.14	0.55	2.42	2.7	3.21	5.81	5.26	7.39	6.85	7.42
	January	8	100.00	11.65	5.37	7.84	6.99	7.99	9.63	9.93	8.51	6.47	5.19
	January	9	100.00	1.74	1.37	2.84	3.53	4.93	8.43	13.67	17.68	16.71	11.57
	January	10	100.00	3.64	1.24	2.36	3.38	5.18	8.35	13.85	17.35	16.21	10.27
	January	11	100.00	3.55	2.91	5.19	5.27	6.32	6.98	8.08	9.68	8.55	7.29
	January	12	100.00	6.68	2.29	4.87	5.86	5.97	8.86	9.58	9.94	8.59	7.11

Figure 4-13. Traffic Axle Load Distribution Input Screen.

4.6.6 Climate

Figure 4-14 presents the climate input screen for a specific weather station. Generally, the left part of screen lets the user select a weather station, and the right part shows the summary of the weather data, such as average temperature or precipitation. The user can look into more detailed information like hourly data by clicking the "Hourly data" tab on the upper right.

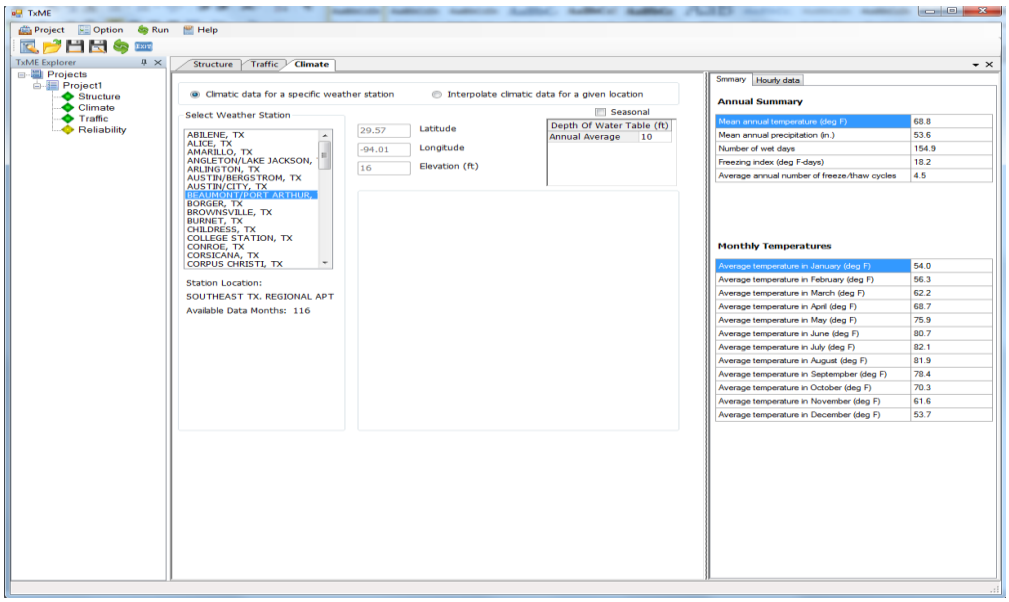

Figure 4-14. Climate for a Specific Weather Station Input Screen.

For a project location without a dedicated weather station, users can choose "Interpolate climatic data for a location," and the application will provide six weather stations nearby for the user to select for interpolation. Figure 4-15 presents the user interface for climate data interpolation. The red lines and numbers such as "#1, #2…" in the graph show the relative positions and distances from the user input project location.

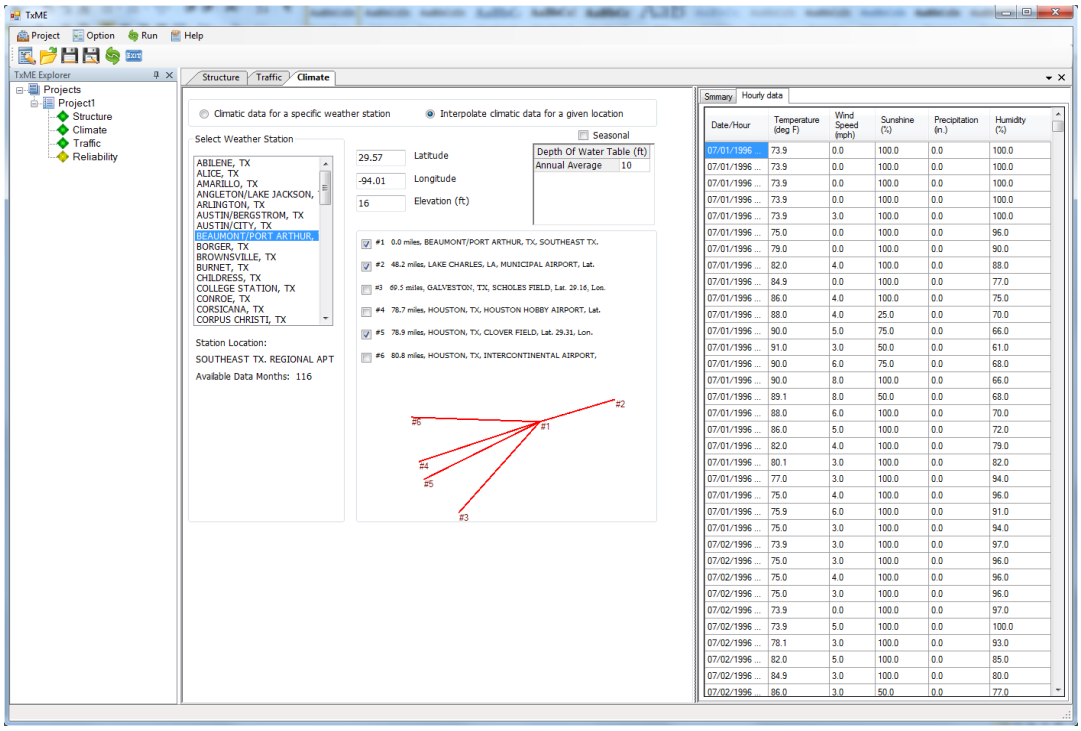

Figure 4-15. Climatic Data Interpolation Input Screen.

4.6.7 Reliability

Figure 4-16 presents the reliability input screen. Two input categories are displayed in this screen. On the left side are the performance criteria inputs, and on the right side are the variability inputs. For the performance criteria inputs, the user supplies the analysis stop criteria (performance limit) and reliability level in terms of percentage. For variability inputs, the user checks the applicable checkboxes and modifies the coefficient of variation value. As mentioned previously, both performance criteria and variability parameters are related to pavement structure type. Whenever the pavement structure type changes, these parameters are changed accordingly.

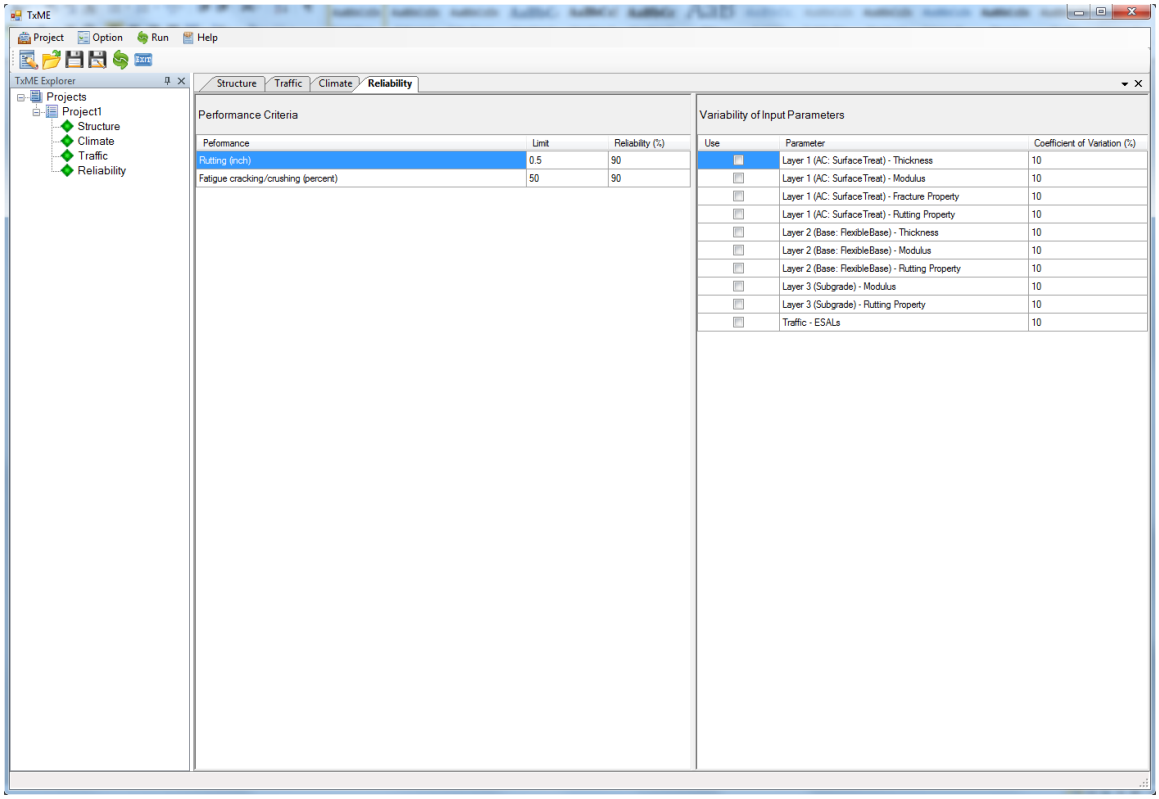

Figure 4-16. Performance Criteria and Reliability Input Screen.

4.7 FLOWCHART

To demonstrate the calculation process of distress development versus time, this report takes AC fatigue cracking as an example and presents the calculation flowcharts in Figures 4-17 and 4-18. The flowcharts can be considered guidance to develop the necessary algorithms to predict pavement distresses.

Figure 4-17 describes the deterministic approach without considering any input variability.

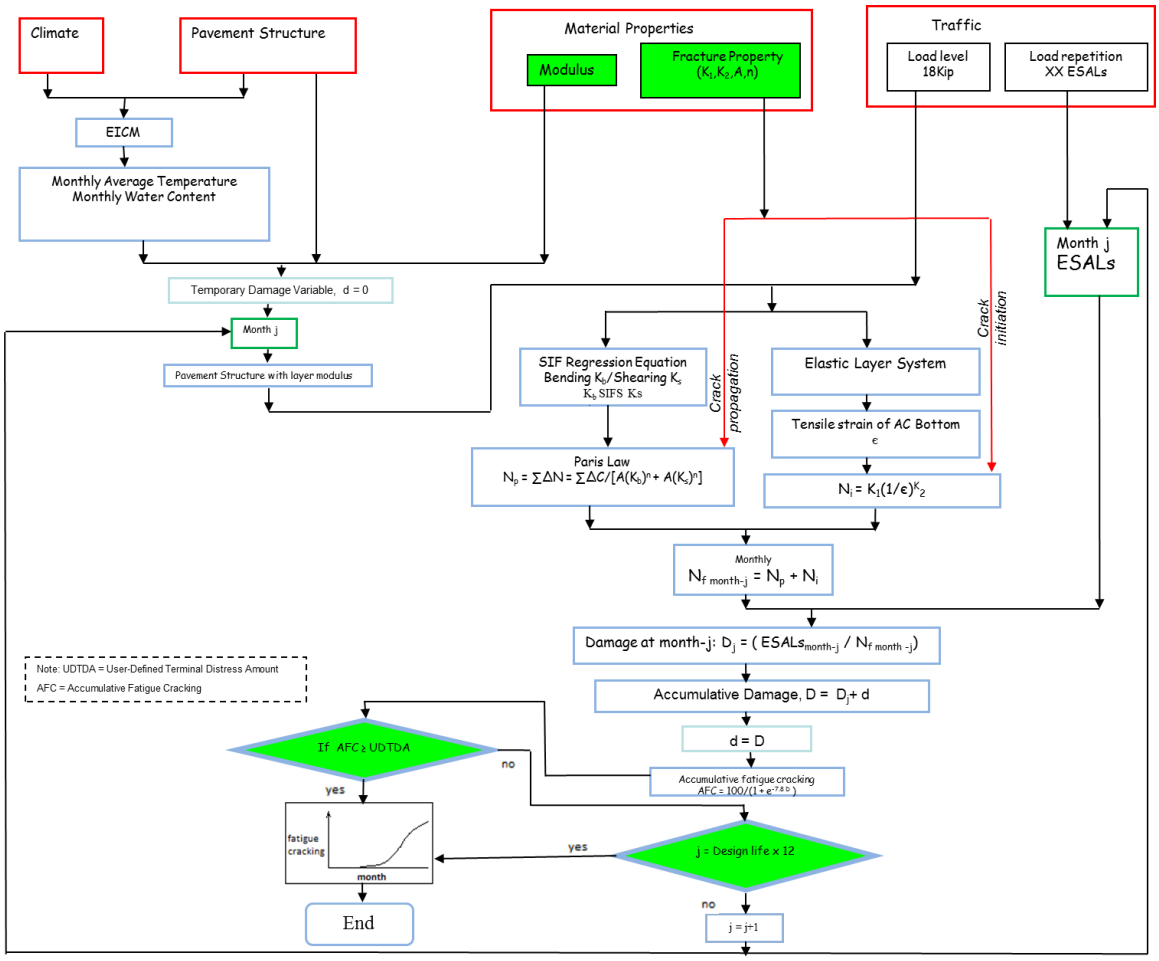

Figure 4-17. Flowchart of Deterministic Approach without Considering Input Variability.

Figure 4-18 describes the approach when considering the input variable uncertainties. As the figure shows, the variables with uncertainty are picked out and combined according to the Rosenblueth method. Thus for each combination, the prediction will be performed just like the aforementioned deterministic approach. After the predictions of all the combinations are complete, the mean and standard deviation of the output will be determined and the final prediction based on the user supplied reliability level can be provided.

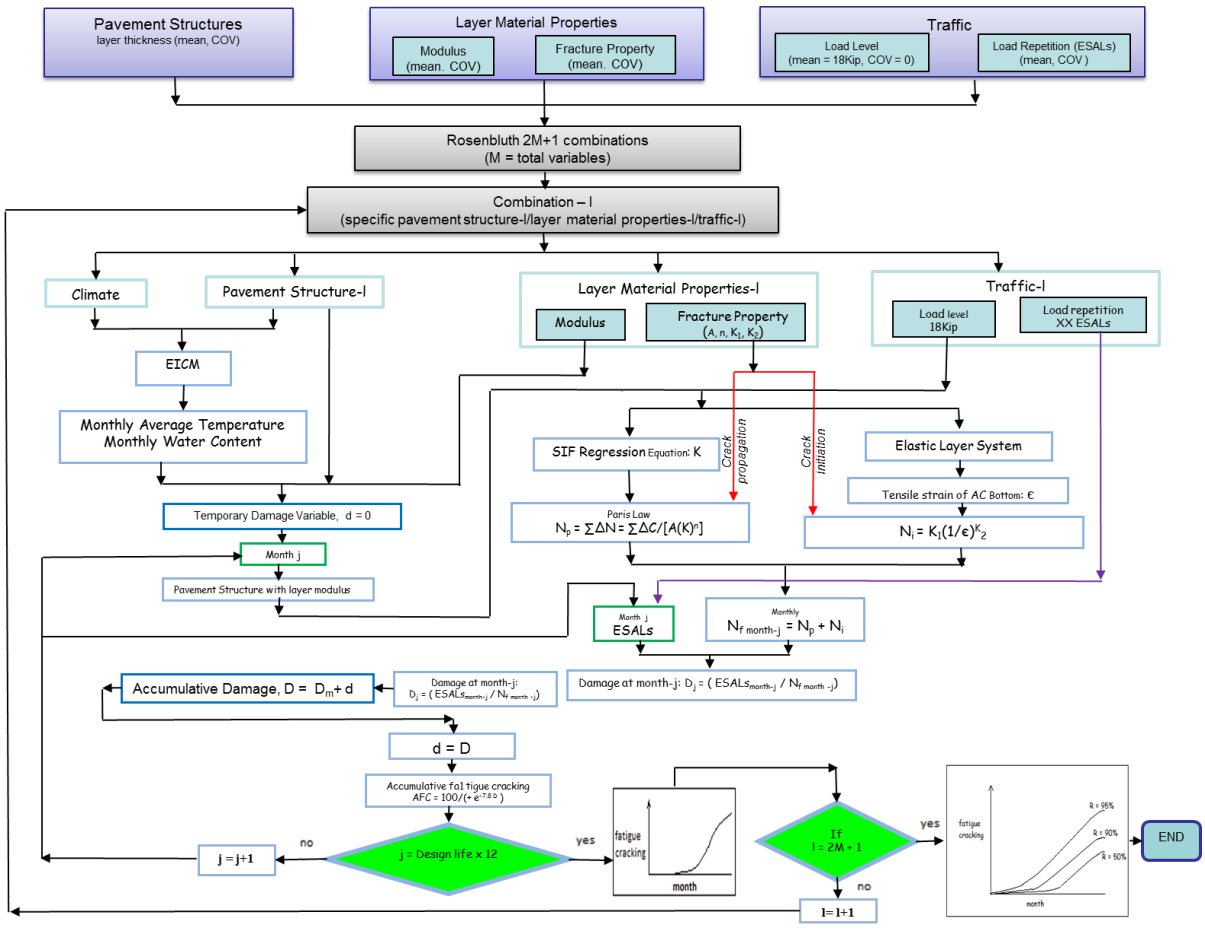

Figure 4-18. Flowchart of Reliability Approach Considering Input Uncertainty.

4.8 SUMMARY

The main goals of the TxME design system framework are to assemble all of the implementable performance models and to develop a user-friendly interface to make the verification/calibration of these models feasible. To achieve these goals, this chapter discusses the following items:

- Pavement structures and associated distress modes. The pavement structures being included are thin-surfaced pavement, conventional pavement, perpetual pavement, and AC overlay. Different pavement structures have different distress modes which will be predicted in accordance with pavement type in the TxME design system.
- Material types and properties. Material properties of each layer are highly related to material types. For each material, modulus and Poisson's ratio are always needed for pavement analysis. Other engineering properties may also be required, depending on anticipated distress modes.
- Traffic loads. Level 2 uses 18 kip ESALs and Level 1 uses detailed load spectra.
- Climate. EICM is proposed to predict in-pavement temperatures and moisture levels.
- Design reliability. The recommended reliability approach is the Rosenblueth $2n+1$ method.
- Descriptions of the user interfaces, which include the connection with FPS, the main screen, pavement structure, traffic, climate, reliability, and several material property user interfaces.
- Presentation of conceptual flowcharts to describe the calculation process of distress prediction. The fatigue cracking prediction was taken as an example to present the flowcharts that can provide guidance for further development.

CHAPTER 5.
CONCLUSIONS AND RECOMMENDATIONS

The primary goal of the new enhanced flexible pavement design system TxME is to enable TxDOT designers to take full advantage of new materials and to make more economical and reliable designs. Therefore, the specific objective of this report was to assemble supporting documentation such as calibrated distress models, traffic loading methodologies, climatic models, design reliability techniques, and to propose the preliminary framework of the TxME design system.

Based on the work presented previously, the following conclusions and recommendations are made:

- The asphalt layer rutting model, asphalt layer fatigue cracking model, reflective cracking model, granular base and subgrade rutting model, stabilized base fatigue cracking model, and stabilized base crushing failure model were well-developed or reviewed in recently completed studies such as 0-5798, 0-4822, 0-5123, and other national studies. Although some of these models might need recalibration based on Texas material and environmental conditions, these were identified as implementable within the TxME framework.

- The low temperature asphalt cracking model, which is similar to the one used in the MEPDG, was proposed. Two significant differences from the MEPDG model are noted:

  - The fracture properties *A* and *n* in the proposed model will be determined by the aforementioned enhanced OT test directly.

  - An alternative cracking amount model was recommended to be consistent with the crack amount model of reflective cracking or fatigue cracking.

- For the top-down longitudinal cracking model, the mechanism has not been fully understood to date and no implementable model was identified. At the moment, the research team cannot recommend any top-down longitudinal cracking model to be included in the TxME design system. Instead, the researchers recommend a specific study on top-down cracking, especially the potential top-down cracking in perpetual pavements in Texas.

- Literature showed that the endurance limit of asphalt mixes does exist, but varies with mix type and temperatures. The best way to describe the endurance limit is to use a cumulative distribution of the tensile strain at the bottom of asphalt layer, as Willis (2008) had proposed. To incorporate the endurance limit into the TxME design system, the research team proposed a two-level design concept:

    - When traffic input is in terms of ESALs, an 18-kip axle load will be applied at the equivalent annual temperature, and the maximum tensile strain at the bottom of asphalt layer will be determined and compared to a single endurance limit value (mix and binder type related).

    - When traffic input is in terms of load spectra, then maximum tensile strains at the bottom of the asphalt layer under different load levels and different temperature conditions will be determined. The corresponding strain distribution will be evaluated and then compared with the user defined strain distribution criteria. Additionally, the research team will keep a close eye on the ongoing NCHRP Project 09-44A "Validating an Endurance Limit for HMA Pavements: Laboratory Experiment and Algorithm Development" to validate/ incorporate the latest findings.

- Several reliability analysis methods were reviewed and compared. The most simple and effective approach is the adjusting-traffic-only approach used in both FPS21W and the AASHTO 1993 design guide, but its major shortcoming is that the impact of the variability of other input parameters cannot be considered. The Monte Carlo simulation approach is a good approach, but the simulation time is often too long to tolerate. The most promising reliability approach for the TxME design system is the Rosenblueth 2*n*+1 method.

- The framework for the TxME design system was proposed, which includes pavement structure, material properties, climate, traffic, reliability inputs, user interfaces, and a distress algorithm flowchart.

REFERENCES

AASHTO Guide for Design of Pavement Structures, American Association of State Highway and Transportation Officials, 1993.

AASHTO TP62-03, *Standard Method of Test for Determining Dynamic Modulus of Hot-Mix Asphalt Concrete Mixtures*, 2003.

Anderson, M., J. D'Angelo, and G. Huber. *Forensic investigation of early cracking on I-25 in Denver, Colorado*, CDOT-DTD-R- 2001-10, Colorado Department of Transportation, 2001.

Andrei, D. *Development of a Predictive Model for the Resilient Modulus of Unbound Materials,* Ph.D. Dissertation, Department of Civil and Environmental Engineering, Arizona State University, Tempe, AZ, May 2003.

Asphalt Institute. *Thickness Design Manual (MS-1)*, 9th ed., the Asphalt Institute, College Park, MD, 1981.

Bagowsky, I. *Reliability Theory and Practice*, Prentice Hall, Englewood Cliffs, NJ, 1961.

Barret, C. R., W. D. Nix, and A. S. Tetelman. *The Principles of Engineering Materials*, Prentice Hall, Englewood Cliffs, NJ, 1973.

Bonnaure, F., A. Gravois, and J. Udron. A New Method of Predicting the Fatigue Life of Bituminous Mixes, *Journal of the Association of Asphalt Paving Technologists*, Vol. 49, pp. 499–529, 1980.

Brademeyer, B. D. *Flexible Pavement Systems: An Analysis of the Structural Subsystem' s Deterioration,* Master of Science Thesis, Massachusetts Institute of Technology, February 1975.

Christensen, D. *Interim Report of Project NCHRP 1-42: Top-Down Fatigue Cracking of Hot-Mix Asphalt Layers*, Advanced Asphalt Technologies, LLC, 2004.

Christensen, D. and R. Bonaquist. Practical Application of Continuum Damage Theory to Fatigue/Phenomena in Asphalt Concrete Mixtures, *Journal of the Association of Asphalt Paving Technologists*, Vol. 74, pp. 963–1001, 2005.

Darter, M, and Hudson, W. R. *Probabilistic Design Concepts Applied to Flexible Pavement System Design*, Report 123-18, Center for Highway Research, University of Texas at Austin, 1973.

Darter, M., L. Khazanovich, T. Yu, and J. Mallela, J. Reliability Analysis of Cracking and Faulting Prediction in the New Mechanistic-Empirical Pavement Design Procedure, *Transportation Research Record*, No. 1936, pp. 150–160, 2005.

Dauzats, M. and A. Rampal. Mechanism of Surface Cracking in Wearing Courses, *Proceedings of the 6th International Conference on the Structural Design of Asphalt Pavements*, Ann Arbor, MI, 1987.

De Beer, M., C. Fisher, and F. J. Jooste. Determination of Pneumatic Tyre/Pavement Interface Contact Stresses Under Moving Loads and Some Effects on Pavement with Thin Asphalt Surfacing Layers, *Proceedings of the 8th International Conference on Asphalt Pavements*, Seattle, WA, 1997.

Deme, I. J., and F. D., Young. Ste. Anne Test Road Revisited Twenty Years Later. *Proceedings, Canadian Technical Asphalt Association*, Vol. 32, pp. 254–283, 1987.

El Halim A. O., Y. Hassan, M. Farha, and W. Bekheet. Surface Cracking: Origin and Causes, Theoretical and Field Studies, *Proceedings of the 5th International RILEM Conference*, Limoges, pp. 19–26, 2004.

Fernando, E., D. Musani, D. Park, and W. Liu. *Evaluation of Effects of Tire Size and Inflation Pressure on Tire Contact Stresses and Pavement Response*, FHWA/TX-06/0-4361-1, Texas Transportation Institute, College Station, TX, 2006.

Finn, F., C. L. Saraf, R. Kulkarni, K. Nair, W. Smith, and A. Abdullah. *Development of Pavement Structural Subsystems*, NCHRP Report 291, Transportation Research Board, Washington, D. C., 1986.

Gerritsen, A. H., C.A. Van Gurp, et al. Prediction and Prevention of Surface Cracking in Asphalt Pavements, *Proceedings of the 6th International conference on the structural design of asphalt pavements*, Ann Arbor, MI, 1987.

Groenendijk, J. *Accelerated Testing and Surface Cracking of Asphalt Concrete Pavements*, PhD Thesis, TU Delft, 1998.

Harmelink, D. and T. Aschenbrener, *Extent of Top-Down Cracking in Colorado*, Report No. CDOT-DTD-R-2003-7, Denver, CO: Colorado Department of Transportation, 2003.

Harmelink, D., S. Shuler, and T. Aschenbrener. Top-Down Cracking in Asphalt Pavements: Causes, Effects, and Cures. *Journal of Transportation Engineering*, Vol. 134:1, pp. 1–6, 2008.

Hiltunen, D. R., and R. Roque. A Mechanics-Based Prediction Model for Thermal Cracking of Asphaltic Concrete Pavements. *Journal of the Association of Asphalt Paving Technologists*, Vol. 63, pp. 81–117, 1994.

Hu, S., X. Hu, F. Zhou., and L. Walubita. SA-CrackPro: A New Finite Element Analysis Tool for Pavement Crack Propagation, In *Transportation Research Record: Journal of the Transportation Research Board*, No.2068, pp. 10–19, 2008.

Hu, S., X. Hu, F. Zhou, and L. Walubita. Development, Calibration, and Validation of a New M-E Rutting Model for HMA Overlay Design and Analysis, *Journal of Materials in Civil Engineering*, Vol. 23, pp. 89–99, 2011.

Huang, Y. H., *Pavement Analysis and Design, Second Edition*, Pearson Education, Inc., Upper Saddle River, NJ, 2004.

Hugo, F. and T. W. Kennedy. Surface Cracking of Asphalt Mixtures in Southern Africa, *Journal of the Association of Asphalt Paving Technologists*, Vol. 54, pp. 454–496, 1985.

Kenis, W. J. *An Interim Design Method for Flexible Pavements Using the VESYS Structural Subsystem*, FHWA Report, RD-77-154, 1978.

Kim, J., R. Roque, and B. Birgisson. Interpreting Dissipated Energy from Complex Modulus Data. *International Journal of Road Materials and Pavement Design*, pp. 223–245, 2006.

Kim, J., R. Roque, and B. Birgisson. Integration of Thermal Fracture in the HMA Fracture Model. *Journal of the Association of Asphalt Paving Technologists*, Vol. 77, pp. 631-662, 2008.

Leahy, R.B., R.G. Hicks, C.L. Monismith, and F.N. Finn. Framework for Performance-Based Approach to Mix Design and Analysis, *Proceedings of the Association of Asphalt Paving Technologists*, Vol. 64, pp 431–473, 1995.

Leech, D. and M. E. Nunn. Deterioration mechanisms in flexible roads, *Proceedings of the 2nd European Symposium on the Performance and Durability of Bituminous Materials*, Leeds, 1997.

Lytton, R.L., R. Roque, J. Uzan, D. R. Hiltunen, E. Fernando, and S. M. Stoffels. *Performance Models and Validation of Test Results,* Strategic Highway Research Program Report A-357, Project A-005, Washington, D.C., 1993.

Lytton, R. L., U. Shanmugham, and B. D. Garrett. *Design of Asphalt Pavements for Thermal Fatigue Cracking*, Research Report No. FHWA/TX-83/06+284-4, Texas Transportation Institute, Texas A&M University, College Station, TX, January 1983.

Lytton, R. L., J. Uzan, E. G. Fernando, R. Roque, D. Hiltumen, and S. M. Stoffels. *Development and Validation of Performance Prediction Models and Specifications for Asphalt Binders and Paving Mixes,* SHRP A-357, National Research Council, Washington, D. C., 1993.

Matsuno, S. and T. Nishizawa, Mechanism of longitudinal surface cracking, *Proceedings of the 7th international conference on asphalt pavements*, Nottingham UK, 1992.

Maupin, G. W., Jr. and J. R. Freeman, Jr. *Simple Procedure for Fatigue Characterization of Bituminous Concrete,* Final Report No. FHWA-RD-76-102, Federal Highway Administration, Washington, D.C., 1976.

Mirza, M. W., and M. W. Witczak. Development of a Global Aging System for Short- and Long-Term Aging of Asphalt Cements. *Journal of the Association of Asphalt Paving Technologists,* Vol. 64, pp. 393–430, 1995.

Moavenzadeh, F. and J. F. Elliott. *Moving Load on Viscoelastic Layered Systems*, Civil Engineering Department, MIT, Cambridge, Mass, 1968.

Monismith, C. L., and D. B. McLean, Structural Design Considerations, *Proceedings of the Association of Asphalt Paving Technologists,* Vol. 41, 1972.

Myers, L., R. Roque, and B. E. Ruth. Mechanisms of Surface Initiated Longitudinal Wheel Path Cracks in High-type Bituminous Pavements. *Journal of the Association of Asphalt Paving Technologists,* Vol. 67, pp. 402–432, 1998.

Myers, L., R. Roque, B. Ruth and C. Drakos. Measurement of Contact Stresses for Different Truck Tire Types to Evaluate Their Influence on Near-Surface Cracking and Rutting. In *Transportation Research Record: Journal of the Transportation Research Board, No.1655,* Transportation Research Board of the National Academies, Washington, D.C., pp. 175–184, 1999.

Myers, L. A. *Development and Propagation of Surface-Initiated Longitudinal Wheel Path Cracks in Flexible Highway Pavements*, Ph.D. Dissertation, Gainesville, FA, University of Florida, 2000.

Myers, L. A., and R. Roque. Top-down Crack Propagation in Bituminous Pavements and Implications for Pavement Management. *Journal of the Association of Asphalt Paving Technologists,* Vol. 71, pp. 651–670, 2002.

NCHRP, *Guide for Mechanistic-Empirical Design of Pavement Structures*, NCHRP Project 1-37A, National Cooperative Highway Research Program, Washington, D.C., 2004.

Nishizawa, T., S. Shimeno, and M. Sekiguchi. Fatigue Analysis of Asphalt Pavements with Thick Asphalt Mixture Layer, *Proceedings of the 8th International Conference on Asphalt Pavements,* Vol. 2. University of Washington, Seattle, WA, pp. 969–976, August 1997.

Nunn, M. Long-Life Flexible Pavement, *Proceedings of the 8th international conference on asphalt pavements,* Seattle, WA, 1997.

Paris, P.C., and E. Erdogan. A Critical Analysis of Crack Propagation Laws, *Journal of Basic Engineering,* Transaction of the American Society of Mechanical Engineering, Series D., Vol. 85, pp. 528–883, 1963.

Priest, A. L. *Calibration of Fatigue Transfer Functions for Mechanistic-Empirical Pavement Design,* Master's Thesis, Auburn University, Auburn, AL, 2005.

Prowell, B. D., E. R. Brown, R. M. Anderson, J. S. Daniel, H. Von Quintus, S.Shen, S. H. Carpenter, S. Bhattacharjee, and S. Maghsoodloo. *Endurance Limit of Hot Mix Asphalt Mixtures to Prevent Fatigue Cracking in Flexible Pavements*, NCHRP Report 646, Transportation Research Board, National Academy of Science, Washington, D.C., July 2010.

Romanoschi, S.A., A.J. Gisi, M. Portillo, and C. Dumitru. The First Findings from the Kansas Perpetual Pavements Experiment, *Transportation Research Board 2008 Annual Meeting*, CD-ROM.

Roque, R., and B. E. Ruth. Mechanisms and Modeling of Surface Cracking in Asphalt Pavements. *Journal of the Association of Asphalt Paving Technologists*, Vol. 59, pp.397–421, 1990.

Roque, R. W.G. Buttlar, B.E. Ruth, M. Tia, S.W. Dickison, and B. Reid. *Evaluation of SHRP Indirect Tension Tester to Mitigate Cracking in Asphalt Pavements and Overlays*. Final Report to the Florida Department of Transportation, August 1997.

Roque, R., B. Birgisson, B. Sangpetngam, and Z. Zhang. Hot-Mix Asphalt Fracture Mechanics: A Fundamental Crack Growth Law for Asphalt Mixtures. *Journal of the Association of Asphalt Paving Technologists*, Vol. 71, pp. 816–827, 2002.

Roque, R., B. Birgisson, C. Drakos, and B. Dietrich. Development and Field Evaluation of Energy-Based Criteria for Top-Down Cracking Performance of Hot-Mix Asphalt. *Journal of the Association of Asphalt Paving Technologists*, Vol. 73, pp. 229–260, 2004.

Roque, R., J. Zou, Y. R. Kim, C. Baek, S. Thirunavukkarasu, B. S. Underwood, and M. N. Guddati. *Top-Down Cracking of Hot-Mix Asphalt Layers: Models for Initiation and Propagation.* Final Report, NCHRP Web-Only Document 162, 2010.

Rosenblueth, E. Point Estimates for Probability Moments. In *Proceedings of National Academic of Science*, USA. 72(10):3812–3814, 1975.

Scrivner, F. H., W. M. Moore, W. F. McFarland, and G. R. Carey, *A Systems Approach to the Flexible Pavement Design Problem*, TxDOT Research Report 32-11, Texas Transportation Institute, Texas A&M University System, 1968.

Sebesta, S., P. Harris, and W. Liu. *Improving Lab Compaction Methods for Roadway Base Materials,* Research Report 0-5135-2, Texas Transportation Institute, Texas A&M University, College Station, TX, 2006.

Soon S. C., A. Drescher, and H. K. Stolarski. Tire-Induced Surface Stresses in Flexible Pavements, In *Transportation Research Record: Journal of the Transportation Research Board*, No.1896, pp. 170–176, 2004.

Soules, T. F., R.F. Busbey, S.M. Rekhson, A. Markovsky, and M. A. Burke. Finite-Element Calculation of Stresses in Glass Parts Undergoing Viscous Relaxation. *Journal of the American Ceramic Society*, Vol. 70, No. 2, pp. 90–95, 1987.

Tsai, B. W., D. Jones, J. T. Harvey, and C. L. Monismith. *Reflective Cracking Study: First-Level Report on Laboratory Fatigue Testing*, Research Report UCPRC-RR-2006-08, Institute of Transportation Studies, University of California, Davis, CA, 2008.

Uhlmeyer, J. S., K. Willoughby, L. Pierce and J. P. Mahoney, "Top-Down Cracking in Washington State Asphalt Concrete Wearing Courses," Submitted to the *Transportation Research Board 79th Annual Meeting*, January 2000, Washington, D.C.

Ullidtz, P., J. T. Harvey, B.-W. Tsai, and C. L. Monismith, *Calibration of Incremental-Recursive Flexible Damage Models in CalME Using HVS Experiments.* Report prepared for the California Department of Transportation (Caltrans) Division of Research and Innovation by the University of California Pavement Research Center, Davis and Berkeley, UCPRC-RR-2005-06, 2006.

Ullidtz, P., J. T. Harvey, I. Basheer, D. Jones, R. Wu, J. Lea, and Q. Lu. CalME, a Mechanistic–Empirical Program to Analyze and Design Flexible Pavement Rehabilitation. In *Transportation Research Record: Journal of the Transportation Research Board*, No. 2087, Transportation Research Board of the National Academies, Washington, D.C., pp. 143–152, 2010.

Walubita, L. F., S. Hu, and T. Scullion. *The Texas Perpetual Pavement Database–Users' Manual*, Technical Report 0-4822-4, Texas Transportation Institute, College Station, TX, 2009.

Wang, J., B. Birgisson, R. Roque. Development of a Windows-Based Top-Down Cracking Design Tool for Florida Based on the Energy Ratio Concept. In *Transportation Research Record: Journal of the Transportation Research Board, No. 2037*, Transportation Research Board of the National Academies, Washington, D.C., pp. 86–96, 2007.

Weissman, S. L. Influence of Tire-Pavement Contact Stress Distribution on Development of Distress Mechanisms in Pavements, In *Transportation Research Record: Journal of the Transportation Research Board*, No.1655, pp. 161–167, 1999.

Willis, J. R. *Field-Based Strain Thresholds for Flexible Perpetual Pavement Design*, Doctoral Dissertation, Auburn University, Auburn, AL, 2008.

Newcomb, D. *Perpetual Pavements: A Synthesis*, APA 101, Asphalt Pavement Alliance, 2002.

Witczak, M. W., and O. A. Fonseca. Revised Predictive Model for Dynamic (Complex) Modulus of Asphalt Mixtures. *Transportation Research Record: Journal of the Transportation Research Board, No. 1540*, Transportation Research Board of the National Academies, Washington, D.C., pp. 15–23, 1996.

Witczak, M.W., R. Roque, D.R. Hiltunen, and W. G. Buttlar. *Project Report—NCHRP Project 9-19: Modification and Re-Calibration of Superpave Thermal Cracking Model*, Arizona State University, Tempe, AZ, 2000.

Wu, Z., Z. Q. Siddique, and A. J. Gisi. Kansas Turnpike–An Example of Long-Lasting Asphalt Pavement, *Proceedings International Symposium on Design and Construction of Long-Lasting Asphalt Pavements*, National Center for Asphalt Technology, Auburn, AL, pp. 857–876, 2004.

Yang, Y., X. Gao, W. Lin, D.H. Timm, A.L. Priest, G.A. Huber, and D.A. Andrewski. *Perpetual Pavement Design in China,* International Conference on Perpetual Pavement, Ohio Research Institute for Transportation and the Environment, 2005.

Zhang, Z., R. Roque, and B. Birgisson. Evaluation of Laboratory-Measured Crack Growth Rate for Asphalt Mixtures. In *Transportation Research Record: Journal of the Transportation Research Board, No. 1767*, Transportation Research Board of the National Academies, Washington, D.C., pp. 67–75, 2001.

Zhou, F., S. Hu, and T. Scullion. *Development and Verification of the Overlay Tester-Based Fatigue Cracking Prediction Approach*, FHWA/TX-07/9-1502-01-8, Texas Transportation Institute, College Station, TX, 2007.

Zhou, F., E. Fernando, and T. Scullion. *A Review of Performance Models and Test Procedures With Recommendations for Use in the Texas M-E Design Program*, FHWA/TX-08/0-5798-1, Texas Transportation Institute, College Station, TX, 2008.

Zhou, F., E. Fernando, and T. Scullion. *Development, Calibration, and Validation of Performance Prediction Models for the Texas M-E Flexible Pavement Design System*, FHWA/TX-08/0-5798-2, Texas Transportation Institute, College Station, TX, 2010.

Zhou, F., and T. Scullion. *VESYS5 Rutting Model Calibrations with Local Accelerated Pavement Test Data and Associated Implementation*. Report No. FHWA/TX-03/9-1502-01-2, Texas Transportation Institute, College Station, TX, 2002.

Zou, J. *Development and Evaluation of an HMA Fracture Mechanics Based Model to Predict Top-Down Cracking in HMA Layers*, PhD Thesis, University of Florida, 2009.

APPENDIX A.
NCHRP 1-42A TOP-DOWN CRACKING MODELS

This appendix summarizes the Top-Down Cracking Models developed under the NCHRP 1-42A. All of the following information is from the final report (Roque et al. 2010).

The models and sub models developed in NCHRP 1-42A project can be divided into four categories:

- Material property models, which determine the AC layer stiffness, AC tensile strength, and Dissipated Creep Strain Energy threshold ($DCSE_f$) at given pavement depth while considering the aging effect.
- Pavement response models, which are used to predict bending-induced maximum surface tensile stresses away from the tire and transverse thermal stresses induced by thermal variation.
- Healing models, which include maximum healing potential model, daily based healing criterion, and yearly based healing criterion.
- Pavement fracture models, which are used to determine the load-associated damage (DCSE per cycle) and thermal-associated damage (DCSE per time interval) based on the tensile stress and thermal stress calculated by pavement response models. Upon accumulating the load-associated damage and thermal-associated damage, healing factors are incorporated. Finally, the crack amount model is used to convert the crack depth over AC layer thickness ratio (C/D) to crack amount.

These models and sub models are described below.

MATERIAL PROPERTY MODEL

Material property model has three sub-models:

- AC stiffness aging model.
- AC tensile strength model.
- DSCE threshold model.

AC Stiffness Aging Model

The AC stiffness aging model was developed on the basis of a binder aging model (Mirza and Witczak 1995) and a dynamic modulus model (Witazk and Fonseca 1996). In this model, the following empirical equation was identified to consider the aging effect on mixture stiffness:

$$|E^*|_t = |E^*|_0 \frac{\log \eta_t}{\log \eta_0} \tag{A-1}$$

where t is aging time, |E*|t and |E*|0 represent the stiffnesses corresponding to aged and unaged conditions, respectively, and ηt and η0 correspond to the aged and unaged binder viscosity. Then the stiffness at the surface of the AC layer can be determined as follows:

$$S(t) = \gamma \times |E^*|_t \ (t = 1800s) \tag{A-2}$$

where γ is reduction factor from compression to tension.

Similarly, for the stiffness at the given depth z of the AC layer, S(t,z) can be calculated by:

$$S(t,z) = \gamma \times |E^*|_{(t,z)} \ (t = 1800s) \tag{A-3}$$

AC Tensile Strength Model

The AC tensile strength aging model was developed by directly relating tensile strength to the AC stiffness aging model based on the following relationship that Deme and Young (*1987*) developed,

$$S_t(t,z) = \sum_{n=0}^{5} a_n \cdot [\log S(t,z)]^n \tag{A-4}$$

where $S_t(t,z)$ is the tensile strength at time t and depth z, and the constants are as follows:

a0=284.01, a1=-330.02, a2=151.02, a3=-34.03, a4=3.7786, a5=-0.1652

DCSE Threshold Model

First, the FE limit surface aging model was conceived and expressed in the following form:

$$FE_f(t) = FE_i - \left[FE_i - FE_{\min}\right] \cdot [S_n(t)]^{k1} \tag{A-5}$$

where

FE_i = the initial fracture energy.

FE_{min} = the minimum value of the *FE* limit after a sufficiently long aging period t_{inf}. FE_{min} was determined based on experience (field specimens) to be 0.2 kJ/m^3, and t_{inf} was chosen as 50 years.

k_1 = an aging parameter to be determined from calibration.

$S_n(t)$ = the normalized change of stiffness at the surface of the AC layer, and is expressed as

$$S_n(t) = \frac{S(t) - S_0}{S_{\max} - S_0} \tag{A-6}$$

where $S(t)$ is the stiffness at the surface of the AC layer. S_0 and S_{max} are $S(t)$ when t is set as 0 and 50 years, respectively. Therefore, it can be seen that $S_n(t)$ is a parameter that varies between 0 and 1. The following relationship was conceived to describe the FE limit versus depth relation:

$$FE_f(t,z) = FE_i - \left[FE_i - FE_f(t)\right] \cdot S(t,z)/S(t) \tag{A-7}$$

Based on the FE limit aging model, the DCSE threshold aging model was developed and is expressed as follows:

$$DSCE_f(t,z) = FE_f(t,z) - S_t^{\,2}(t,z)/(2 \cdot S(t,z)) \tag{A-8}$$

PAVEMENT RESPONSE MODELS

The pavement response model has two sub-models: the load response model and the thermal response model.

Load Response Model

The load response model was primarily used to predict bending-induced maximum surface tensile stresses away from the tire. The model first estimated the AC modulus based on the temperature profiles and aging conditions. The model then automatically searched for the maximum tensile stress on the surface of the AC layer. Figure A-1 shows the schematic plot. A 9-kip circular load was applied repeatedly to the surface of a pavement to simulate cyclic traffic loading. Each cycle included a 0.1 sec haversine loading period and 0.9 sec resting period. The stiffness gradient due to the temperature and aging effects was taken into account by dividing the AC layer into multiple sub-layers with different stiffnesses.

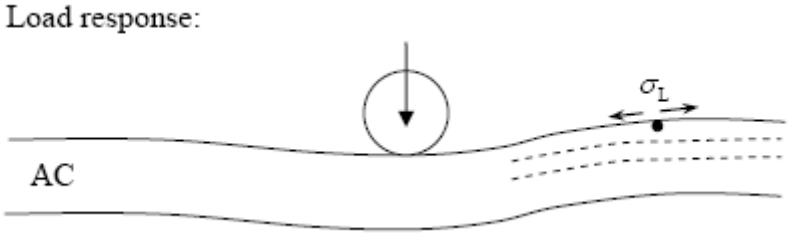

Figure A-1. Schematic Plot for Load Response at the Surface of the AC Layer (after Roque et al. 2010).

Thermal Response Model

The thermal response model predicts the thermally induced stresses in the transverse direction of asphalt concrete pavement. It was developed based on a thermal stress model for predicting thermal cracking (Hiltunen and Roque 1994). The existing model was intended to predict thermal stresses in the longitudinal direction. However, top-down cracking is known to occur in the longitudinal direction, so transverse, as opposed to longitudinal, thermal stresses are of particular relevance. Different boundary conditions to which the AC layer is subjected in these two directions caused the difference in transverse and longitudinal thermal stresses:

- The AC layer is subjected to a fixed boundary condition in the longitudinal direction, which can induce very high longitudinal thermal stresses and are the main cause of thermal cracking.
- However, the AC layer can move in the transverse direction once the maximum friction that the base provided is reached.
- Therefore, the transverse thermal stress, which contributes to top-down cracking, cannot exceed the friction limit. The limit value was determined to be 10 psi for typical HMA and base materials based on a separate calculation. Figure A-2 shows the transverse thermal stresses due to change of temperature in an AC layer.

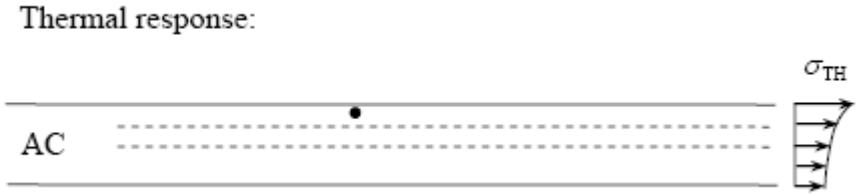

Figure A-2. Schematic Plot for Thermal Response in the AC Layer (after Roque et al. 2010).

HEALING MODELS

The healing models were completed in two steps. First, a maximum healing potential aging model was obtained based on the research of Kim and Roque (2006). Then, a simplified empirically based healing model and criteria were proposed.

Maximum Healing Potential Aging Model

The following relationship describes the maximum healing potential surface aging model:

$$h_{ym}(t) = 1 - [S_n(t)]^{FE_i/1.67} \quad \text{(A-9)}$$

where, h_{ym} is the yearly maximum healing potential, FEi is the initial fracture energy, $S_n(t)$ is the normalized change of stiffness at the surface of the AC layer, and t is time in years. The maximum healing potential versus depth relation is:

$$h_{ym}(t,z) = 1 - [1 - h_{ym}(t)] \cdot \frac{S(t,z)}{S(t)} \tag{A-10}$$

where $S(t,z)$ is the AC stiffness at time t and depth *z*, considering aging effect. $S(t)$ is the stiffness at surface of AC layer.

Daily-Based Healing Criterion

A daily based healing criterion was developed to estimate the recovered damage on any particular day. It was assumed that the damage generated in a day would be healed according to a daily normalized healing parameter, h_{dn}, which is defined as

$$h_{dn} = 1 - \frac{DCSE_{d\_remain}}{DCSE_{d\_induced}} \tag{A-11}$$

where $DCSE_{d\_induced}$ is the dissipated energy induced during the day, and $DCSE_{d\_remain}$ is the dissipated energy remaining at the end of the day after healing.

The daily normalized healing parameter, h_{dn}, is dependent on depth, time, and temperature. It was correlated with the daily lowest stiffness S_{low} of the AC layer. The rationale is that healing potential is believed to be closely related to the AC material's capacity to flow. Since S_{low} is the lowest stiffness of a day, it represents the highest flow capacity of the material on that day, which was used to estimate the material's healing potential.

The daily lowest stiffness can be determined using the daily highest temperature at any depth of the AC layer (refer to AC stiffness aging model). The corresponding daily lowest stiffness S_{low} for five successive years (each year was started from July 1st), after taking the effects of aging into account, are plotted in Figure A-3. In addition, two critical stiffness values S_{cr1} and S_{cr2} are also shown in the figure, which divide the S_{low} profile into the following three zones:

- S_{cr1} is the Lower Bound Value. It was assumed that the daily normalized healing parameter, h_{dn}, reached the maximum value of a year, i.e., h_{ym} representing the highest healing potential of the mixture for that year, when $S_{low} \leq S_{cr1}$ (i.e., when S_{low} falls into Zone A).

- S_{cr2} is the Upper Bound Value. It was assumed that h_{dn} reached the minimum value of a year, i.e., 0 representing the lowest healing potential of the mixture, when $S_{low} \geq S_{cr2}$ (i.e., when S_{low} falls into Zone C).
- For any S_{low} value that is between S_{cr1} and S_{cr2} (i.e., when S_{low} is in Zone B), h_{dn} can be determined by linear interpolation between 0 and h_{ym}, representing intermediate healing potentials.

S_{cr1} and S_{cr2} can be determined by the following example.

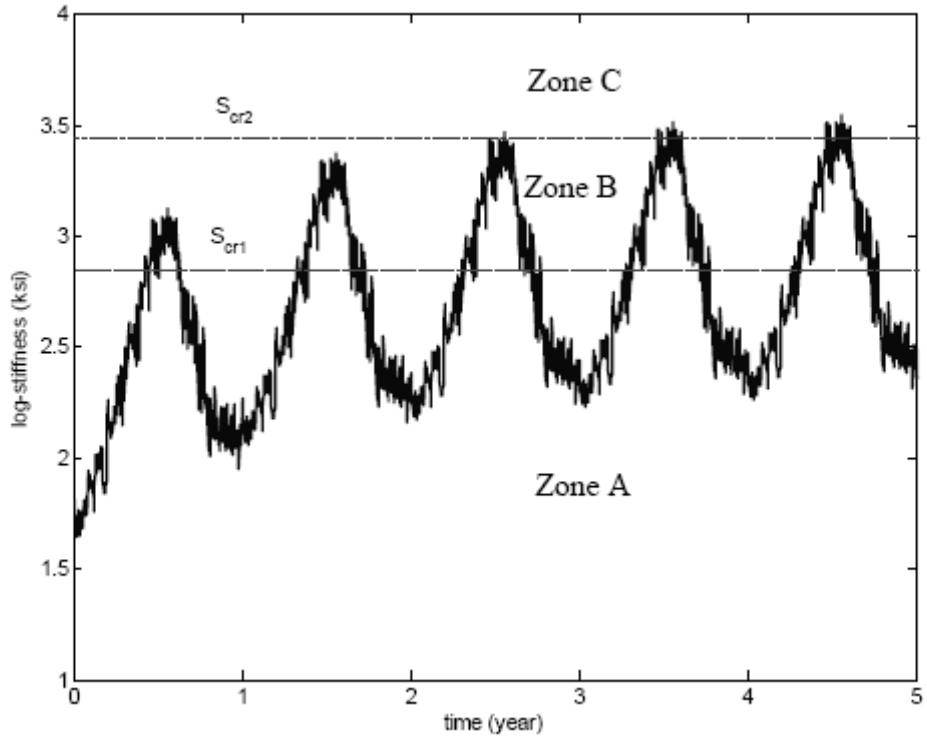

Figure A-3. Daily Lowest AC Stiffness (S_{low}) Profile and Two Critical Values (S_{cr1} & S_{cr2}) (after Roque et al. 2010).

To determine these two critical values S_{cr1} and S_{cr2}, the daily lowest AC stiffness curves in the aged and unaged sections are plotted in Figures A-4 and A-5, respectively. These test sections were built in Gainesville, Florida, for Accelerated Pavement Testing (APT). As shown, the stiffnesses of the aged section are much higher than the unaged section. As the measured binder viscosity indicates, the asphalt mixture at the surface of the aged section was extensively aged. Because this was greater than any value determined from field cores in typical Florida pavement, it was believed that no healing would occur in the mixture of this section. According to the definitions of healing zones, the S_{low} values for this section should be close to S_{cr2}. Therefore, the value for S_{cr2} was selected to be 2000 ksi.

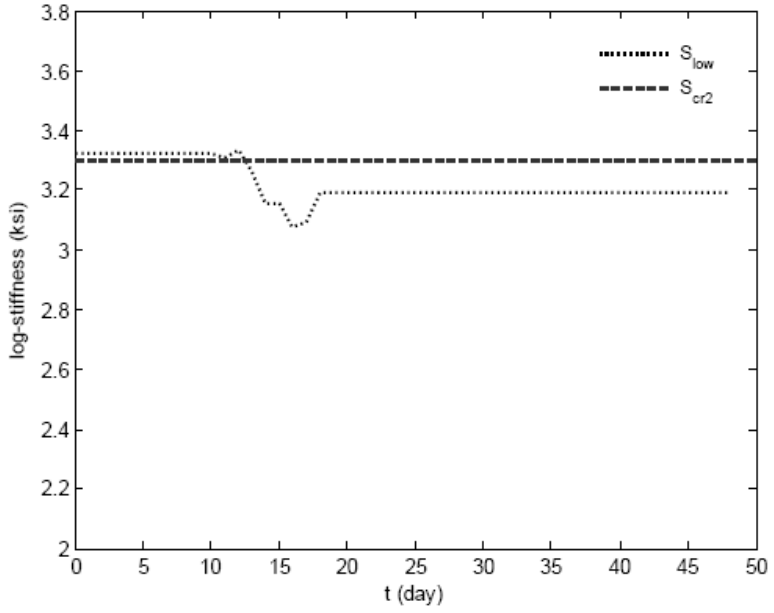

Figure A-4. Daily AC Stiffness of the Aged Section (after Roque et al. 2010).

On the other hand, the viscosity test results showed that the mixture in the unaged section was only slightly aged. This mixture was thus believed to have full healing potential. According to the definitions of healing zones, the S_{low} values for this section should be close to S_{cr1}. As a result, S_{cr1} was selected to be 320 ksi (see Figure A-5).

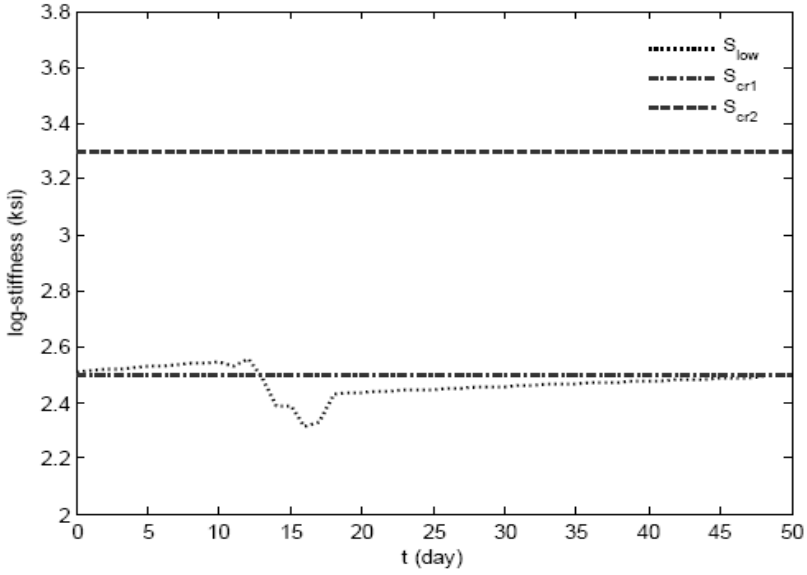

Figure A-5. Daily AC Stiffness of the Unaged Section (after Roque et al. 2010).

Yearly Based Healing Criterion

In the daily based healing criterion, the damage generated in any particular day will be healed only once during that day, after which no healing will be applied to remaining damage. This does not agree well with the observation from laboratory healing tests that indicated damage can be healed successively during any rest period that follows. Thus, a yearly based healing criterion was developed to address continuous healing. In this healing criterion, it was assumed that all damage accumulated during a yearly period (started from July 1st) can be at least partially healed according to a yearly normalized healing parameter h_{yn} which is defined as,

$$h_{yn} = 1 - \frac{DCSE_{y\_remain}}{DCSE_{y\_induced}} \tag{A-12}$$

where $DCSE_{y\_induced}$ is the dissipated energy induced during the year, and $DCSE_{y\_remain}$ is the dissipated energy remaining at the end of the year after healing.

The yearly normalized healing parameter h_{yn} was determined based on an average daily lowest stiffness S_{low} over a prolonged period T_p (i.e., the last 40 days of the yearly period being analyzed).

PAVEMENT FRACTURE MODELS

The pavement fracture model consists of three sub-models:

- Crack initiation model.
- Crack growth model.
- Crack amount model.

Crack Initiation Model

The load-associated damage per cycle (or, DCSEL/cycle) is calculated as:

$$DCSE_L / cycle = \int_0^{0.1} \sigma_{AVE} \sin(10\pi t)\, \dot{\varepsilon}_{p\max} \sin(10\pi t)\, dt \tag{A-13}$$

where σ_{AVE} is the average stress within the portion of the asphalt mixture being analyzed to determine whether a crack will initiate or propagate along that zone, and $\dot{\varepsilon}$ pmax is the maximum creep strain rate, which is determined from IDT creep tests at 1000-second loading time. Since:

$$\dot{\varepsilon}_p = \sigma_{AVE} \frac{dD(t)}{dt} = \sigma_{AVE} D_1 m t^{m-1} \tag{A-14}$$

where D_1 and m are the creep compliance power law parameters.

Then the following equation can be obtained:

$$DCSE_L / cycle = \tfrac{1}{20}\sigma_{AVE}[\sigma_{AVE} D_1 m(1000)]^{m-1} \quad \text{(A-15)}$$

The thermal-associated damage over the time interval from (t - Δt) to t (or, $DCSET/\Delta t$) is expressed as:

$$DCSE_T / \Delta T = [\sigma(t) - \sigma(t-\Delta t)] \cdot [\varepsilon_{cr}(t) - \varepsilon_{cr}(t-\Delta t)] / 2 \quad \text{(A-16)}$$

where ε_{cr} is creep strain at time t. It can be expressed as

$$\varepsilon_{cr}(t) = \varepsilon_{cr}(t-\Delta t) + \frac{1}{2 \cdot \eta_v}[\xi(t) - \xi(t-\Delta t)] \cdot [\sigma(t) + \sigma(t-\Delta t)] \quad \text{(A-17)}$$

where $\sigma(t)$ is thermal stress calculated using a thermal response model.

In the crack initiation model, the rule for crack initiation is given as follows:

$$DCSE_{norm}(t) = \frac{DCSE_{remain}(t)}{DCSE_f} \geq 1.0 \quad \text{(A-18)}$$

where $DCSE_{remain}$ is the accumulated dissipated energy when taking healing into account, $DCSE_f$ is the $DCSE$ limit accounting for its degradation with aging, and $DCSE_{norm}$ is the normalized damage accumulation. The threshold for crack initiation is 1.0. The $DCSE_{remain}$ during each time interval Δt can be further expressed as follows:

$$DSCE_{remain}(\Delta t) = (1 - h_{dn}) \cdot [n \cdot (DCSE_L / cycle) + DCSE_T(\Delta t)] \quad \text{(A-19)}$$

where n is number of load cycles in Δt.

Crack Growth Model

In the crack growth model, load-induced tensile stresses ahead of the crack tip were predicted using the DDBE model (Sangpetngam et al. 2003) as follows:

The pavement structure was discretized using quadratic displacement discontinuity (DD) boundary elements.

An initial crack was assumed to have a length of 6 mm (0.25 in.), which is about one-half of the nominal maximum aggregate size of typical asphalt mixtures. It was placed vertically at the location of the maximum surface tensile stress and discretized using DD boundary elements.

The load used for the 2-D model was adjusted so that the maximum tensile stress at the surface of the pavement that the 2-D model predicted can be matched with the prediction of the 3-D LEA program.

The near-tip thermal stresses were estimated by applying the stress intensity factor (SIF) of an edge crack to the thermal stresses predicted using the thermal response model.

The load-associated damage and thermal-associated damage were then calculated in the same manner as introduced in the crack initiation model. The same rule as used for determination of crack initiation was adopted in the crack growth model. Once the rule was satisfied (i.e., the $DCSE_{norm}$ reached 1.0), the crack started to grow.

Some key terms used during simulation of step-wise crack growth are explained below:

- Potential crack path: The potential crack path was predefined in front of the crack tip at the beginning of crack growth simulation. It was composed of a series of zones of constant length heading toward the bottom of the AC layer.
- Zone (in the potential crack path): The zone is a means used to discretize the potential crack path to facilitate the calculation of crack growth. A constant zone length was used because it is far more computationally efficient than using variable zone lengths, with relatively little effect on the crack growth prediction. It was observed from lab testing that cracking develops in a stepwise manner in asphalt mixtures. For typical asphalt mixtures with a nominal maximum aggregate size (NMAS) of 12.5 mm, the stepwise-developed crack length is about one-half of the NMAS, which is about 6 mm. So, 6 mm (0.25 in.) was selected as the constant zone length.
- Critical crack depth (CDc): The critical crack depth is the final crack depth in the crack growth model, which was preset to be one-half the depth of the AC layer, as field observations showed that top-down cracking generally does not exceed that depth.

Crack Amount Model

The crack amount model was developed based on the following assumptions:

- For a 100-ft long pavement section, the maximum crack amount was assumed to be 330 ft. The pavement was determined to be severely cracked if total crack amount exceeded 330 ft.

- The crack amount, between 0 and the specified maximum value, was assumed to be linearly proportional to the crack depth over AC layer thickness ratio (C/D), which ranges from zero to 0.5 (i.e., when crack depth is equal to CDc). The rationale is that generally, as a crack gets deeper, the crack mouth opening gets wider. Also, for a crack of the same depth (i.e., same C), the crack mouth opening is wider in a thinner

layer than in a thicker layer. Therefore, it seems logical to assume that the probability that a crack is visible and counted as a crack (and therefore the probability of increase in crack amount) increases as the C/D ratio increases. The assumption that the relationship is linear is a first order approximation.

- In accordance with the definition for crack initiation in terms of the crack depth (refer to crack initiation model), the onset of a crack in terms of the crack amount was assumed to be triggered by observing an amount of cracking of at least 12 ft.

Based on the above assumptions, the crack amount versus time relationship can be obtained from the crack depth versus time relationship that the crack growth model predicted. Using this model, the predicted amount of cracking at initiation is greater than 12 ft for any pavement that has an HMA layer thickness of no larger than 12 in.

NCHRP 1-42A TOP-DOWN CRACKING MODELS PREDICTION RESULTS

The model predictions were compared between with and without consideration of the healing effect.

Model Predictions without Healing

When the healing effect was not considered, the predicted load passes to induce crack initiation for the aged and unaged sections are given in Figure A-6. As seen in the figure, the predicted number of loads to cracking for the unaged section was only about 41,700 loads, which was much less than the 128,300 loads for the aged section. The predictions in terms of DCSE norm versus time also showed the trend that the unaged section required less time for crack initiation than the aged one.

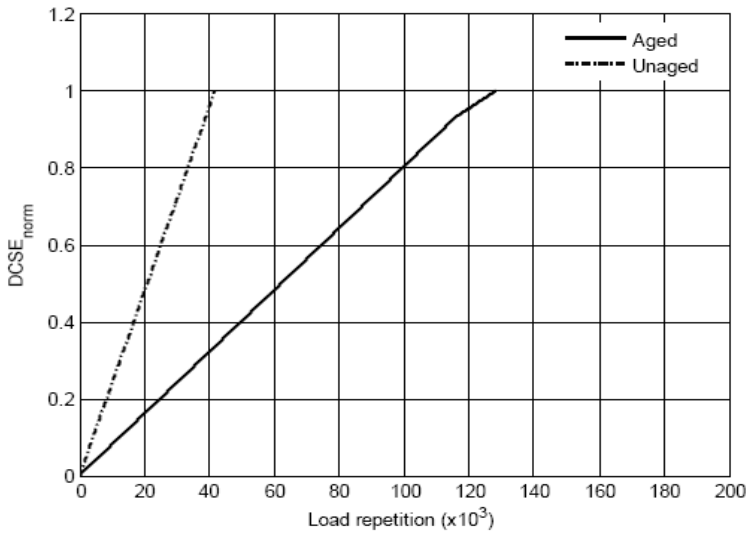

Figure A-6. Prediction of Crack Initiation without Healing: Damage versus Load Repetition (after Roque et al. 2010).

Figure A-7 shows the step-wise increase of crack depth with load passes for both the aged and unaged sections. In general, the crack propagates at a relatively low rate initially (e.g., for the first zone). The rate of growth then increases for the next few zones, beyond which the rate slows down again. As also shown in Figure A-6, the load repetitions to the critical crack depth (i.e., 3 in. for these two sections) is about 129,200 for the unaged section. Meanwhile, the load repetitions to 3 in. depth of the aged section is about 295,900, which was much more than that for the unaged section. Given the time to crack initiation, an average crack growth rate in the unaged section can be estimated to be 0.34 in/day, which is more than 1.5 times the value, i.e., 0.20 in/day obtained for the aged section.

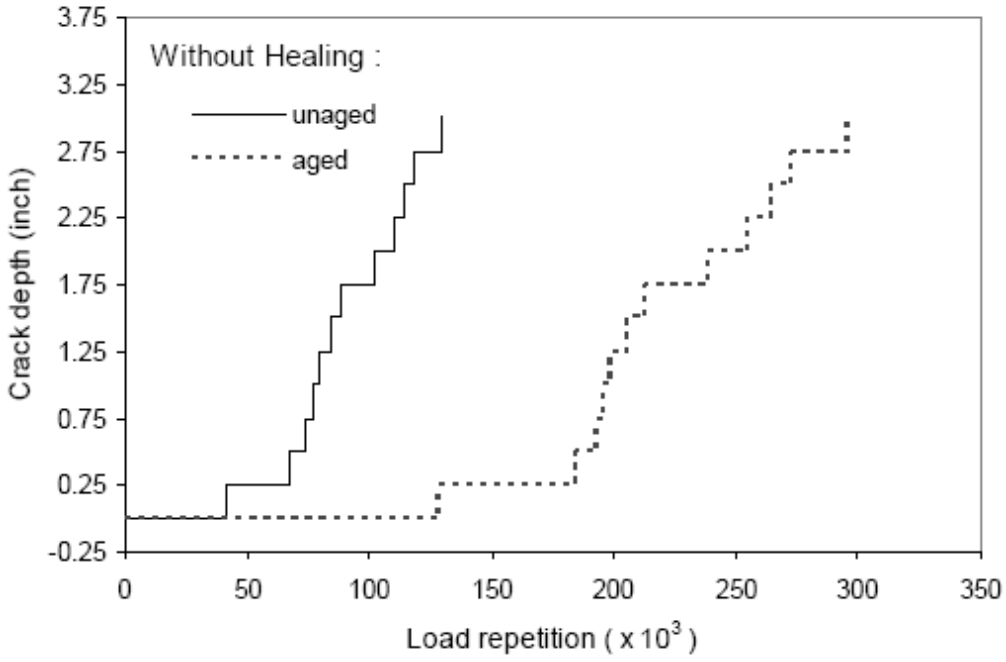

Figure A-7. Prediction of Crack Growth without Healing: Crack Depth versus Load Repetition (after Roque et al. 2010).

It is clear that the predicted results in terms of both crack initiation and propagation in the unaged section do not make sense (Roque et al. 2010).

Model Predictions with Healing

Another set of predictions were made using the performance model after incorporating the healing model (see Figures A-8 and A-9). The predictions after incorporation of the healing model agreed well with observations from cores, which indicated that the crack had propagated to about half the depth of the AC layer of the aged section (Roque et al. 2010).

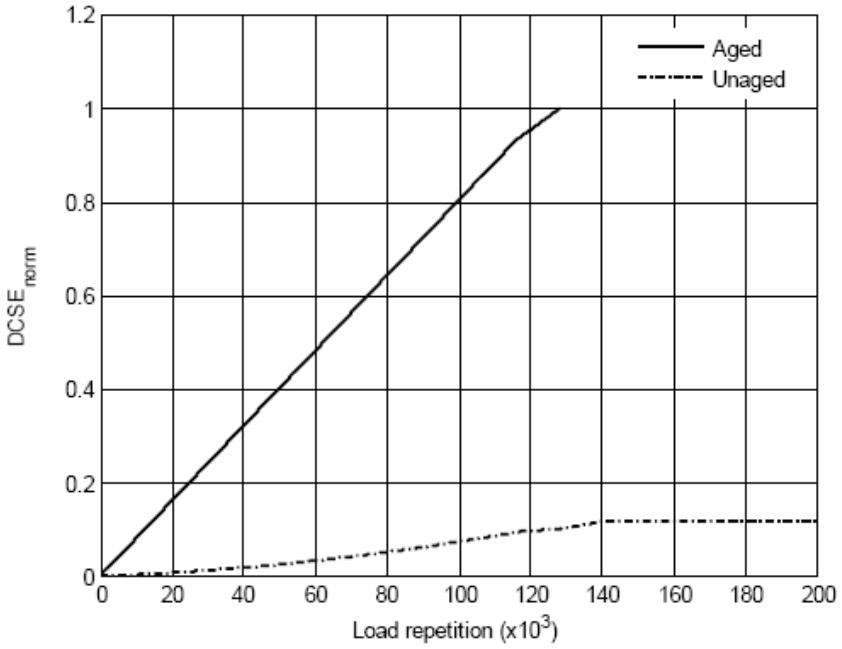

Figure A-8. Prediction of Crack Initiation with Healing: Damage versus Load Repetition (after Roque et al. 2010).

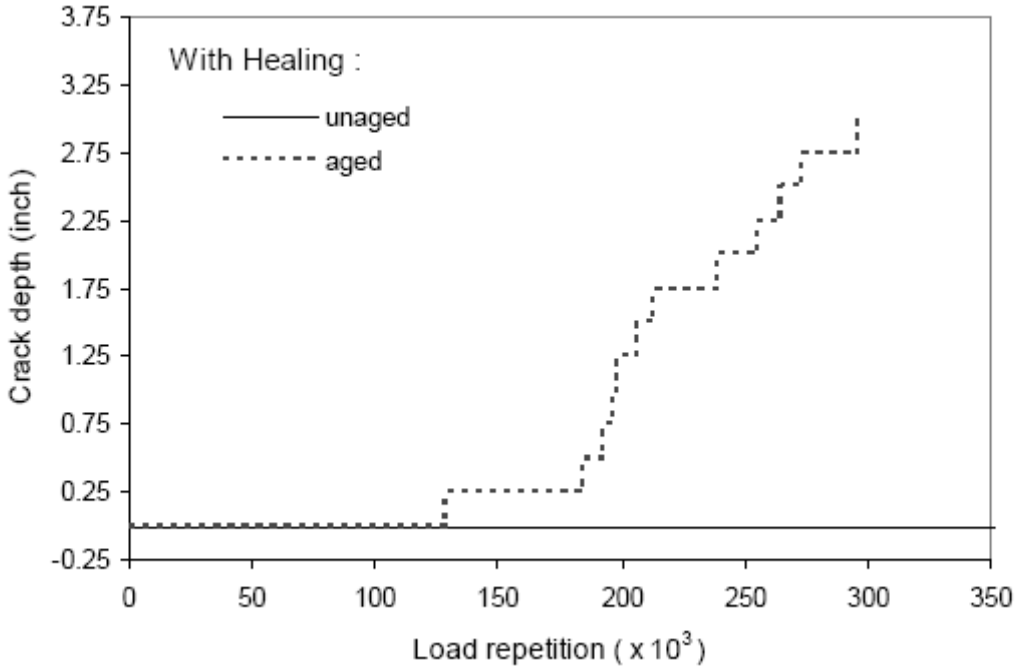

Figure A-9. Prediction of Crack Growth with Healing: Crack Depth versus Load Repetition (after Roque et al. 2010).

REFERENCES

Kim, B., and R. Roque. Evaluation of Healing Property of Asphalt Mixtures. *Transportation Research Record: Journal of the Transportation Research Board, No. 1970*, Transportation Research Board of the National Academies, Washington, D.C., pp. 84–91, 2006.

Roque, R., J. Zou, Y. R. Kim, C. Baek, S. Thirunavukkarasu, B. S. Underwood, and M. N. Guddati. *Top-Down Cracking of Hot-Mix Asphalt Layers: Models for Initiation and Propagation.* Final Report, NCHRP Web-Only Document 162, 2010.

Sangpetngam, B., B. Birgisson, and R. Roque. Development of Efficient Crack Growth Simulator Based on Hot-mix Asphalt Fracture Mechanics. In *Transportation Research Record: Journal of the Transportation Research Board, No. 1832*, Transportation Research Board of the National Academies, Washington, D.C., pp. 105–112, 2003.

APPENDIX B.
RELIABILITY APPROACHES USED IN DIFFERENT PAVEMENT DESIGN AND ANALYSIS SYSTEMS

Several methods can be adopted to perform reliability-based design, ranging from closed-form approaches to simulation-based methods. However, some methods may be more suitable than others given the complexities of the design procedure. The following approaches will be reviewed and discussed below.

- Reliability approach used in TxDOT's current FPS system.
- Reliability approach used in the AASHTO 1993 design guide.
- Reliability approach used in the VESYS design system.
- Reliability approach used in the MEPDG.
- Reliability approach used in the CalME.

FLEXIBLE PAVEMENT DESIGN

FPS21 is currently used statewide in Texas for flexible pavement designs. The first version of FPS (FPS11) was developed in 1968 (Scrivner et al. 1968) under the American Association of State Highway Officials (AASHO) Road Test study. Following that version, Darter and Hudson (1973) pioneered the use of a reliability-based approach for pavement design in the FPS (FPS13). The reliability factor was introduced in the system to take into account the inherent variability that exists in pavement design and construction. Then Scullion and Michalak (1997) embedded a multilayered linear elastic program to compute the pavement response directly and formed the FPS19 and then FPS19 Windows version, FPS19W (Liu and Scullion 2006). The latest version of FPS is FPS21W, which TxDOT has approved.

FPS11

FPS11 included a pavement performance equation, which predicts serviceability loss as a function of the structural curvature index (SCI), layer materials stiffness coefficients, initial and terminal serviceability, equivalent single axle loads, and temperature and swelling clay parameters (Scrivner et al. 1968). The performance equation developed for FPS is as follows:

$$\log N = \log Q + \log \alpha - 2\log SCI - \log B + 6.0 \quad \text{(B-1)}$$

where

Q $= \sqrt{5-P2} - \sqrt{5-P1}$.

$P2$ = minimum acceptable serviceability index.
$P1$ = initial serviceability index.
B = regression coefficient.
SCI = surface curvature index of pavement structure, in inches * 10^{-3}; SCI is a function of a_i (stiffness coefficient) and Di (thickness) for each pavement layer and subgrade.
N = number of predicted equivalent 18-kip single-axle load applications.
α = harmonic mean temperature.

FPS11 uses a *deterministic* approach. By comparing the predicted N with the applied ESALs during the design period, a series of pavement structure combinations which meet the requirement can be screened out.

FPS13

To take into account the inherent variability that exists in pavement design and construction, Darter and Hudson (1973) developed a reliability-based approach for FPS. This approach is a *closed-form approach based on a Taylor's Series expansion technique* (Huang 2004):

$$V[f(x_i)] \approx \sum_{i=1}^{n} \left(\frac{\partial f}{\partial x_i} \right)^2 V(x_i) \tag{B-2}$$

where V is the variance σ^2 and f means function.

For example, Equation B-1 can be expressed as

$$\log N = \log(\sqrt{5-P2} - \sqrt{5-P1}) + \log \alpha - 2\log SCI - \log B + 6.0 \tag{B-3}$$

The variance of $log\ N$ (V_{logN}) can be determined directly according to Equation B-2:

$$V[\log N] \approx (\frac{\partial \log N}{\partial P1})^2 V[P1] + (\frac{\partial \log N}{\partial \alpha})^2 V[\alpha] + (\frac{\partial \log N}{\partial SCI})^2 V[SCI] \tag{B-4}$$

where $V[SCI]$ can be determined in a similar way as Equation B-2 since SCI is an explicit function of a_i (stiffness coefficient) and D_i (thickness) for each pavement layer and subgrade combination (*Scrivner et al. 1968*).

It means that $V[a_i]$, $V[D_i]$, and the final standard deviation of N (σ) can be determined directly given the standard deviations of each input parameter, such as $V[P_1]$, $V[\alpha]$. Then,

$$\log N_r = \overline{\log N} + Z\sigma \text{ , (Z <0)} \quad \text{(B-5)}$$

where

$$\overline{\log N} = \log(\sqrt{5 - P2} - \sqrt{5 - \overline{P1}}) + \log \overline{\alpha} - 2\log \overline{SCI} - \log B + 6.0 \quad \text{(B-6)}$$

and *Z* is normal deviate that depends on level of reliability (or confidence level) and *Nr* is the final predicted *N*, and $\sigma = \sqrt{V[\log N]}$.

The prerequisite of the closed-form approach is that all the calculations should have explicit formulations and the first-order and second-order partial derivatives of these formulations can be deduced.

FPS19W/FPS21W

In the current version, FPS19W/FPS21W, the use of a linear elastic multilayered model has replaced the use of stiffness coefficients to calculate surface deflections under the load and at 0.3 m from the point of load application. It uses pavement layer moduli, Poisson's ratio, and thickness to predict pavement deflections in calculating the *SCI*. Since explicit formulations cannot express this calculation, the variance of *SCI* cannot be determined directly; regression equations were developed to determine this value empirically. For simplicity, some default standard deviations of input parameters (such as P_1 and α) were provided in the program so that users do not need to input these values. The reliability in FPS19W/FPS21W is considered by adjusting the estimated traffic (ESALs in 20 years).

AASHTO 1993 PAVEMENT DESIGN GUIDE

AASHTO 1993 pavement design guide defines reliability in terms of the number of predicted equivalent single axle loads to terminal serviceability being less than the number of equivalent single axle loads actually applied to the pavement (AASHTO 1993).

The reliability factor is comprised of two variables: standard normal deviate Z_R and combined standard error, S_0. Z_R corresponds to a desired probability of exceedance level. For example, a designer may specify that there should only be a 5 percent chance that the design does not last a specified number of years (e.g., 20 years). This is the same as stating that there should be a 95 percent chance that the design does last the specified number of years (e.g., 20 years). Then, the reliability is 95 percent (100 percent − 5 percent), and the corresponding Z_R value is −1.645 for one-sided confidence interval (AASHTO 1993).

S_0 defines how widely the two basic design inputs, traffic and performance, can vary. For instance, traffic may be estimated at 2,000,000 ESALs over 20 years. However, actual traffic may turn out to be 2,500,000 ESALs over 20 years due to unanticipated population growth.

Similarly, pavement design factors may turn out to be different than estimated. What these two brief examples are expressing is that structural design input values can vary from those initially chosen and the performance equation must account for this somehow. The more these values vary, the higher the value of S_0.

The basic 1993 AASHTO Guide flexible design equation is:

$$\log_{10}(W_{18}) = 9.36 \times \log_{10}(SN+1) - 0.2 + \frac{\log_{10}(\frac{\Delta PSI}{2.7})}{0.4 + \frac{1094}{(SN+1)^{5.19}}} + 2.32 \times \log_{10}(M_R) - 8.07 \quad \text{(B-7)}$$

where

W_{18} = predicted number of 80 kN (18,000 lb) ESALs.
SN = $\Sigma a_i D_i m_i$
a_i = i^{th} layer coefficient.
D_i = i^{th} layer thickness (in.).
m_i = i^{th} layer drainage coefficient.
ΔPSI = difference between the initial design serviceability index, p_0, and the design terminal serviceability index, p_t.
M_R = subgrade resilient modulus (in psi).

The right side of the above equation is then augmented with S_0 (to account for input value variability) and Z_R (to establish a confidence level that a certain design will perform as intended) to obtain the final form of the equation:

$$\log_{10}(W_{18}) = Z_R \times S_0 + 9.36 \times \log_{10}(SN+1) - 0.2 + \frac{\log_{10}(\frac{\Delta PSI}{2.7})}{0.4 + \frac{1094}{(SN+1)^{5.19}}} + 2.32 \times \log_{10}(M_R) - 8.07 \quad \text{(B-8)}$$

Values of Z_R are always negative. Therefore, the quantity ($Z_R \times S_0$) is always negative and will serve to decrease the predicted number of 80 kN (18,000 lb) ESALs that a particular design can accommodate.

Each agency that uses the 1993 AASHTO Guide design equation can choose its own levels of reliability. However, the 1993 AASHTO Guide provides some recommended levels (reproduced in Table B-1).

Table B-1. Suggested Levels of Reliability for Various Functional Classifications (after AASHTO 1993).

Functional Classification	Recommended Level of Reliability	
	Urban	Rural
Interstate and Other Freeways	85–99.9	80–99.9
Principal Arterials	80–99	75–95
Collectors	80–95	75–95
Local	50–80	50–80

Typical values of S_0 used are 0.40 to 0.50 for flexible pavements.

AASHTO 1993 reliability approach sometimes results in a net effect of a thick pavement that implies higher reliability, but thicker pavements are not always the answer because there are other critical aspects that the design guide considers (Darter et al. 2005).

VESYS DESIGN SYSTEM

In the VESYS design system, the reliability of a pavement system at any time *t*, is given by the probability that the serviceability index PSI is above some unacceptable level PSI_f which has been established beforehand (Kenis 1978):

$$\text{Reliability}=\Pr\{PSI > PSI_f\}=1-F(PSI_f) \quad \text{(B-9)}$$

where,
PSI = present serviceability index at time *t*.
PSI_f = limiting or failure level of present serviceability index.
$F(PSI_f)$ = cumulative distribution of *PSI* evaluated at PSI_f (see Figure B-1).

The distribution of *PSI* is obtained assuming a Gaussian distribution (normal distribution).

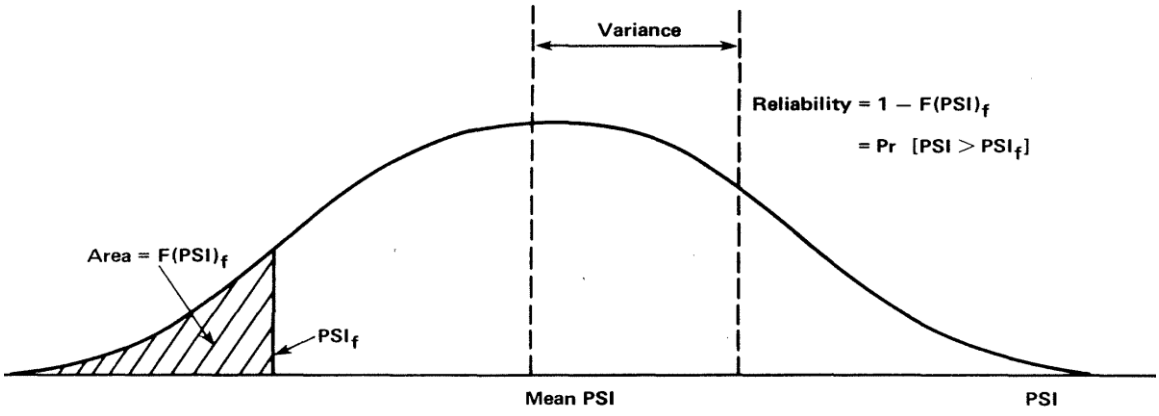

Figure B-1. Schematic of PSI Probability Density Function.

PSI is defined as follows:

$$PSI = PSI_I - (1.91)\log_{10}(1+SV) - (1.38)R_D^2 - 0.01Cr^{0.5} \quad \text{(B-10)}$$

where

PSI_I = initial serviceability index.
SV = slope variance, radian*10^{-6}.
R_D = average rut depth, in.
Cr = area cracked, $ft^2/1000\ ft^2$.

Equation B-11 is the roughness model, where,

$$SV = \frac{2B}{C^2} Var(\eta) E[R_D]^2 \quad \text{(B-11)}$$

B and C are pavement system properties defining correlation along the pavement.
η is a random variable expressing the variation in material properties along the pavement.
E[R_D] is the mean of rut depth.

The rutting model to determine the R_D is as follows:

$$R_D = \int_{N1}^{N2} U_s^{+} \frac{e_t}{e_s} \mu_{sub} N^{\alpha_{sub}} + \sum_{i=1}^{n-1} \int_{N1}^{N2} (U_i^{+} - U_i^{-}) \mu_i N^{\alpha_i} \quad \text{(B-12)}$$

where

U_s^{+} = deflection at top of the subgrade due to single axle load.
U_i^{+} and U_i^{-} = deflection at top and bottom of finite layer *i* due to axle group.
e_t = compressive strain at top of subgrade due to the axle group.
e_s = compressive strain at top of subgrade due to a single axle.
μ_{sub} and α_{sub} = permanent deformation parameters of the subgrade.
μ_i and α_i = permanent deformation parameters of layer *I*; n is total number of layers.

The cracking model to determine C_r is:

$$E[Cr] = \sum_{q=1}^{Q} E[n_q] E[\frac{1}{N_q}] \quad \text{(B-13)}$$

where n_q= current number of load repetitions in the q^{th} incremental analysis period and
N_q=number of load repetitions to fatigue failure in the q^{th} incremental analysis period, and

$$N_q = k_1 \varepsilon^{-k_2} \quad \text{(B-14)}$$

where ε=maximum tensile stain, k_1 and k_2 are model parameters.

In VESYS, the primary response models to determine stress, strain, or deformation are established based on a three-layer semi-infinite continuum such that the upper two layers are finite in thickness while the third layer is infinite.

There are closed-form probabilistic solutions for this three-layer linear viscoelastic boundary value problem (Moavenzadeh and Elliott 1968, Brademeyer 1975). It is valid for single stationary circular loading at the pavement's surface and the geometry of the three-layered system should be deterministic (such as layer thicknesses, radius of applied load, and horizontal offset of the point of interest from the axis of the applied loading etc.).

In summary, VESYS is also a closed-form reliability approach. It can only be used to analyze three-layer systems and the layer thicknesses have to be deterministic.

MEPDG

Depending on user choice, MEPDG design reliability can be considered

- Directly for each key distress type.
- By using an overall measure of pavement performance (such as ride quality).
- Both methods (NCHRP 2004).

Definition of Reliability in MEPDG

Design reliability, *R*, is defined as the probability, *P*, that each of the key distress types and smoothness will be less than a selected critical level over the design period.

R=*P*(distress over design period < critical distress level)

Design reliability is defined for smoothness (IRI) as follows:

R=*P*(IRI over design period < critical IRI level).

MEPDG Reliability Evaluation Approach

Dater et al. (2005) proposed the Monte Carlo method and preliminarily incorporated this simulation into the MEPDG JPCP cracking prediction after using neural networks (NNs) as a substitute for the ISLAB2000 finite element (FE) model and found a promising result. However, when the research team attempted to develop a similar approach for flexible pavement, they found the reliability analysis to be computationally prohibitive. Because the reliability analysis was supposed to be the same for rigid and flexible pavements, the MEPDG development team was forced to consider alternative solutions, which are described below.

To evaluate the reliability of a selected pavement structure, the current MEPDG procedure utilizes the overall standard deviation of the measured distresses, obtained from calibration against distressed pavements, in comparison with predicted values.

For example, to calibrate bottom-up fatigue (alligator) cracking, first the data were grouped based on the predicted log(Damage [%]), then the standard deviation of measured cracking data of each corresponding group was calculated. See Tables B-2 and B-3. Following that calculation, the relationship between standard deviation of measured cracking and mean predicted cracking log(Damage[%]) was established (see Figure B-2 [NCHRP 2004]).

Table B-2. Group of Predicted log(Damage [%]) Data.

Group	Range of Predicted log(Damage [%])	Number of Data Points	Mean of the Predicted log(Damage [%])
1	<−2	18	−2.5
2	−2 to −1	47	−1.4
3	−1 to 0	161	−0.45
4	0 to 1	158	0.45
5	>1	77	1.3

Table B-3. Standard Deviation of Measured Cracking for Each Group.

Group	Standard Deviation of Measured Cracking (%)
1	0.681458
2	0.562037
3	1.811323
4	6.224589
5	12.04897

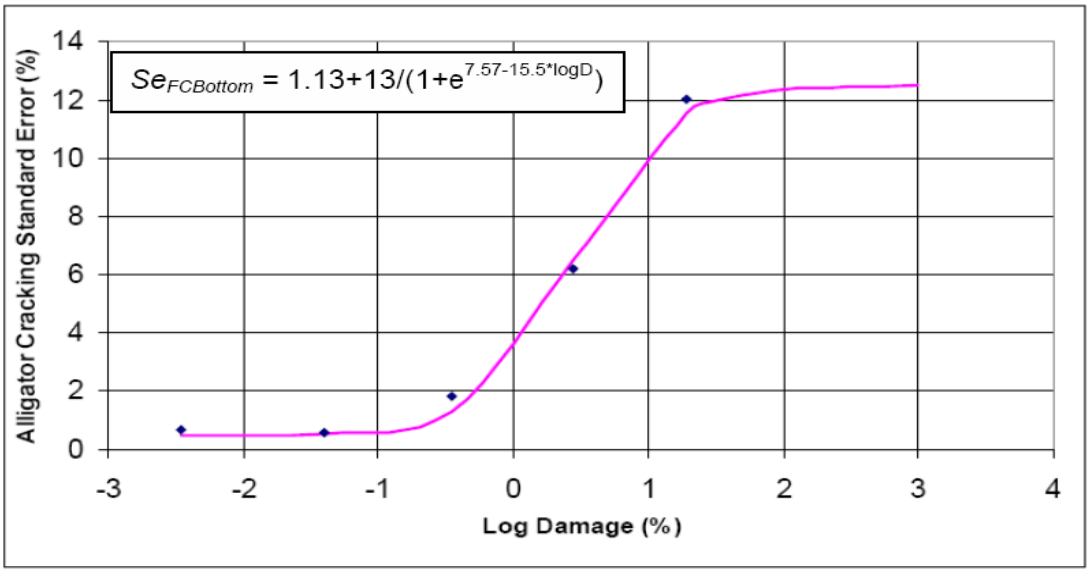

Figure B-2. Relationship between Standard Deviation of Measured Cracking and Mean Predicted Cracking Log(Damage [%]).

The key point of this technique is using the standard deviation of measured data as a substitute for the standard deviation of predicted data. According to the relationship in Figure B-2, the standard deviation corresponding to a given mean predicted data can be obtained.

With a known standard deviation for each distress, the MEPDG adjusts distresses for the desired reliability level using the following relationship:

$$Distress\_P = Distress\_mean + STD_{distress\_mea} \times Z_P \quad \text{(B-15)}$$

where,

Distress_P = distress level corresponding to the reliability level *P*.

Distress_mean = distress predicted using the MEPDG deterministic model with mean inputs (corresponding to 50% reliability).

$STD_{distress\_mean}$ = standard deviation of distress corresponding to distress predicted using the deterministic model with mean inputs.

Z_P = standardized normal deviate corresponding to reliability level *P*.

This technique is relatively simple compared to the closed-form method or the Monte Carlo simulation method. It also represents a step forward compared with AASHTO 1993 reliability analysis because in this way the standard deviation was related to the mean predicted value rather than a single, predefined empirical value. However, it is far from accurate because this procedure is inherently incapable of predicting the cumulative effect of the uncertainties in input variables. It relies on a set of predetermined variability values obtained from a performance

database rather than on those based on the site-specific input parameters that induce such uncertainty in distress prediction.

CALME

CalME is a computer program developed by the California Department of Transportation for analysis and design of flexible pavement rehabilitation strategies, asphalt overlay requirements, and new/reconstruction of flexible pavements. CalME was developed beginning in the late 1990s using research products from SHRP (1989–1993), subsequent research and development sponsored by Caltrans, and models and data from research programs around the world. CalME was developed to fill the needs listed above through a mechanistic-empirical analysis tool for use in California (Ullidtz et al. 2010).

CalME has the ability to consider variability through Monte Carlo simulation with reasonable run times. It can run one simulation per minute on a 2007 model X61s Lenovo laptop computer (Ullidtz et al. 2010). For nine uncertain variables, 1000 simulations may be needed based on the opinions of CalME researchers.

CalME researchers are also developing a method for determining convergence in the Monte Carlo simulation procedure, allowing one to, on the one hand, have confidence that the result of simulation is close to the true result and, on the other hand, to not perform more simulations than necessary to achieve that accuracy. Basically, the Monte Carlo simulation technique consists of five essential steps (Thyagarajan 2009):

Step 1: Formulate the problem in terms of all the random variables. This first step in simulation is to identify the variables having uncertainty or variability. The given problem is defined in terms of identified random variables. The deterministic variables are substituted into the explicit or implicit relations available to reduce the problem in terms of only response and random variables.

Step 2: Quantify the probabilistic characteristics of all the random variables in terms of their probability density functions and the corresponding parameters.

Step 3: Generate the values of these random variables. Random numbers are generated according to a specific distribution. In general, all modern computers have the capability to generate uniformly distributed random numbers between 0 and 1. Corresponding to an arbitrary seed value, the generators will produce the required number (N) of uniform random numbers between 0 and 1. By changing the seed value, different sets of random numbers can be generated. Depending on the size of the computer, the random numbers may be repeated after generating large quantities.

Step 4: Evaluate the problem deterministically for each set of realizations of all the random variables. The generated uniformly random variables (u) between 0 and 1 are to be converted to

a required distribution of the corresponding random variable X. The process requires transformation of uniform random variables to standard normal variables and then to random numbers with the appropriate characteristics. This process is commonly known as the inverse transformation technique or inverse cumulative density function (CDF) method (Nowak and Collins 2000).

Step 5: Extract the probabilistic information from N such realizations. N corresponding realizations of random numbers (Xi) were obtained from N uniform random numbers generated for each of the random variables (Xi) in the problem.

Thus, solving the problem using these N realizations deterministically will give N response variables. These variables can then be used to calculate all the required sample statistics, the histogram, the frequency diagram, the corresponding CDF, and the probability of failure considering various performance criteria. The accuracy of the technique increases as the number of simulations N increases.

Appendix C has detailed information and demonstrations about the Monte Carlo simulation.

REFERENCES

AASHTO Guide for Design of Pavement Structures, American Association of State Highway and Transportation Officials, 1993.

Darter, M., and W.R. Hudson. *Probabilistic Design Concepts Applied to Flexible Pavement System Design*, Report 123-18. Center for Highway Research, University of Texas at Austin, 1973.

Darter, M., L. Khazanovich, T. Yu, and J. Mallela. Reliability Analysis of Cracking and Faulting Prediction in the New Mechanistic-Empirical Pavement Design Procedure, *Transportation Research Record*, No. 1936, pp. 150–160, 2005.

Liu, W., and T. Scullion. *Flexible Pavement Design System FPS 19W: User's Manual (Reprint)*, TxDOT Research Report 0-1869-1, Texas Transportation Institute, Texas A&M University System, 2006.

Kenis, W. J. *An Interim Design Method for Flexible Pavements Using the VESYS Structural Subsystem*, FHWA Report, RD-77-154, 1978.

NCHRP, *Guide for Mechanistic-Empirical Design of Pavement Structures*, NCHRP Project 1 37A, National Cooperative Highway Research Program, Washington, D.C., 2004.

Nowak, A. S. and K. Collins. *Reliability of Structures*. McGraw-Hill Publisher, 2000.

Scrivner, F. H., W. M. Moore, W. F. McFarland, and G. R. Carey, *A Systems Approach to the Flexible Pavement Design Problem*, TxDOT Research Report 32-11, Texas Transportation Institute, Texas A&M University System, 1968.

Scullion, T., and C. H. Michalak. *Flexible Pavement Design System (FPS) 19: User's Manual*, TxDOT Research Report 1987-2, Texas Transportation Institute, Texas A&M University System, 1997.

Thyagarajan. S. *Improvements to Strain Computation and Reliability Analysis of Flexible Pavements in the Mechanistic-Empirical Pavement Design Guide*, PhD Dissertation, Washington State University, Pullman, WA, 2009.

Ullidtz, P., J. T. Harvey, I. Basheer, D. Jones, R. Wu, J. Lea, and Q. Lu. CalME, a Mechanistic–Empirical Program to Analyze and Design Flexible Pavement Rehabilitation. In *Transportation Research Record: Journal of the Transportation Research Board*, No. 2087, Transportation Research Board of the National Academies, Washington, D.C., pp. 143–152, 2010.

APPENDIX C.
EXAMPLES AND COMPARISONS AMONG CLOSED-FORM METHOD, ROSENBLUETH METHODS, AND MONTE CARLO SIMULATION METHOD

This appendix presents three examples to demonstrate the Closed-form method, Rosenblueth's 2^n and $2n+1$ methods (Rosenblueth 1975), and the Monte Carlo simulation method, and compares the accuracy of each method with the closed-form method.

EXAMPLE 1

*Y=X1*X2*X3*, where *X1*, *X2*, and *X3* are independent variables, and their distribution characteristics are listed in Table C-1.

Table C-1. Mean Value, Standard Deviation, CV, and Distribution Type of Variables.

	Mean value (μ)	Std. Dev. (σ)	CV (%)	Distribution type
X1	10	2	20	Normal
X2	4	1	25	Normal
X3	5	1.5	30	Normal

Closed-Form Solution

$$\frac{\partial y}{\partial x1} = X2 * X3\big|_{\mu} = 4 * 5 = 20 \tag{C-1}$$

$$\frac{\partial y}{\partial x2} = X1 * X3\big|_{\mu} = 10 * 5 = 50 \tag{C-2}$$

$$\frac{\partial y}{\partial x3} = X1 * X2\big|_{\mu} = 10 * 4 = 40 \tag{C-3}$$

$$\frac{\partial^2 y}{\partial x1^2} = \frac{\partial^2 y}{\partial x2^2} = \frac{\partial^2 y}{\partial x3^2} = 0 \tag{C-4}$$

$$\mu_y = u_{x1} \times \mu_{x2} \times \mu_{x3} + 0.5 \times \left[(\frac{\partial^2 y}{\partial x1^2}) \times \sigma_{X1}{}^2 + (\frac{\partial^2 y}{\partial x2^2}) \times \sigma_{X2}{}^2 + (\frac{\partial^2 y}{\partial x3^2}) \times \sigma_{X3}{}^2 \right] = 200 \tag{C-5}$$

$$\sigma_y = \sqrt{\left[(\frac{\partial y}{\partial x1}) \times {\sigma_{X1}}^2 + (\frac{\partial y}{\partial x2}) \times {\sigma_{X2}}^2 + (\frac{\partial y}{\partial x3}) \times {\sigma_{X3}}^2 \right]} = \sqrt{20^2 \times 2^2 + 50^2 \times 1^2 + 40^2 \times 1.5^2}$$
$$= 87.7496$$

(C-6)

Rosenblueth's 2^n Simulation Method

Table C-2 lists the calculation process for Rosenblueth's 2^n simulation method. Note that 2^3=8 calculations of *Y* were performed. In this table, X_i^- equals μ_{xi} - σ_{xi}, and X_i^+ equals μ_{xi} + σ_{xi}, respectively.

Table C-2. Results of Rosenblueth's 2^n Simulation Method.

	x1	*x2*	*x3*	*Y=X1X2X3*
$X1^-$ $X2^-$ $X3^-$	8	3	3.5	84
$X1^-$ $X2^-$ $X3^+$	8	3	6.5	156
$X1^-$ $X2^+$ $X3^-$	8	5	3.5	140
$X1^-$ $X2^+$ $X3^+$	8	5	6.5	260
$X1^+$ $X2^-$ $X3^-$	12	3	3.5	126
$X1^+$ $X2^-$ $X3^+$	12	3	6.5	234
$X1^+$ $X2^+$ $X3^-$	12	5	3.5	210
$X1^+$ $X2^+$ $X3^+$	12	5	6.5	390
Mean (μ_y)				200
Std. Dev. (σ_y)				90.4323

Rosenblueth's 2n+1 Simulation Method

Table 3 lists the calculation process for Rosenblueth's 2*n*+1 simulations method. Note that 2*3+1=7 calculations of *Y* were performed. In this table, X_i^- equals μ_{xi} - σ_{xi}, and X_i^+ equals μ_{xi} + σ_{xi}, respectively.

Table C-3. Result of Rosenblueth's 2*n*+1 Simulations Method.

x1	*x2*	*x3*	*Y=X1X2X3*	$(y_i^- + y_i^+)/2$	$(y_i^- - y_i^+)/2$	$(y_i^- - y_i^+)^2/(y_i^- + y_i^+)^2$
10 (μ_{x1})	*4 (μ_{x2})*	*5 (μ_{x3})*	*200 (y_0)*	*N/A*	*N/A*	*N/A*
8 (X_1^-)	*4 (μ_{x2})*	*5 (μ_{x3})*	*160 (y_1^-)*			
12 (X_1^+)	*4 (μ_{x2})*	*5 (μ_{x3})*	*240 (y_1^+)*	200	-40	0.04
10 (μ_{x1})	*3 (X_2^-)*	*5 (μ_{x3})*	*150 (y_2^-)*			
10 (μ_{x1})	*5(X_2^+)*	*5 (μ_{x3})*	*250 (y_2^+)*	200	-50	0.0625
10 (μ_{x1})	*4 (μ_{x2})*	*3.5 (X_3^-)*	*140 (y_3^-)*			
10 (μ_{x1})	*4 (μ_{x2})*	*6.5(X_3^+)*	*260 (y_3^+)*	200	-60	0.09

$$\mu_y = y_0 \times \frac{\frac{1}{2}(y_1^- + y_1^+)}{y_0} \times \frac{\frac{1}{2}(y_2^- + y_2^+)}{y_0} \times \frac{\frac{1}{2}(y_3^- + y_3^+)}{y_0} = 200 \qquad \text{(C-7)}$$

$$\begin{aligned}\sigma_y &= y_0 \times \sqrt{(1+\left[\frac{(y_1^- - y_1^+)}{(y_1^- + y_1^+)}\right]^2) \times (1+\left[\frac{(y_2^- - y_2^+)}{(y_2^- + y_2^+)}\right]^2) \times (1+\left[\frac{(y_3^- - y_3^+)}{(y_3^- + y_3^+)}\right]^2) - 1} \\ &= 200 \times \sqrt{(1+0.04) \times (1+0.0625) \times (1+0.09) - 1} \\ &= 90.4323 \end{aligned} \qquad \text{(C-8)}$$

As Rosenblueth (1975) mentioned, if the function is the production of independent variables, the result of the 2*n*+1 method exactly equals to the 2^n simulation method.

Monte Carlo Solution

As stated previously, to achieve a Monte Carlo solution, the generation of the values of these random variables should be performed. In this case, random variables *X1*, *X2*, and *X3* are normally distributed. To generate normally distributed random variables, uniformly distributed random numbers between 0 and 1were generated, and then these values were converted to a normal distribution of the corresponding random variable Xi based on the inverse transformation technique described below.

Assuming that a set of uniformly distributed random variables $u_1, u_2, \ldots, u_n$ ($0<u_i<1$) were generated, then the corresponding standard normal random numbers $z_1, z_2, \ldots, z_n$ can be given as (Nowak and Collins 2000) :

$$z_i = \phi^{-1}(u_i) = -t + \frac{C_0 + C_1 t_i + C_2 t_i^2}{1 + d_1 t_i + d_2 t_i^2 + d_3 t_i^3} \ldots\ldots \qquad \text{(C-9)}$$

where Φ^{-1} is the inverse of the standard normal cumulative distribution function, and

$t_i = \sqrt{-\ln(u_i^2)}$;

C_0= 2.515517; C_1=0.802853; C_2=0.010328;

d_1= 1.432788; d_2=0.189269; d_3=0.001308

$$\text{if } u_i>0.5,\ z_i=-\Phi^{-1}(1-u_i) \qquad \text{(C-10)}$$

In the case of normally distributed random variable X with mean μ_x and standard deviation σ_x, the basic relationship between the normal distributed variables x_i and the standard normal variables z_i is

$$x_i = \mu_x + z_i\sigma_x \qquad \text{(C-11)}$$

After N corresponding random values ($X1_i$, $X2_i$, $X3_i$), i=1, 2 …, N, were obtained, these values can be used deterministically and get N response variables $Y_i=X1_i*X2_i*X3_i$. The N response variables Y_i can then be used to calculate all the required statistical characteristics, such as mean value, standard deviation, and the histogram.

It is well-known that the accuracy and repeatability of the Monte Carlo solution increases as the simulation number N increases. To demonstrate how the simulation number N affects the results in this case, the simulation number N of 20, 100, 500, 1000, 3000, 5000, and 10,000 were tried; for each case of a different simulation number, the Monte Carlo simulations were repeated 10 times and 10 different results were recorded.

Figure C-1 shows the repeatability for the different number of simulations by comparing the fluctuation of mean value σ_y among the 10 repeats. When the simulation number is larger than 3000, the fluctuation is pretty small. Thus, all the following Monte Carlo solutions and demonstrations will be based on the 3000 simulations results.

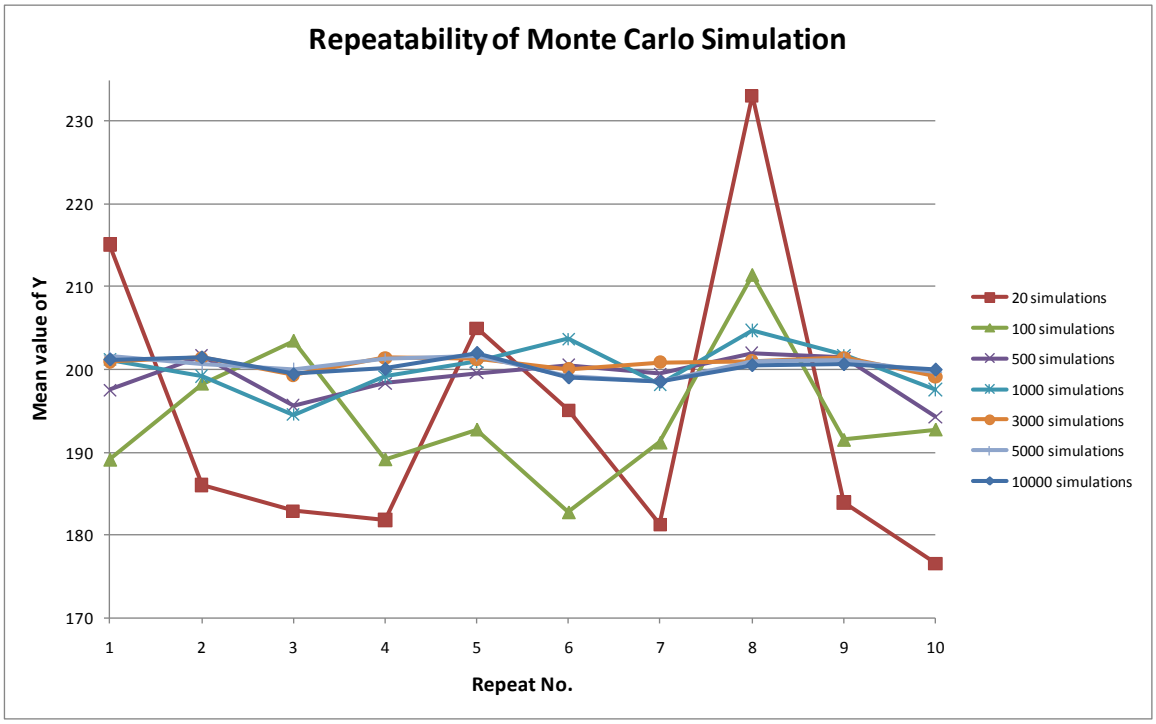

Figure C-1. Repeatability of Monte Carlo Solution for Function *Y=X1*X2*X3*.

Figures C-2 to C-4 show the *X1*, *X2*, and *X3* simulated values distribution (*N*=3000), respectively.

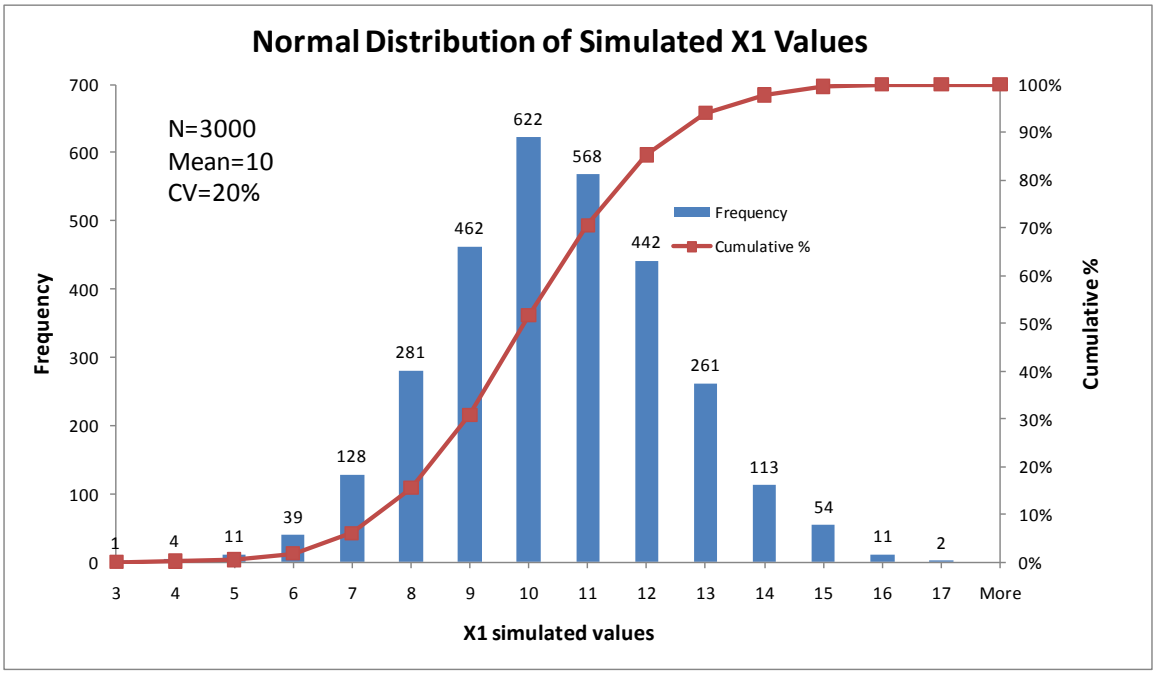

Figure C-2. Normal Distribution of Simulated *X1* Values.

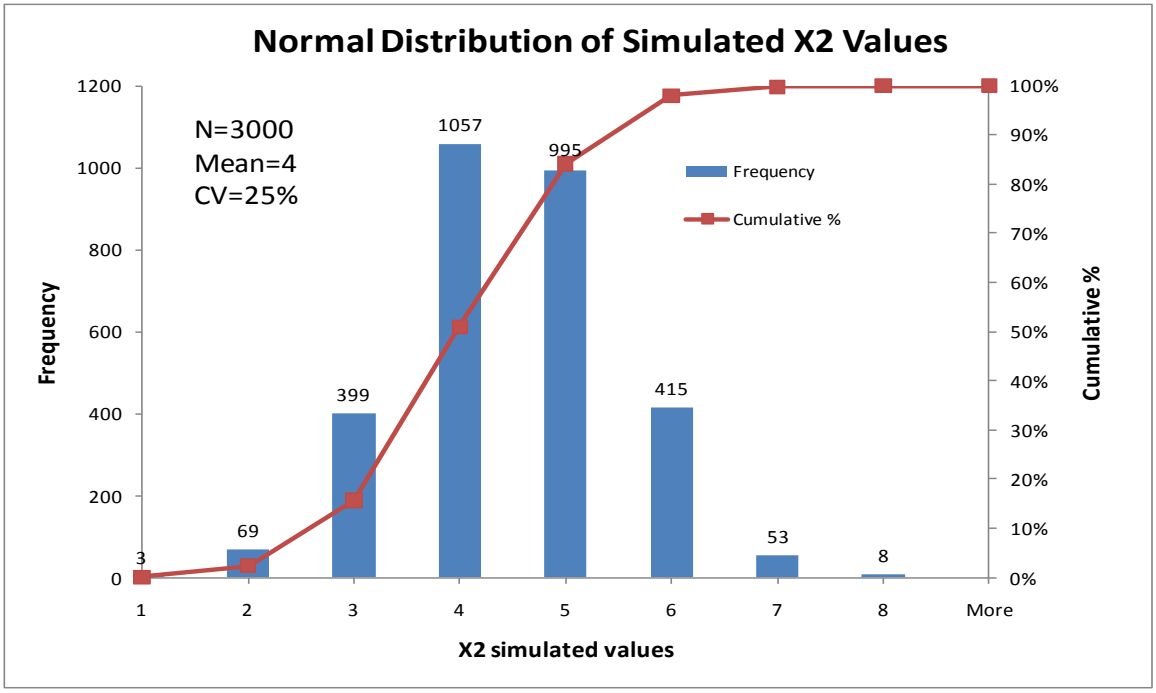

Figure C-3. Normal Distribution of Simulated *X2* Values.

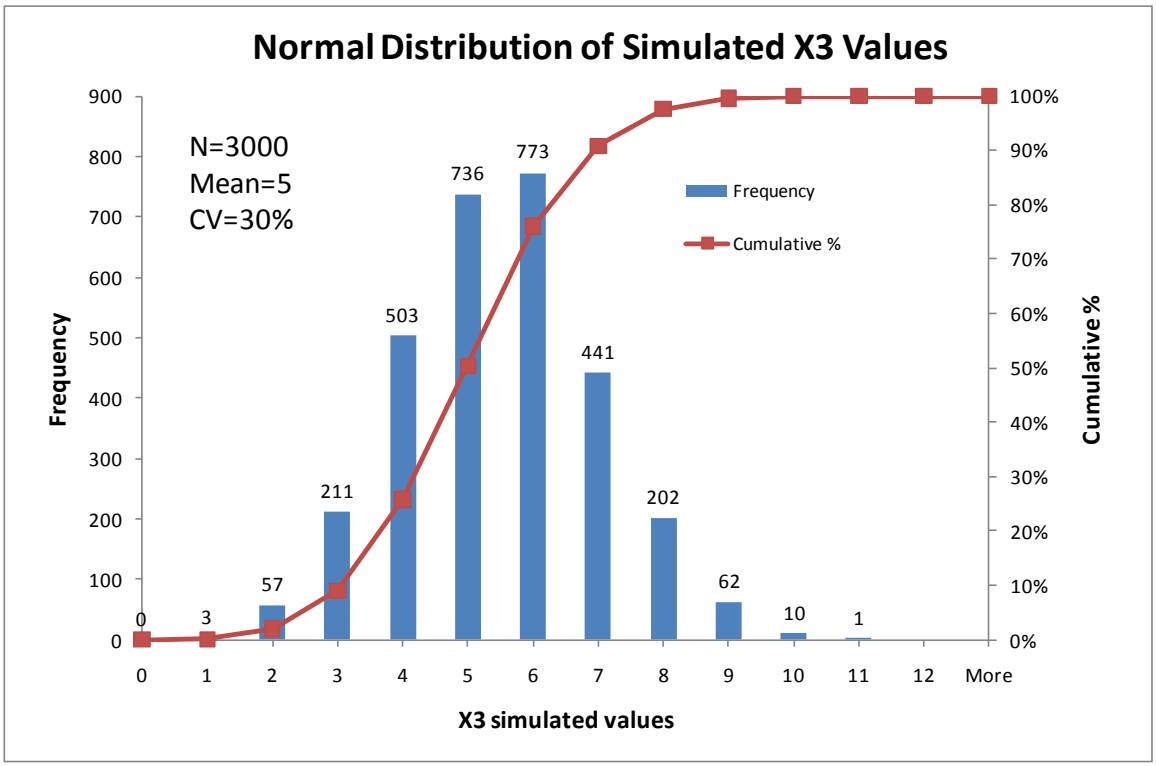

Figure C-4. Normal Distribution of Simulated *X3* Values.

Figure C-5 shows the distribution of calculated *Y* values (*N*=3000). The mean value and standard deviation value were also provided in this figure. To be easily compared, the closed-form result, Rosenblueth result, and Monte Carlo result for this example are listed in Table C-4.

Table C-4. Comparison among Different Methods for *Y=X1*X2*X3*.

	Mean value (μ)	Std. Dev. (σ)	CV (%)
Closed-form method	200	87.7496	44
Rosenblueth 2^n simulation method	200	90.4323	45
Rosenblueth 2n+1 simulation method	200	90.4323	45
Monte Carlo method	199.57	90.4957	45

Theoretically, the production of normally distributed variables is not normally distributed again. In this figure, based on the mean value and standard deviation value, two cumulative % curves were added (one is assumed to be a normally distributed and the other is assumed to be a lognormally distributed) to compare with the real cumulative % curve.

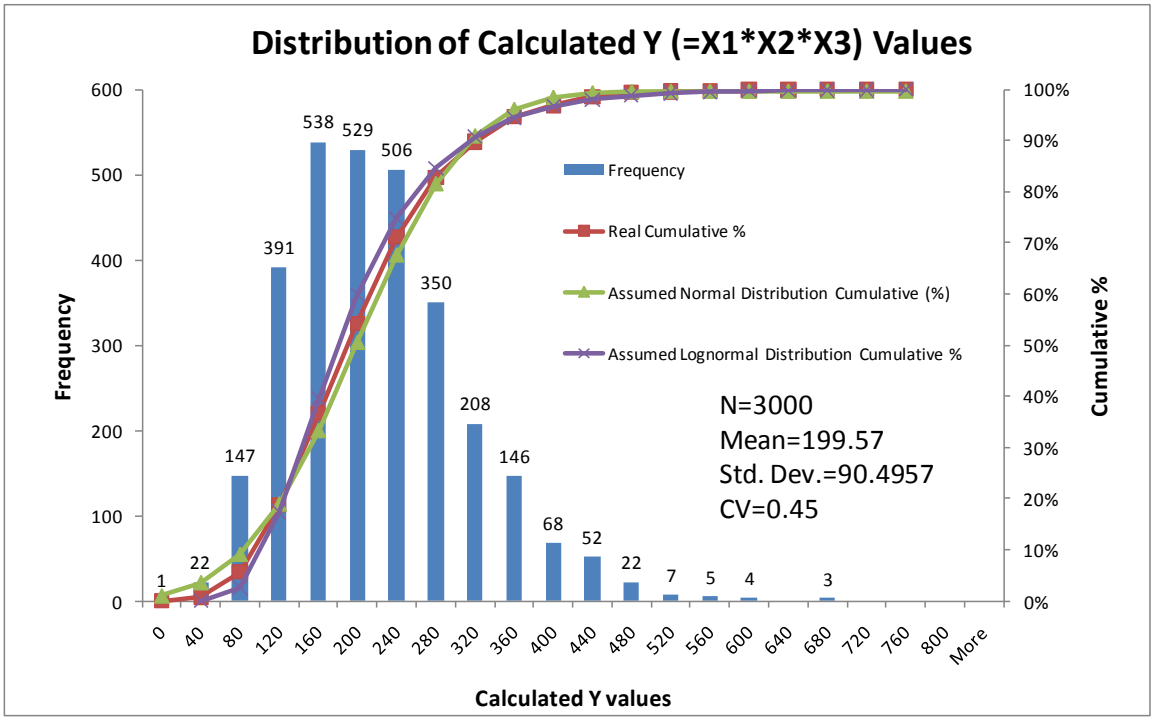

Figure C-5. Distribution of Calculated Y Values (*Y=X1*X2*X3*).

EXAMPLE 2

$Y=X1*X2+X3^2$, where *X1*, *X2*, and *X3* are the same independent variables as in Example 1. Similar calculations can be performed as in Example 1, and Table C-5 presents the results comparison.

Table C-5. Comparison among Different Methods for $Y=X1*X2+X3^2$.

	Mean value (μ)	Std. Dev. (σ)	CV (%)
Closed-form method	67.25	19.7231	29
Rosenblueth 2^n simulation method	67.25	19.8242	29
Rosenblueth 2n+1 simulation method	67.25	19.5945	29
Monte Carlo method	67.1801	19.7454	29

Note, now that the function *Y* is not the simple product of independent variables, the standard deviation result of the Rosenblueth 2*n*+1 method (19.5945) is not exactly equal to the result of the 2^n method (19.8242). However, they are still very close, which confirms that these two methods are equally valid, provided that the standard deviations of the input variables are not too large.

Figure C-6 shows the distribution of calculated $Y=X1*X2+X3^2$ values (*N*=3000), the mean value, and the standard deviation value. Similarly, based on the mean and standard deviation values, two cumulative % curves were added (one is assumed to be normal distribution and the other is assumed to be lognormal distribution) to compare with the real cumulative % curve.

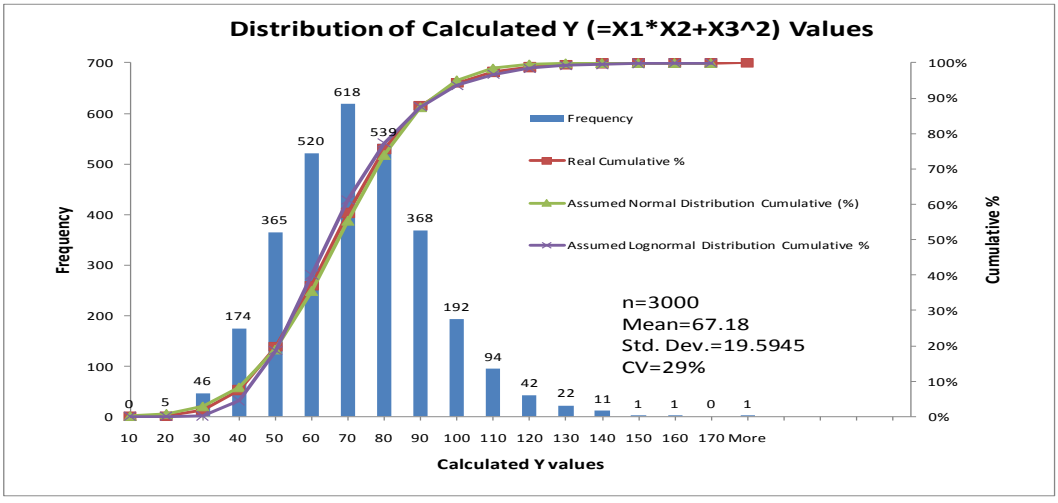

Figure C-6. Distribution of Calculated Y Values; $Y=X1*X2+X3^2$; *X1*, *X2*, and *X3* All Have Normal Distributions.

EXAMPLE 3

$Y=X1*X2+X3^2$, where *X1*, *X2*, and *X3* have the same mean values and standard deviation values as in Example 1, but the distributions are different. Among them, *X1* still has a normal distribution, *X2* has a uniform distribution, and *X3* has a lognormal distribution.

In this case, because the distribution type does not affect closed-form results or Rosenblueth results, only the Monte Carlo solution needs to be recalculated. Figures C-7 and C-8 present the distributions of simulated *X2* and *X3* variables, respectively.

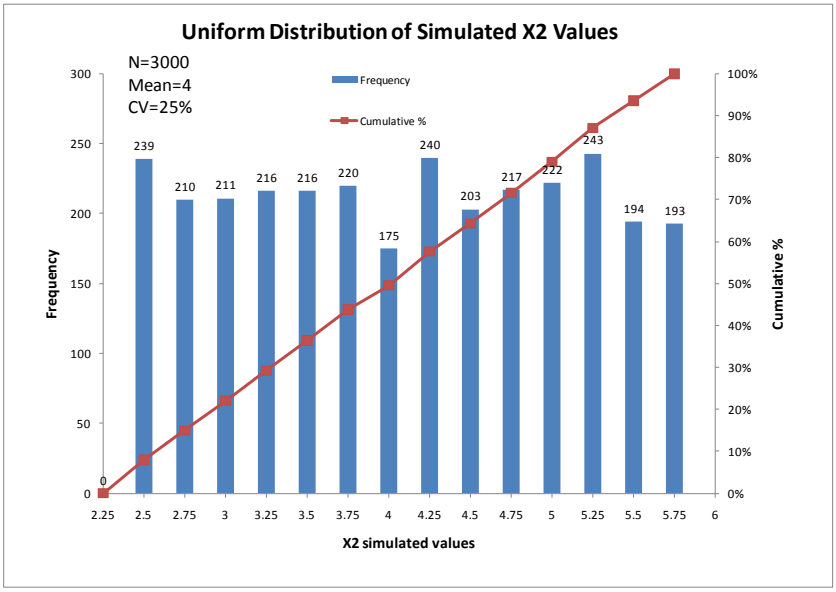

Figure C-7. Uniform Distribution of Simulated *X2* Values.

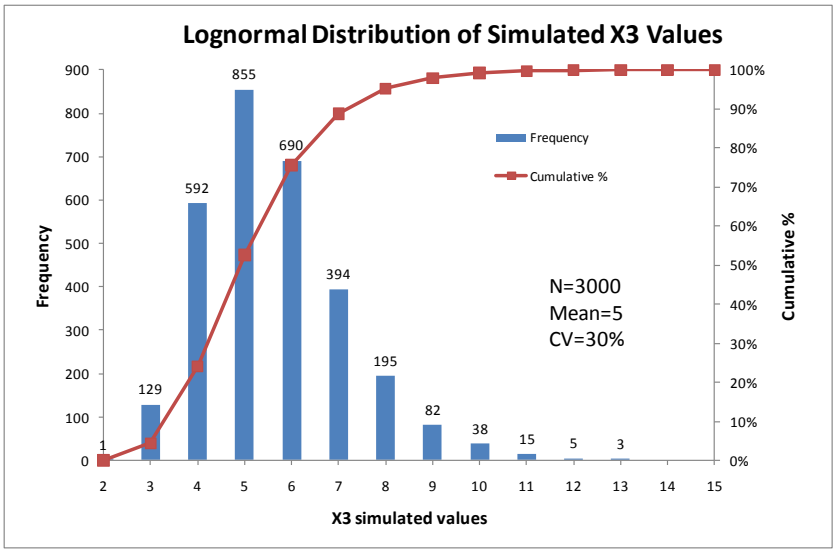

Figure C-8. Lognormal Distribution of Simulated *X3* Values.

Figure C-9 presents the distribution of calculated $Y=X1*X2+X3^2$ values (N=3000), the mean value, and the standard deviation value. Again, based on the mean value and standard deviation value, two cumulative % curves were added (one is assumed normally distributed and the other is assumed lognormally distributed) to compare with the real cumulative % curve.

Comparing the results with Example 2 shows that distribution type does have some influence on the final result. However, this influence is not significant: mean value (68.6 vs 67.18), standard deviation (22.065 vs 19.5945), and coefficient of variation (32 percent vs 29 percent). Comparing the two cumulative % curves in one figure shows that the resulting distributions are also very close (see Figure C-10). This verifies the validity of the closed-form method and Rosenblueth method since these methods only consider the mean value and standard deviation value and ignore the distribution type.

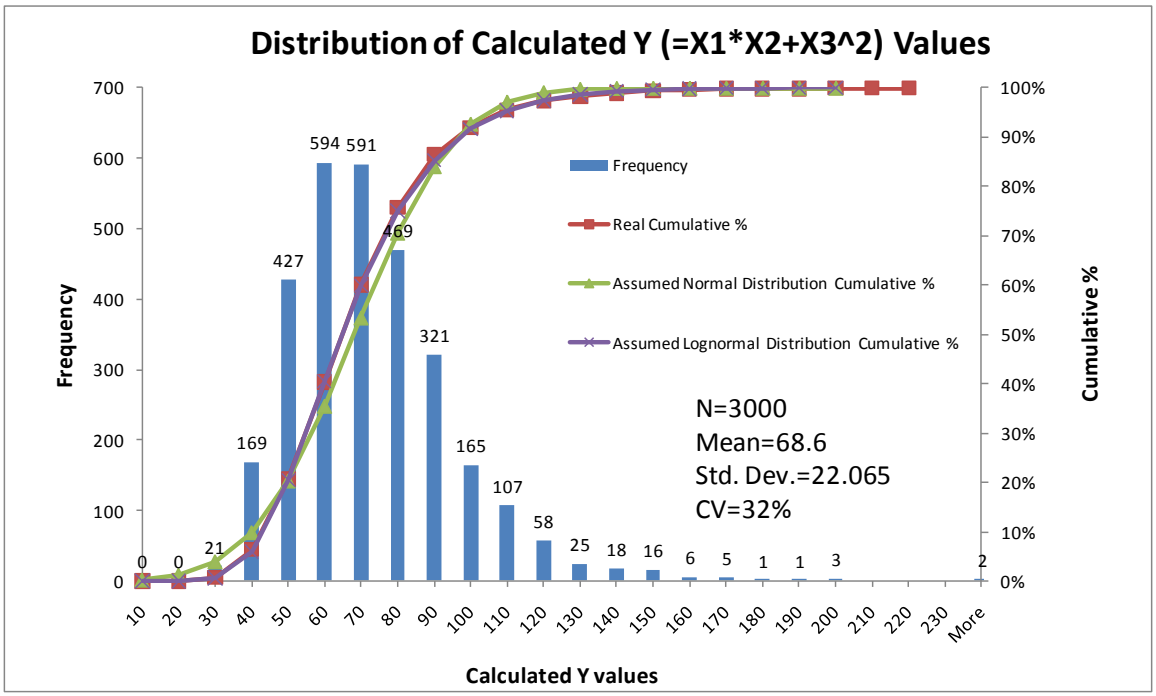

Figure C-9. Distribution of Calculated Y Values, $Y=X1*X2+X3^2$ (*X1* has normal distribution, *X2* has uniform distribution, and *X3* has lognormal distribution.)

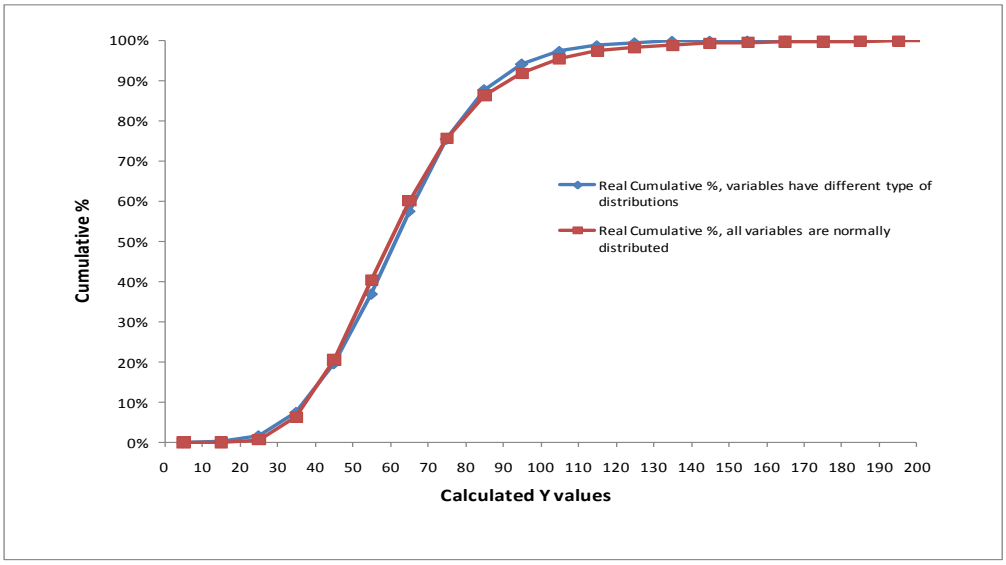

Figure C-10. Comparison of Cumulative % Curves between Examples 2 and 3.

SUMMARY

Based on the results presented above, the following conclusions can be drawn:

- The results for the Closed-form method, Rosenblueth 2^n simulation method, Rosenblueth $2n+1$ simulations method, and Monte Carlo method are all comparable to each other as verified by using different functions and different distribution types for selected input variables.
- For the Monte Carlo method, the simulation number N is recommended to be equal to or greater than 3000 to assure good repeatability and accuracy.
- Leaving the mean value and standard deviation value (or coefficient of variation) unchanged, the input variable distribution type has some but not a significant influence on the final response function in terms of the Monte Carlo solution.
- Both the closed-form and Rosenblueth methods do not need to know the distribution type of the input variables. Neither of them can obtain the cumulative distribution function curve of the response variable.
- Both normal distribution and lognormal distribution could be employed to fit the response cumulative distribution function curve with little error.
- The Rosenblueth $2n+1$ simulations method has high practical benefit when the calculations are very complicated and the derivatives are hard to obtain.

REFERENCE

Nowak, A. S. and K. Collins. *Reliability of Structures*. McGraw-Hill Publisher, 2000.

Rosenblueth, E. Point Estimates for Probability Moments. In *Proceedings of National Academic of Science*, USA. 72(10):3812-3814, 1975.